이학박사학위논문

Hybrid phase transition in complex systems

복잡계에서의 하이브리드 상전이

2020년 2월

서울대학교 대학원

물리·천문학부

박 진 하

이학박사학위논문

Hybrid phase transition in complex systems

복잡계에서의 하이브리드 상전이

2020년 2월

서울대학교 대학원

물리·천문학부

박 진 하

Hybrid phase transition in complex systems

복잡계에서의 하이브리드 상전이

지도교수 강 병 남

이 논문을 이학박사 학위논문으로 제출함

2020년 2월

서울대학교 대학원

물리·천문학부

박 진 하

박진하의 박사 학위논문을 인준함

2019년 12월

위 원 장: 정현석 (인)

부위원장: 강병남 (인)

위 원: 양범정 (인)

위 원: 백용주 (인)

위 원: 고광일 (인)

Abstract

Hybrid phase transition in complex systems

Jinha Park
Department of Physics and Astronomy
The Graduate School
Seoul National University

Complex organization of elements can bring in new phases and novel critical effects. The phase transition of a complex system can be rich and unique. More is different, and details matter. In particular, complexification may yield hybrid phase transition, a discontinuous transition which accompanies critical phenomena. This novel type of phase transition has been discovered across diverse complex systems, including k-core percolation, cascade failures of interdependent networks, generalized epidemic spreading, restricted percolation, Kuramoto oscillators with flat-topped frequency distribution, and restricted synchronization. In this dissertation, it is investigated that how a complex system exhibits a discontinuous jump of the order parameter together with the critical phenomena at the same transition point. In particular, hybrid percolation transition and hybrid synchronization transition are focused. Several universal (or potentially universal) mechanisms are noticed. There are hybrid percolation transitions of cascade class and of merging class, hybrid synchronization transitions of Kuramoto models with flat natural frequency distribution and of restricted Kuramoto model with ranking-based shuffling dynamics. Hybrid phase transitions of complex systems may be classified on the basis of those mechanisms.

Keywords: Hybrid phase transition, Complex system, Synchronization, Percolation, Kuramoto model, restricted Erdős-Rényi model, restricted Kuramoto model

Student number: 2014-21361

Contents

List of Figures

Chapter 1

Introduction

Complex organization of elements can bring in new phases and novel critical effects. More is different [1] and details matter [2]. How is the phase transition and critical phenomena affected by a complexification? One possibility is to introduce disorders. The presence of disorders does not necessarily destroy the phase transition of a clean system [3], and long-range order is also possible [4]. Under presence of disorders, a sharp phase transition still occurs, although new critical points and new critical exponents may appear. For example, network represents a structural disorder. Heterogeneity in connections is described by a simple power exponent λ of the degree distribution, for instance in the scale-free network, while the outcomes of introducing such a nontraditional power is not so simple [5–7]. In a coupled non-identical oscillator system, a change in the shape of intrinsic frequency distribution can significantly change the type of phase transitions [8–13]. Other possibilities include, introducing competing species [6, 14–21], multiplexing network [6, 22], and so on, where at each stage, a complex organization leads to further new complex physics.

1.1 What is a hybrid phase transition?

Phase transition is either continuous or discontinuous. A continuous phase transition is characterized by a critical point where correlations over all scales holds the system to a unique critical phase. A discontinuous transition has two or more phases are allowed at the transition point. The macroscopic transformation bridging a phase to another phase further requires some equilibrium or nonequilibrium dynamic processes.

Hybrid phase transition is a type of phase transition which exhibits properties of both discontinuous (jump of the order parameter) and continuous (critical phenomena) phase transitions at the same transition point. Such a transition has been discovered in diverse equilibrium [6,23–32] and nonequilibrium complex systems [7,9,11–13,20,22,33–55]. A practical implication of a hybrid phase transition is the presence of a diverging precursor associated to the upcoming catastrophic abrupt change of the complex system. But how can a complex system undergo a discontinuous transition and exhibit a diverging quantity at the same time? Several mechanisms have been proposed for the hybrid phase transitions of complex systems, yet more are left to be revealed.

The term hybrid phase transition was coined in context of the k-core percolation of complex networks, which originally specified a discontinuous jump of the order parameter which also accompanies a square-root singularity [33,39,53]. An analogous square-root singularity is often noticed from a spinodal critical point, the end of a metastable line in the first-order phase transitions. Although, the spinodal critical point is rarely realized in the ordinary equilibrium thermodynamics. However, this point might be considerable under a strong nonequilibrium drive, e.g. quenching [26]. Hybrid transition has been observed in complex systems as well, for example, in cascade failure of interdependent networks [22,34], generalized disease spreading [40,41,43,44], and the restricted percolation [48–51]. Hybrid transition also appears in synchronization with a nontrivial critical exponent $\beta = 2/3$ [7,11,13,20].

On the other hand, there are mixed-order phase transitions of the equilibrium complex systems, characterized by order parameter jump and diverging susceptibility at the same transition point [6,23–25,27,28,31,32,41]. In a loose sense, the mixed-order transition can be called a hybrid phase transition, whilst the hybrid phase transition in the original restricted sense refers to the presence of a peculiar singularity at the order parameter jump. Mixed-order transition can occur at a critical endpoint, a point in the phase diagram where a second order transition line ends at a first order transition line. At a critical endpoint, we observe discontinuous transition of the order parameter and diverging susceptibility which originates from the continuous phase transition. Diverging susceptibility is owing to the vanishing second

derivative of the free energy. Landscape inversion phase transition of magnetic colloids also causes a mixed order phase transition [27], where the flat energy landscape at the transition point introduces the critical phenomena to the discontinuous transition. It is remarked that an analogous flat landscape perspective may possibly hold for some nonequilibrium hybrid phase transitions. For example, a pseudo free energy is constructed in Ref. [56] as a phenomenological approach to the hybrid synchronization transition. This pseudo free energy becomes flat at the hybrid phase transition point in the thermodynamic limit $N \to \infty$.

The hybrid phase transition of the original k-core percolation context and the mixed order phase transition of equilibrium/nonequilibrium systems are sometimes distinguished. In the former, a singularity lies in the order parameter curve at the top end of the jump. In the later, diverging susceptibility is noted at the discontinuous transition point, regardless of the existence of such a continuous-type singularity in the order parameter curve. Moreover, a single nonequilibrium model can sometimes exhibit both mixed-order transition and hybrid transition, depending on the initial conditions. For example, in the generalized epidemic spreading model with initial infectious seeds of orders of system size, pandemics is reached through a hybrid phase transition [42]. With a single infectious seed, epidemic order parameter exhibits no singularity at the top end of the jump, but the transition is also marked by divergence of mean finite outbreak size [41].

There are two classes of hybrid percolation transitions, cascade or merging, depending on the character of the underlying dynamic process in the model. The hybrid percolation transition of k-core percolation, cascade failure of interdependent networks, and generalized epidemic spreading are examples of hybrid phase transition induced by pruning processes. This class of hybrid phase transitions follows a universal mechanism, namely a crossover from critical branching to supercritical branching process [46]. On the other hand, the hybrid percolation transition can also be induced by a cluster aggregation process. In the restricted percolation model [48–51], clusters are sorted by their size and partitioned into two groups, and merging of two big-size clusters are suppressed. The restricted merging process involves a back-and-forth group-switching dynamics of clusters, which organizes a critical state and

an abrupt transition [51].

Absence of synchronization seed leads to hybrid synchronization transition in the Kuramoto model with flat-topped intrinsic frequency distributions [11–13,20]. Evenly dispersed oscillators are maximally competitive, and hence frequency clustering occurs in an abrupt manner. An analogous balancing was provided in the first-order explosive synchronization models as well, by correlating the segregation and aggregation [57–63]. Indeed, hybrid synchronization transition could possibly occur as a special case in an explosive model [7]. However, the suppressive modification [62] is not a necessary condition for a jump of synchrony in the oscillator model. Rather, second-order, first-order and hybrid synchronization transitions are all possible already in the original Kuramoto model, depending on the shape of intrinsic frequency distribution. This is in contrast to percolation, where a global suppressive rule [64] was a necessary condition for a discontinuous jump.

Further introduction of competing, mixed-signs coupling constants generates tiered synchronization patterns such as π or traveling-wave states [19, 20]. Correspondingly, a rich synchronization dynamics involving more than two phases occurs at a single transition point, where a collection of metastable intermediate states is noticed on the way to traveling wave synchronization [20].

Finally, motivated by restricted percolation, a ranking-based group reclassification is applied to synchronization, and a distinct class of hybrid synchronization transition is obtained. In contrast to the previous hybrid synchronization models, the restricted synchronization model exhibits hybrid phase transition even with unimodal natural frequency distributions. A macroscopic population of oscillators is frequency clustered, forming a traveling wave steady state. However, the frequency cluster also involves intricate internal switching dynamics and the switching interval distribution follows a power law [65].

1.2 A critical singularity at the discontinuous transition

Hybrid phase transition is a type of discontinuous transition which also accompanies critical phenomena at the same transition point. The hybrid phase transition which has been found in

many nonequilibrium complex systems [11,13,20,33,39,48,49,53] is characterized by a singular point after jump in the order parameter. The order paramter curve $m(t)$ asymptotically behaves near the transition point t_c as

$$m(t) = \begin{cases} 0 & t < t_c \\ m_0 + A(t - t_c)^\beta & t \geq t_c \end{cases} \tag{1.1}$$

and with an associated singularity at the terminal point of the jump. By singularity we mean $\partial t(m)/\partial m = 0$ at $m = m_0$, and it is characterized by a non-integer exponent $0 < \beta < 1$. Here, m_0 is the size of jump, A is a constant, and t is a control parameter. This exponent after jump is distinct from the usual β of the continuous transition defined at $m = 0$, which becomes zero in presence of discontinuity ($\beta = 0$). The singularity at $m = m_0$ may further relate to some other critical phenomena as well. For instance, finite size clusters of the restricted percolation model follow a power law size distribution $n_s \sim s^{-\tau}$ at $m = m_0$ [49]. For such a reason we call β the (hybrid) critical exponent of the order parameter. However, the relationship between a hybrid singularity and criticality is not that obvious. In particular, recall that ordinary continuous percolation transition of the Erdős-Rényi model is characterized by critical exponents $\beta = 1$ and $\tau = 5/2$. There β is not an integer and therefore the slope is not divergent, but there is a bifurcation of order parameter curve from zero to a nontrivial branch. In a hybrid phase transition, order parameter curve is discontinuous, and hence it is already singular at the bottom of the jump $t = t_c, m = 0$. The continuous-type singularity at the top of the jump is something extra.

The $(k \geq 3)$-core percolation shows a hybrid phase transition with square-root singularity $\beta = 1/2$ [33, 38, 39]. Cascade failures of interdependent networks [22, 34, 47] and generalized epidemic spreadings [40, 42] also exhibit square-root singularities. Hybrid synchronization transitions [7, 11, 13, 20] can exhibit an unusual exponent $\beta = 2/3$. Further, continuously varying β is obtained for some hybrid percolation models [49, 50] and hybrid synchronization models. See for example Ref. [12] and also a model presented in chapter 5.

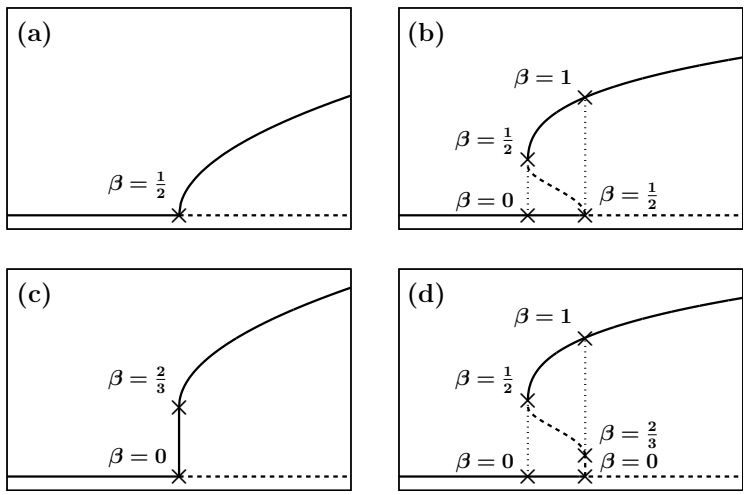

Figure 1.1: With asymptotics $\sim x^{\beta}$, $0 < \beta < 1$ implies a diverging (vertical) slope. A discontinuous transition is usually characterized by $\beta \to 0$ at the foot of the jump. Looking at the curves after turning one's head, note $\beta = 1/2$ corresponds to an extremum of a parabola. $\beta = 1$ implies a linear response to the change of control parameter. A tangent of a curve obtains a finite slope most of the time. $\beta > 1$ results a zero (horizontal) slope. The schematic figures present order parameter curves of (a) second-order type (b) first-order type (c) supercritical hybrid type and (d) subcritical hybrid type phase transitions.

1.3 Hybrid phase transition of equilibrium complex systems

A similar square-root critical singularity is often noticed in first-order phase transition, at the end of the metastable branch of the order parameter curve. However, such a critical point is rarely realized in the ordinary thermodynamics. In presence of thermal fluctuations, i.e. equilibrium processes, global free energy minimum is favored instead of the metastable states. A full hysteresis involving spinodal point might be considerable instead under a strong nonequilibrium drive, for example, in the rapid heating and cooling of metals, where there is a bottleneck of heat transfer [26].

On the other hand, some equilibrium and nonequilibrium complex systems exhibit a mixed-order phase transition. For example, metamagnets [27], Ashkin-Teller spin model [6], and one-dimensional Ising model under long-range interaction [23, 24, 28, 29], where we

find a discontinuous transition occurs together with a diverging susceptibility. Such a transition is described under the framework of Landau theory. Let us denote m the Landau order parameter near the transition point. In the language of magnetic systems, m is the average magnetization. In the paramagnetic phase $T > T_c$, disordered state $m = 0$ is the unique global minimum of the Landau free energy $f(m)$ and $f(0) = f'(0) = 0, f''(0) > 0$. Phase transition occurs at $T = T_c$. For a discontinuous jump to occur, another minimum (or minima) is required at some $m_0 \neq 0$. At the transition point, there are two (or more) global minima $f(m_0) = f'(m_0) = 0, f''(m_0) > 0$ and $f(0) = f'(0) = 0$. Additionally, if $f''(0) = 0$ or $f''(m_0) = 0$ is satisfied, such a flatness implies an additional second-order-like singularity which gives diverging susceptibility; then the transition is mixed order. In the ferromagnetic phase ($T < T_c$) $m_0(T) \neq 0$ becomes the global minimum (minima) and $f(0) = f'(0) = 0, f(m_0) < 0, f'(m_0) = 0, f''(m_0) \geq 0$. Notice that these conditions are met at the critical endpoint, where the second order line ($f(0) = f'(0) = f''(0) = 0$) ends at the first order line.

1.3.1 Ashkin-Teller magnet on scale-free network

The study of Ashkin-Teller model on scale-free networks [6] is one of many pedagogical examples relevant to discuss about the richness of the complex system paradigm of research. The Ashkin-Teller system is composed of two species of Ising spins s and σ at each site. It is an equilibrium system where the Landau theory applies. Two perspectives should be noticed. First, more is different. The two species generalization not only results a paramagnetic or ferromagnetic phases characterized by $\langle s \rangle$ or $\langle \sigma \rangle$, but also introduces a product phase characterized by the order parameter $\langle \sigma s \rangle$. In turn, Ashkin-Teller model on d-dimensional lattice exhibits tricritical points. Second, scale-free network introduces a new structural exponent λ to consider. It introduces a nontraditional term of order $m^{\lambda-1}$ in the free energy $f(m)$, which is hence no longer a simple polynomial form. The structural modification from a lattice to scale-free network extends the first-order line, and separates each tricrtical point into a critical endpoint and a critical point [6]. Remarkably, the Ashkin-Teller model on scale-free

networks can exhibit continuous, discontinuous, mixed-order, and successive phase transitions (second-order transition followed by discontinuous transition), depending on the model parameters [6].

At the critical endpoint, a second-order line falls on top of the first-order line. Thus, mixed-order phase transition occurs. Susceptibility is divergent near the high temperature side of the transition point $f''(0) = 0$. And a jump occurs in the magnetization order parameter. At the second-order transition line excluding the critical endpoint, a λ-dependent the critical exponent $\beta = 1/(\lambda - 3)$ is noticed. However, precisely at the critical endpoint, this second-order singularity hides at the foot of the first-order jump.

1.3.2 Spin chain under long range interaction

Another notable example is one-dimensional Ising model with a ferromagnetic long range interaction $J(r) \propto r^{-\sigma}$, where r is the distance between two sites. For $1 < \sigma < 2$, the model exhibits a continuous transition with $\beta = 2 - \sigma$ [23, 29]. In contrast, for a shorter range interactions of $\sigma > 2$, formation of domain walls is favored and the long range order is impossible [23, 29]. For $\sigma > 2$ it is immediately noticed that the first moment

$$M_1 = \sum_{i=0}^{\infty} iJ(i)$$

becomes finite. Notice additionally that this quantity relates to the energy difference of perfectly ordered state and a single domain wall state as $E_1 - E_0 = 2M_1$, if the Ising spin variables are assumed to take the values $s_i = \pm 1$. A mathematical proof that long range ordering is impossible for when M_1 is finite is provided in [30]. If $\sigma > 2$, the domain wall is allowed at any finite temperatures, which breaks the long-range ordering.

An interesting case is when with inverse square law $\sigma = 2$, where not only a first-order transition, but also mixed order phase transition had been suggested (Thouless effect) [23]. Thouless had predicted that a discontinuous transition should occur in the marginal case of $\sigma = 2$. Moreover, he suggested another possibility where the distribution of magnetization

becomes flat. Aizenman et al. showed that the discontinuous transition indeed occurs, using Fortuin-Kasteleyn formalism and mathematical inequalities [28]. There is a mixed order terminal point in the first-order line [24]. However, the $\sigma = 2$ model was not exactly solvable. Recently, a solvable modification of this $\sigma = 2$ model has been presented by Bar and Mukamel [24], where the long-range interaction was confined within the domain walls. They found an interesting phase diagram where mixed-order lines appear.

1.3.3 Colloidal metamagnet

Landscape inversion phase transition in magnetic colloids is another example of a mixed order phase transition [27]. A flat energy landscape at the transition point induces critical phenomena to the discontinuous transition. Paramagnetic colloidal particles float around the top of a two dimensional magnetic substrate, which is striped with oppositely magnetized domains. The particles acquire magnetic dipoles due to superposition of the substrate magnetic field and the external magnetic field $m \propto H \pm H_s$, and they assemble in lines above the magnetic domain walls. Ferri- and ferro- magnetic orderings are possible. Moreover, dipolar interactions lead to a structural ordering characterized by the lattice angle α. By controlling the external magnetic field, the energy landscape can become flat at (and inverted beyond) the transition point $H = H_s$ as in Fig. 1.2(a). Correspondingly, the crystal experiences a discontinuous structural transition (in α), together with a transition from a ferrimagnetic to ferromagnetic ordering. Such a flat landscape at the transition point induces critical phenomena such as diverging correlation length and the lattice angle fluctuations. The order parameter curve is given as a step function and it is not the kind of a hybrid phase transition characterized by critical β. It is a mixed order phase transition which involves diverging correlation lengths and diverging lattice angle fluctuations.

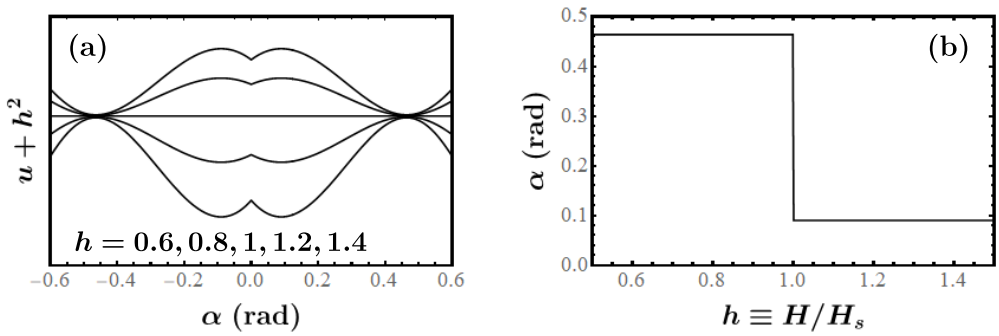

Figure 1.2: (a) The landscape inversion phase transition and the corresponding (b) order parameter curve of lattice angle $\alpha(h)$. This is a reproduction of Fig.1 in Ref. [27].

1.4 Structure and goal of this dissertation

Hybrid phase transition is a very general concept which may apply to a variety of equilibrium and nonequilibrium systems. Hybrid phase transitions frequently occur in complex systems, where many of which are nonequilibrium systems. How can critical phenomena occur simultaneously with the discontinuous transition in those systems? In contrast to the equilibrium critical phenomena, hybrid phase transition does not have a single theoretical framework which leads to systematic and rigorous understandings. For example, we do not know how the renormalization concept could be applied to the hybrid phase transition of complex systems. In particular, a hybrid phase transition may involve two or more distinct diverging length scales and in such a case we do not know how to coarse-grain the system [50]. The critical phenomena of hybrid phase transitions are rich and the underlying mechanisms can be diverse. The goal of this dissertation is not to provide a single unification theory of the hybrid phase transition. Rather, hybrid phase transitions of complex systems are grouped into several classes, on the basis of the underlying mechanisms. Specifically, hybrid phase transitions of percolation and synchronization are focused. The structure of this dissertation is mainly two-fold: we review properties and mechanisms of both hybrid percolation transition and hybrid synchronization transition.

Percolation transition is known as one of the most robust continuous transitions. It was

revealed recently that global suppression is an indispensable factor for a discontinuous percolation transition. It brings up another perspective: "what are the necessary factors for a hybrid percolation transition?" Hybrid percolation transition is a discontinuous percolation transition accompanied by one or more critical phenomena.

- In chapter 2, some preliminary concepts on the continuous percolation transition are reviewed and discussed. Recent attempts to build discontinuous percolation transition are briefly mentioned. Two classes of hybrid percolation transitions, namely the cascade class and the merging class are reviewed.

- In chapter 3, novel dynamic critical behaviors of the merging class hybrid percolation model is presented.

Kuramoto model is a simple phase oscillator model which exhibits synchronization phase transition. In the thermodynamic limit, the type of transition may be continuous or discontinuous, depending on the natural frequency distribution formed by the oscillators. Especially, it is often categorized by many literatures that unimodal or bimodal natural frequency distribution leads to continuous or discontinuous synchronization transition, respectively [8, 66–71]. However, there exists a marginal category of having flat-topped distributions, which can neither be classified as unimodal nor bimodal. A class of hybrid synchronization transitions occurs for flat-topped natural frequency distributions. Another class of hybrid synchronization transition is presented later in chapter 7.

- In chapter 4, self-consistency theory of Kuramoto is reviewed. Continuous or discontinuous synchronization transition occurs in the Kuramoto model with unimodal or bimodal natural frequency distribution, respectively.

- In chapter 5, flat-topped class of hybrid synchronization transition is discussed. For uniform distribution or flat-topped distribution with additional presence of long range tails, we find a critical exponent $\beta = 2/3$ or $\beta = 2/5$, respectively. Here the synchronized phase is a fully phase locked state.

- In chapter 6, mixed signs of couplings is introduced to the Kuramoto model and investigate how the presence of this additional disorder affects hybrid synchronization transition. Passive type and active type interactions are considered. In the hybrid synchronization transition of an active model, we find emergence of traveling wave phase characterized by a nontrivial angular velocity, which deviates from the mean natural frequency of the system. Also, the synchronization dynamics at the hybrid critical point involves metastable states. We obtain rich phase diagrams involving three phases, and first-order and hybrid transition lines. In the hybrid synchronization transition of a passive model, we find an unusual hybrid critical exponent in the subleading order, which is different from that of the continuous phase transition. Such an effect can be observed in the finite size systems.

Finally, ranking-based restriction idea of the merging class percolation is applied to synchronization problem. A leader-follower dichotomy based on oscillators' angular velocity rankings is considered. Interaction of leader oscillators is suppressed in the restricted synchronization model, analogously to the suppression of coagulation of big clusters in the restricted percolation model.

- In chapter 7, we present the restricted Kuramoto model and investigate its phase transitions. With presence of a ranking-based leader-follower reclassification and with a restricted interaction among leader oscillators, we find that discontinuous (hybrid) synchronization transition is also possible for a unimodal frequency distribution. This is in stark contrast to the ordinary Kuramoto model, where a unimodal frequency distribution leads to a continuous transition. We find hybrid synchronization transition or second-order synchronization transition, depending on the leader fraction. Oscillators cooperatively self-organize a heavy-tailed intervent time distribution of leader-follower set switching intervals.

Chapter 2

Hybrid percolation transition

In this chapter we briefly review the theory of continuous percolation transition and define the critical exponents. Then we discuss the possibility of discontinuous transitions in some variant percolation models. Finally, hybrid percolation models are introduced.

2.1 The theory of continuous percolation transition

Percolation transition is an emergence of macroscopic connection. It is a purely geometric transition from unconnected to connected state, which accounts for a variety of natural and social phenomena such as sol-gel transition [72], metal-insulator transition [73], resistive switching [74], disease spreading [75], and social opinion formation [76].

The information on how parts are connected in the system is conveniently provided by an abstract object: network (or graph). Adjacency matrix a_{ij}, for example, is a representation of connection ($a_{ij} = 1$) or disconnection ($a_{ij} = 0$) between the two elements i and j. For a statistical mechanics treatment, we first need a collection of networks. A network ensemble is considered, for example, by specifying the complete degree sequence $\{k_1, \cdots, k_N\}$ (microcanonical) [77, 78], or by fixing the total number of nodes and links (canonical), or by fixing number of nodes N and linkage probability p which has fluctuating number of links (grandcanonical) [79]. The probability that a grandcanonical network ensemble (N, p) contains a specific graph G is given as

$$P(G) = Z^{-1} \prod_{(i,j)\in G} p \prod_{(i,j)\notin G} (1-p) \tag{2.1}$$

where (i, j) denotes a link between two nodes i and j. A homogeneous connection probability $p_{ij} = p$ corresponds to an ensemble of Erdős–Rényi random network with Poissonian degree distribution [80, 81]. Details will be followed in section 2.2. It is remarked that a random network ensemble with heterogeneous connection probability p_{ij} is also possible, e.g. $p_{ij} = w_i w_j$ with $w_i \propto i^{-\mu}$ is capable of generating an ensemble of networks having random Poissonian degree distributions to an ensemble of networks having highly heterogeneous degree distributions $P_k \sim k^{-(1+\mu)/\mu}$ and with presence of hubs [82].

Now, take a network and fill links with conducting materials randomly by a probability p. The network is an insulator at $p = 0$ and becomes a conductor at $p = 1$. In between, at which p, do we expect a metal-to-insulator transition? The probability of coloring a graph in such a percolation problem is given as

$$P(G) = Z^{-1} \prod_{\langle ij \rangle} p^{a_{ij}} (1-p)^{1-a_{ij}} \tag{2.2}$$

where $\langle ij \rangle$ denotes adjacent node pairs in the background network and a_{ij} is the adjacency matrix of the filling network. The graph ensemble average of any graph-dependent physical quantity $A(G)$ can be calculated as

$$\langle A \rangle = \sum_{G} P(G) A(G). \tag{2.3}$$

On a lattice geometry, the presence of a connecting path between two opposite ends, or the presence of a spanning cluster naturally defines the percolation. On networks, the order parameter of the percolation transition is defined as the fraction of nodes belonging to the giant cluster.

2.1.1 Fortuin-Kasteleyn mapping to magnetic system

Fortuin and Kasteleyn had noted that solving the graph coloring or percolation problem of (2.2) is infact equivalent to solving a spin model [83–85]. Here, we start with the q-state

Potts Hamiltonian

$$H = -J \sum_{ij} (\delta_{\sigma_i,\sigma_j} - 1) \tag{2.4}$$

where $J > 0$ is the ferromagnetic coupling, and σ is the spin variable which can take q different values. Hence, Ising model is $q = 2$–state Potts model and Ashkin-Teller model is $q = 4$–state Potts model. The partition function is given by (see Appendix A)

$$Z = \sum_{\sigma} e^{-\beta H} = \sum_{\sigma} \prod_{\langle ij \rangle} \left((1-p) + p\delta_{\sigma_i,\sigma_j} \right) \tag{2.5}$$

with the summation over all spin configurations σ and with $p = 1 - \exp(-\beta J)$. By randomly distributing links with probability p between all pairs of nearest neighbor sites in the same spin state, the partition function Z is also written in the form [83–88]

$$Z = \sum_{n} \left[\prod_{\langle ij \rangle} p^{n_{ij}} (1-p)^{1-n_{ij}} q^{c(n)} \right]. \tag{2.6}$$

where the summation is over all link configurations n and $c(n)$ is the number of Fortuin-Kasteleyn clusters (see Appendix A). It is important to note in (2.6) that the spins of the system do not appear. The spin configurations had been one-to-one mapped to cluster configurations by connecting nearest neighbor spins of the same orientation. The partition function is given entirely in terms of link configurations. Now observe from the partition function (2.6) that the percolation problem (2.2) corresponds to the $q = 1$ limit of the Potts model. In the following section, we briefly review the continuous percolation phase transition and its critical phenomena.

2.1.2 Critical phenomena of the percolation phase transition

Near the transition point the cluster size distribution spans a broad range of values. The moments of the cluster size distribution thus contain singular parts which define the critical

exponents as follows.

$$\Big[\sum_s n_s\Big]_{sing.} \propto |p - p_c|^{2-\alpha} \tag{2.7}$$

$$\Big[\sum_s s n_s\Big]_{sing.} \propto (p - p_c)^{\beta} \tag{2.8}$$

$$\Big[\sum_s s^2 n_s\Big]_{sing.} \propto |p - p_c|^{-\gamma} \tag{2.9}$$

The cluster size distribution n_s is defined as the number of clusters of size s divided by the system size N. The zeroth moment (2.7) is analogous to number of magnetic domains, boundary of which had related to the total energy in the magnetic system. The order parameter $m(p)$ is defined as the fraction of nodes belonging to the giant cluster, which emerges at the percolation threshold p_c and thus it becomes the singular part in the total number of nodes (2.8). The order parameter relates to the total number of nodes in the finite clusters by the identity $\sum' s n_s = 1 - m$, where the primed summation goes over finite clusters. The second moment (2.9) is mean cluster size at which a randomly selected node belongs to. The mean finite cluster size diverges at the transition point, which is analogous to the magnetic susceptibility.

In case of a continuous percolation transition the order parameter exhibits critical behavior near the percolation threshold p_c as

$$m(p) = \begin{cases} 0 & p < p_c, \\ A(p - p_c)^{\beta} & p \geq p_c \end{cases} \tag{2.10}$$

in the thermodynamic limit $N \to \infty$. Here, β is the critical exponent of the order parameter and A is some constant. The susceptibility is defined as the mean finite cluster size

$$\chi_m \equiv \frac{\sum_s{}' s^2 n_s(p)}{\sum_s{}' s n_s(p)}. \tag{2.11}$$

Near the transition point, the size distribution of finite clusters behaves as

$$n_s(p) \sim s^{-\tau} e^{-s/s_c}, \tag{2.12}$$

where the characteristic cluster size s_c scales as

$$s_c \sim |p - p_c|^{-1/\sigma}. \tag{2.13}$$

Precisely at the transition point $p = p_c$, the size distribution of finite clusters follows a power law $n_s(p_c) \sim s^{-\tau}$. Thus the moments of n_s become

$$\sum_s{}' n_s \sim s_c^{1-\tau} \sim |p - p_c|^{(\tau-1)/\sigma}, \tag{2.14}$$

$$\sum_s{}' s n_s \sim s_c^{2-\tau} \sim (p - p_c)^{(\tau-2)/\sigma}, \tag{2.15}$$

$$\sum_s{}' s^2 n_s \sim s_c^{3-\tau} \sim |p - p_c|^{-(3-\tau)/\sigma}. \tag{2.16}$$

Hence, the susceptibility χ_m diverges for $2 < \tau < 3$. For the normalization condition of the total number of nodes $\tau > 2$ is required. The scaling relations are followed:

$$\beta = \frac{\tau - 2}{\sigma}, \tag{2.17}$$

$$\gamma = \frac{3 - \tau}{\sigma}. \tag{2.18}$$

The divergence of correlation length $\xi \sim |p - p_c|^{-\nu}$ is usually characterized by the critical exponent ν. The correlation length can be defined as the linear size of a typical cluster. $s_c \sim \xi^d \sim |p - p_c|^{-\bar{\nu}}$ where $\bar{\nu} \equiv d\nu$. Correspondingly, the total number of clusters in the system scales as $N/\xi^d \sim N(p - p_c)^{\bar{\nu}}$. The hyperscaling relations are followed:

$$\bar{\nu}\sigma = \tau - 1, \tag{2.19}$$

$$\alpha + 2\beta = \bar{\nu}. \tag{2.20}$$

2.2 Erdős–Rényi model

Now we discuss an analytically solvable random network model which exhibits a continuous percolation phase transition.

2.2.1 The original random network model

Erdős–Rényi (ER) model [80, 81] is a random network construction model. In the original model, there are initially N nodes and an edge is added between each possible pair of nodes with probability p. The expected number of links is $\langle L\rangle = N(N-1)p/2$. The degree distribution of the ER model follows from the standard combinatorics:

$$P(k) = \binom{N-1}{k} p^k (1-p)^{N-1-k} \tag{2.21}$$

where the degree k is number of edges attached to a node which ranges from 0 to $N-1$. For large $N \to \infty$ and fixed mean degree $\langle k\rangle = 2\langle L\rangle/N = (N-1)p$, the binomial distribution can be well approximated by the Poisson distribution.

$$P(k) \simeq \frac{e^{-\langle k\rangle}\langle k\rangle^k}{k!}. \tag{2.22}$$

Note the probability of obtaining a large degree node decreases rapidly with increasing k. Hence in the random network no hubs are present. In contrast, scale-free network with hub is characterized by a long tail in the degree distribution. In this model, a giant cluster emerges at the transition point $p_c = 1$ or $\langle k\rangle_c = 1$ [80] and its expected size increases continuously beyond the transition point. Precisely at the transition point, the giant cluster size is of order $O(N^{2/3})$ [89]. Beyond the transition point $p > p_c$ the giant size scales as $(p-p_c)N$, which is linearly proportional to the system size (see eq. (2.38)). A maximal giant size N is reached for dense connections beyond $p \simeq \log N/N$, because of the following reasoning. At some point we expect a single isolated node in the system. The proabability that a randomly selected node does not have connections to the giant cluster is $(1-p)^{N-1}$. Hence the expected number of

isolated nodes are $N(1-p)^{N-1} \approx Ne^{-Np} \approx 1$ which yields $p \approx \log N/N$, beyond this value of p the network becomes fully connected.

2.2.2 Random graph process

As an equivalent model, we can consider the random graph process [90], which adds an edge at a time between a pair of randomly chosen nodes if the edge is not already occupied. We define the normalized time as the link fraction $t \equiv L/N$. In the thermodynamic limit $N \to \infty$, the giant cluster emerges at $t_c = 1/2$ and grows its size continuously from zero beyond the transition point $m(t) \sim (t - t_c)^\beta$ with $\beta = 1$.

The Erdős–Rényi random graph process exhibits continuous phase transition. Here, the generating function approach by Newman et al. is followed [78, 91]. Suppose the probability distribution of vertex degrees k of a network is $P(k)$ and $G_0(x)$ is generating function of the degree distribution $P(k)$.

$$G_0(x) = \sum_{k=0}^{\infty} P(k)x^k. \tag{2.23}$$

Since a probability distribution is positive and normalized, absolute convergence of the generating function is gauranteed for any $|x| \leq 1$. The generating function generates the moments of the probability distribution. For example, the mean degree of the graph is a first-order derivative of $G_0(x)$.

$$\langle k \rangle = \sum_k kP(k) = G_0'(1). \tag{2.24}$$

The generating function approach can further yield the cluster size distribution during the random graph process. To obtain the sizes of the connected components, information is required on how a node is connected to other nodes on the graph. By recursively following consecutive connections from a node, size of the component which it belongs to can be tracked. In this regard, suppose an edge is randomly chosen and is followed to one end. Let $P_{NN}(k)$ be

the probability that the end node has k additional links ($k \geq 0$), other than the one that has been already chosen and followed. It is important to note that the degree distribution of an end node of a randomly chosen link $P_{NN}(k)$, i.e. the nearest neighbor degree distribution, is different from the degree distribution $P(k)$ [53]. For uncorrelated networks,

$$P_{NN}(k) = \frac{kN_k}{2L} = \frac{kP(k)}{\langle k \rangle} \tag{2.25}$$

The corresponding generating function is written as

$$G_1(x) = \sum_{k=0}^{\infty} P_{NN}(k)x^k = \sum_{k=1}^{\infty} \frac{kP(k)}{\langle k \rangle} x^{k-1} \tag{2.26}$$

The subscripts 0 and 1 in the generating function is used as mnemonics to denote the association to nodes and links, respectively. Combined use of G_0 and G_1, for example, yields the generating function of the next nearest neighbors $\sum_k P(k)[G_1(x)]^k = G_0\big(G_1(x)\big)$ and the average number of next nearest neighbors as

$$\langle k_{n.n.n.} \rangle = \frac{d}{dx} G_0\big(G_1(x)\big)\big|_{x=1} = G_0'(1)G_1'(1). \tag{2.27}$$

Now introduce the generating function $H_1(x)$ for the distribution of sizes of connected components following a randomly chosen edge. It satisfies a recursion relation, or a self-consistency equation.

$$H_1(x) = xP_{NN}(0) + xP_{NN}(1)H_1(x) + xP_{NN}(2)\left[H_1(x)\right]^2 + \cdots \tag{2.28}$$

$$= xG_1(H_1(x)). \tag{2.29}$$

Here, the power of x denotes the cluster size and the coefficient denotes the probability. The leading x^1 denotes the unit contribution made by the initial node to the node counting. This node at the end of a randomly chosen edge may or may not lead to extra connections. Instead of a link, if we start from a randomly chosen node, the generating function for the component

size the node belongs to is

$$H_0(x) = xG_0(H_1(x)). \tag{2.30}$$

In principle, given $G_0(x)$ and $G_1(x)$ we can solve for (2.29) and then substitute to (2.30) to obtain $H_0(x)$. For example, the average cluster size is

$$\langle s \rangle \stackrel{?}{=} \sum_{s=1}^{\infty} sP(s) = H_0'(1) = 1 + G_0'(1)H_1'(1), \tag{2.31}$$

where (2.29) gives $H_1'(1) = 1 + G_1'(1)H_1'(1)$ and hence

$$\langle s \rangle \stackrel{?}{=} 1 + \frac{G_0'(1)}{1 - G_1'(1)} = 1 + \frac{\langle k \rangle^2}{\langle k \rangle - \langle k_{n.n.n.} \rangle}. \tag{2.32}$$

This expression is ill-defined when $G_1'(1) = 1$, when the number of consecutive connections are critically branched $\langle k \rangle = \langle k_{n.n.n.} \rangle$; which marks the phase transition [77]. The giant component exists if and only if $\langle k_{n.n.n} \rangle > \langle k \rangle$. When the graph includes a giant cluster, normalization of the probability distribution $H_0(1)$ is no longer unity but

$$H_0(1) = 1 - m, \tag{2.33}$$

where m is the fraction of the nodes that are included in the giant cluster. The generating function $H_0(x)$ by definition generates the probability distribution of the size of "finite" clusters. Thus the correct expression of the mean cluster size (2.31), (2.32) requires a normalization factor

$$\langle s \rangle = \frac{\sum_{s=1}^{\infty} sP(s)}{\sum_{s=1}^{\infty} P(s)} = \frac{H_0'(1)}{H_0(1)}. \tag{2.34}$$

For Erdős–Rényi network which has Poissonian degree distribution (2.22), the corresponding generating functions G_0 and G_1 of the degree distribution $P(k)$ and nearest neighbor degree

distribution $P_{NN}(k) = kP(k)/\langle k\rangle$ are equal to

$$G(x) = e^{\langle k\rangle(x-1)}. \tag{2.35}$$

Self consistency equations (2.29) and (2.30) are identical in the Erdős–Rényi graph.

$$H(x) = xG(H(x)). \tag{2.36}$$

In turn, the giant size m satisfies the following self-consistency equation

$$m = 1 - e^{-\langle k\rangle m} \tag{2.37}$$

which has a trivial solution $m = 0$ and nontrivial solution(s) when $\langle k\rangle \geq 1$. The giant cluster emerges and continuously grows its size beyond the phase transition point $\langle k\rangle = \langle k\rangle_c = 1$. For a small m, series expansion of the above equation $m \approx \langle k\rangle m - \langle k\rangle^2 m^2/2! + \cdots$ yields

$$m \simeq \frac{2(\langle k\rangle - \langle k\rangle_c)}{\langle k\rangle^2} \sim \Delta^\beta \tag{2.38}$$

with $\Delta \equiv \langle k\rangle - \langle k\rangle_c$ and $\beta = 1$. The cluster size distribution $\mathcal{P}_s$ is formally written as

$$\mathcal{P}_s = [x^s]H(x) = \frac{1}{s!}\frac{d^s H(x)}{dx^s}\bigg|_{x=0} = \frac{1}{2\pi i}\oint \frac{H(z)}{z^{s+1}}dz. \tag{2.39}$$

where $H_0(x) = H_1(x) = H(x)$ for the Erdős–Rényi network. Using the eqs. (2.30), (2.29), and by applying the Cauchy formula several times an exact result is found.

$$\begin{aligned}
\mathcal{P}_s &= [x^s]H(x) = [x^{s-1}]\frac{H(x)}{x} && (2.40)\\
&= \frac{1}{(s-1)!}\left[\frac{d^{s-1}}{dx^{s-1}}G(H(x))\right]_{x=0} && (2.41)\\
&= \frac{1}{(s-1)!}\left[\frac{d^{s-2}}{dx^{s-2}}G'(H(x))H'(x)\right]_{x=0} && (2.42)\\
&= \frac{1}{2\pi i(s-1)}\oint \frac{G'(H(z))H'(z)}{z^{s-1}}dz && (2.43)
\end{aligned}$$

$$= \frac{1}{2\pi i(s-1)} \oint \frac{G'(h)}{(h/G(h)))^{s-1}} dh \tag{2.44}$$

$$= \frac{\langle k \rangle}{2\pi i(s-1)} \oint \frac{G(h)^s}{h^{s-1}} dh \tag{2.45}$$

$$= \frac{\langle k \rangle}{(s-1)!} \left[\frac{d^{s-2}}{dh^{s-2}} G(h)^s \right]_{h=0} \tag{2.46}$$

$$= \frac{(s\langle k \rangle)^{s-1} e^{-s\langle k \rangle}}{s!}. \tag{2.47}$$

Finally, near and at the critical point $\langle k \rangle = 1 + \Delta$, the distribution is obtained as

$$\mathcal{P}_s \simeq \frac{s^{-3/2}}{\sqrt{2\pi}\langle k \rangle} e^{-s\Delta^2/2} \tag{2.48}$$

after applying the Stirling's formula. The probability distribution follows a power law precisely at the critical point $\Delta = 0$. Near the critical point the probability distribution has an exponential cutoff which diverges as Δ approaches zero and

$$\mathcal{P}_s = s n_s \sim s^{1-\tau} e^{-s/s_*}, \tag{2.49}$$

$$s_* \sim |\Delta|^{-1/\sigma} \tag{2.50}$$

where n_s is the cluster size distribution and the critical exponents take the values $\tau = 5/2$ and $\sigma = 1/2$. Also, equation (2.34) yields the mean cluster size as [78]

$$\langle s \rangle = \frac{1}{1 - \langle k \rangle + \langle k \rangle m} \sim \frac{1}{|\Delta|}, \tag{2.51}$$

which gives the critical exponent $\gamma = 1$.

2.2.3 Random cluster aggregation process

In the ER random graph process, an added edge may connect two separate clusters (intercluster edge) or the edge may instead connect two nodes already in the same cluster (intracluster edge). The intercluster connections happen much more frequently than the intracluster con-

nections until the percolation threshold. For simplicity, a cluster aggregation process is considered, which ignores the detailed substructure of a cluster, but just keeps the information on the cluster sizes. In the thermodynamic limit $N \to \infty$, the random graph process and the random cluster aggregation process will result in the same transition point and exhibit the same the critical phenomena.

The random cluster aggregation process is described as follows. The system is initially composed of N monomers. At each time two clusters of size i and j are randomly chosen with probabilities proportional (multiplicative) to their sizes, and merged. The size of the resulting merged cluster is the sum of the sizes of the two clusters. The cluster aggregation process is described by a Smoluchowski equation [92] in terms of the density variables n_i as follows:

$$\frac{dn_s(t)}{dt} = \sum_{i,j} in_i jn_j \delta_{i+j,s} - 2sn_s. \tag{2.52}$$

where $n_i(t) \equiv N_i(t)/N$ is the density of size i clusters at time t and in_i is the probability of choosing a cluster of size i. The random cluster aggregation process is exactly solvable. With help of the generating function $G(z,t) = \sum_{s=1}^{\infty} sn_s(t)e^{zs}$, the above equation is written as

$$\frac{\partial G}{\partial t} = 2(G-1)\frac{\partial G}{\partial z}. \tag{2.53}$$

Using method of characteristics, we obtain $G(z,t) = H(z+2(G(z,t)-1)t)$ for an arbitrary initial condition $G(0,z) = H(z)$. For a monodisperse initial condition $G(0,z) = e^z$, the equation is written $Ge^{-2Gt} = e^{z-2t}$, which becomes in the form

$$X = Ye^{-Y} = f(Y) \tag{2.54}$$

with substitutions $X = 2te^{z-2t}, Y = 2Gt$. Using Lagrange inversion formula we obtain

$$[X^n]Y(X) = \frac{1}{2\pi i}\oint \frac{Y}{X^{n+1}}dX \tag{2.55}$$

$$= \frac{1}{2\pi i}\oint \frac{Y}{f(Y)^{n+1}}f'(Y)dY \tag{2.56}$$

$$= \frac{1}{2\pi i}\oint \frac{Y}{(Ye^{-Y})^{n+1}}(1-Y)e^{-Y}dY \tag{2.57}$$

$$= \frac{1}{2\pi i}\oint \sum_{k=1}^{\infty}\frac{n^k}{k!}(Y^{k-n} - Y^{k+1-n})dY \tag{2.58}$$

$$= \frac{n^{n-1}}{n!} \tag{2.59}$$

where $[X^n]Y(X)$ gives the n-th order series coefficient A_n of the series expansion $Y(X) = \sum_{n=1}^{\infty} A_n X^n$. Thus,

$$G(z,t) = \sum_{k=1}^{\infty}\frac{(2k)^{k-1}}{k!}t^{k-1}e^{-2kt}e^{zk}. \tag{2.60}$$

The order parameter $m(t) = 1 - G(0,t)$ satisfies the self-consistency equation

$$m(t) = 1 - e^{-2m(t)t} \tag{2.61}$$

which has a nontrivial solution emerging at $t_c = 1/2$ and with $\beta = 1$.

$$m(t) \sim 4(t - t_c) + O(t - t_c)^2. \tag{2.62}$$

Near the transition point $t_c = 1/2$, the cluster size distribution becomes

$$n_s(t) = [e^{zs}]G(z,t) = \frac{(2s)^{s-1}}{s!}t^{s-1}e^{-2st} \tag{2.63}$$

$$\approx \frac{(2s)^{s-2}}{\sqrt{2\pi s}}\left(\frac{e}{s}\right)^s e^{s\log t - 2st} \tag{2.64}$$

$$\sim \frac{e^{-2s(t-t_c)^2}}{4\sqrt{2\pi}s^{5/2}}, \quad \text{as } t \to t_c. \tag{2.65}$$

Therefore at the transition point of the random cluster aggregation model, the characteristic cluster size diverges $s_* \sim |t - t_c|^{-1/\sigma}$ where $\sigma = 1/2$ and the cluster size distribution obeys the power law $n_s(t_c) \sim s^{-\tau}$ with $\tau = 5/2$.

2.3 Search for a discontinuous percolation transition

Percolation transition is a robust continuous phase transition. Recently, researchers have raced for finding a discontinuous percolation model. One of the most notable variants of the Erdős–Rényi percolation model is the explosive percolation model, which adopts the Achlioptas rule [52,64,93–97]. At each step, two potential edges are randomly picked. Then, one of them is selected according to some rule and connected. The product rule chooses the edge which minimizes the product of the sizes. Sum rule chooses the edge which produces the smallest cluster [93]. Bohman-Frieze rule chooses the first one if it joins two isolated nodes, and the second one otherwise [98]. Such rules have also been further generalized to the so-called best-of-m rules. In common, such competitive selection rules delay the percolation transition and result an explosive increase of the order parameter. At first, the explosive percolation was claimed as a discontinuous transition [93]. However it has been revealed that the explosive increase of the order parameter in those models are actually continuous [64,95,96]. A rate equation study [95] has obtained a continuous transition with a nonzero critical exponent $\beta \approx 0.05$ of the order parameter. A number of numerical analyses and finite size scaling studies involving [96] also supported this result, but some careful methods were necessary in order to genuinely distinguish the explosive yet continuous transition from a truly discontinuous transition ($\beta = 0$). A rigorous argument was provided by the authors of [64], who proved that any rule based on a finite number of random candidates results a continuous transition. Once the relative number of nodes in large components reaches some constant fraction of the system, those clusters rapidly merge to form a giant component. Such a set of nodes were called as the powder keg to explosive increase of order parameter [99].

2.4 Hybrid percolation transition

The community was thrilled by the discovery of a discontinuous and also critical percolation transition, characterized by the singularity in the order parameter curve as in eq (1.1). The hybrid percolation transition may occur during cluster merging process or during pruning process, where characteristics and mechanisms of the two classes differ [54]. The hybrid percolation transitions induced by pruning processes [22, 34–36] have a universal description in the language of branching theory [46]. On the other hand, the hybrid percolation transitions induced by the cluster merging process [48–51] have a unique self-organization mechanism.

2.4.1 k-core percolation

k-core percolation with $k \geq 3$ is a hybrid phase transition induced by pruning process. k-core of a network is obtained after consecutive removal of all nodes with degree less than k. In a bootstrap percolation, initially, a fraction p of sites are randomly occupied, and then k-core of the occupied sites is obtained. The obtained size of the k-core is set as the order parameter. k-core percolation on a Bethe lattice with $k \geq 3$ shows a discontinuous transition together with a square-root singularity of the order parameter $\beta = 1/2$ [33]. Similar behavior was obtained from the k-core organization of a randomly damaged network [38, 39, 53]. Furthermore, strong critical fluctuations, a diverging correlation length at the transition point was noticed [37].

Let m_k be the size of the k-core giant and R be the probability that the given end of an edge is not connected to the giant cluster. The recursion relations are given as

$$m_k = p \sum_{q \geq k} P_d(q) \binom{q}{n} R^{q-n} (1-R)^n \tag{2.66}$$

$$R = (1-p) + p \sum_{n=0}^{k-2} \sum_{q=n+1}^{\infty} \frac{q P_d(q)}{\langle q \rangle} \binom{q-1}{n} R^{q-n-1} (1-R)^n, \quad k \geq 2 \tag{2.67}$$

Solving the self consistent R gives m_k. Notice that $R = 1$ is a trivial solution. With the

definition of [38]

$$f_k(R) \equiv \frac{1}{1-R}\left[1 - \sum_{n=0}^{k-2}\sum_{q=n+1}^{\infty} \frac{qP_d(q)}{\langle q\rangle}\binom{q-1}{n} R^{q-n-1}(1-R)^n\right] \tag{2.68}$$

$$= \frac{1}{1-R}\left[1 - \sum_{n=0}^{k-2} \frac{(1-R)^n}{n!}\frac{d^n G_1(R)}{dR^n}\right] \tag{2.69}$$

and the generating function $G_1(x)$ as (2.26), the self consistency equation is compactly written as $pf_k(R) = 1$. Noting $f_k(R) \to 0$ as $R \to 1$ and $0 < f_k(0) < 1$, a nontrivial $0 \le R < 1$ solution first appears at the maximum of $f_k(R)$, i.e. at some R_0 where $f_k'(R_0) = 0$, or at $R = 0$. Usually a saddle node bifurcation with a stable solution $R_0 - R \sim (p - p_c)^{1/2}$ occurs. Also, the square-root critical singularity $m_k - m_{k0} \sim (p - p_c)^{\beta},\ \beta = 1/2$ is yielded [33,38,39]. In contrast to ordinary percolation, the emergence of $(k \ge 3)$-cores does not associate to the divergence of finite clusters. Instead, divergence in the size of corona cluster was noticed as the associated critical phenomenon [37]. A k-core's corona is defined as a subset of nodes in the k-core having exactly k nearest neighbors in the k-core, which is the minimum possible number of connections. The mean total size of corona clusters N_{crn} diverges at the k-core transition point

$$N_{crn}(p) \sim (p - p_c)^{-1/2} \tag{2.70}$$

Thus in the k-core percolation, size of corona cluster plays the role of susceptibility. The corresponding exponent $\gamma = 1/2$ is clearly different from that of the ordinary percolation transition.

2.4.2 Hybrid percolation transition induced by pruning process

A universal mechanism in k-core percolation, cascade failure, and generalized epidemic spreading models One class of hybrid percolation transition is induced by pruning processes. The examples include cascade of failures on interdependent networks [22,34], k-core percolation [35, 36] and generalized epidemic spreadings [40, 41, 43, 44]. In those systems,

failure of one node by its removal (or by pruning of a link) may lead to a recursive failure of other nodes. Depending on whether this recursion terminates after several rounds or it long lasts, the failures may remain localized or spread systemwide. The pruning process causes a continuous decrease of order parameter above the transition point, while the same process causes a discontinuous drop of order parameter for the system at the transition point. Such a qualitative difference in the progression of a cascade can be rephrased into mathematical terms by using the theory of branching process. A subcritical branching has a branching ratio less than unity, which means that the number of offsprings in the next generation is lesser than the number of current generation. Thus the subcritical branching process by nature has to cease after some rounds. On the other hand, critical branching has a mean offspring equal to unity, which can thus long last. Supercritical branching, with mean branching ratio greater than unity, exhibits an explosive growth in populations. Removal of a node from the giant cluster triggers an avalanche which can be viewed as a branching process. The cascade process of the hybrid percolation models induced by pruning process corresponds to a critical (subcritical) branching at (above) the transition point. At the transition point, an avalanche can be either finite (localized) or infinite (systemwide). At the hybrid transition point, a single infinite avalanche which undergoes an initial period characterized by a critical branching eventually follows a supercritical branching after a crossover time of $O(N^{1/3})$ [46]. Such a crossover is not only noticed in the cascade failure model, but also noticed universally in the k-core percolation and in the generalized epidemic spreading models [46]. Finite avalanches at the hybrid transition point, on the other hand, follows a power-law probability distribution.

In the generalized epidemic spreading model proposed by Janssen and Stenull [40], each node takes one of the four states: susceptible (S), weakened (W), infected (I) and recovered (R). In addition to the single-step infection and recovery processes $S+I \to I+I$ and $I \to R$, two-step contagion process via the weakened state is possible, by the second encounter of an infected node, i.e. $S + I \to W + I$ and $W + I \to I + I$. Recall now that precisely at the percolation transition of the Erdős–Rényi random graph, the giant cluster is of size $O(N^{2/3})$ and its connection topology is largely tree-like which has a depth of $O(N^{1/3})$ [89]. A period

of critical branching which is characterized by the balance of infection and recovery processes persists only up to $O(N^{1/3})$ steps. The density of infectious nodes is maintained, but the weakened nodes steadily accumulate. The golden time to prevent the potential pandemics is until then. Recall also that the giant cluster has a large loop beyond this depth because of the finite size of the network. So beyond the $O(N^{1/3})$ time, such a long range loop channel becomes effective and it will connect the infectious node front to the weakened nodes fallen behind. In turn, the net infection suddenly becomes supercritical, causing an explosive jump of the order parameter [46].

Avalanche processes in the k-core percolation and cascade failure of interdependent networks can be understood in a similar context. At the transition point, the avalanche process may be infinite or finite, each of which contributes to discontinuous aspect or critical aspect of the hybrid phase transition, respectively. In the k-core, say, deletion of a single node i leads to a macroscopic avalanche of orders of system size. This node i corresponds to the initial infectious seed I. At the next time step, any neighbor of the node i with exactly k neighbors are deleted, or infected in the language of the epidemic spreadings. Therefore, the nodes in the corona cluster are analogous to the susceptibles S, which are potentially destructible in the next time step if it encounters an infected neighbor. A core node initially with a number of neighbors greater than k is weakened and eventually becomes fallen down (infected) by two or more successive infections.

An interdependent network can be equivalently represented by a single layer network with two types of links [47]. A collective well-functioning of two or more layers of interdependent networks requires well-functioning at each layer, e.g. internet and electricity. Here, a necessary concept is mutual percolation [22]. More specifically, the collective functionality is characterized by mutually connected component, in which every pair of nodes are connected following each type of link. Removal of a single node (together with its attached links) can trigger a cascade of failures. Again this node corresponds to the infectious node I. The vulnerable nodes correspond to susceptibles S. An effective degree is defined as the number of links which leads to the giant mutually connected cluster, which is decreased (weakened)

throughout the cascade dynamics. See Ref. [46] for more details.

2.4.3 Hybrid percolation transition induced by cluster merging process

The other class of hybrid percolation transition is induced by cluster merging. Examples include the restricted Erdős–Rényi model [48, 49, 51] and restricted model on two dimensional lattice [50]. Restricted percolation involves a cluster merging process in contrast to the pruning processes of the previous subsection. The restricted percolation models has a restriction parameter $0 < g < 1$. The restriction–free limit ($g \to 1$) reduces the model to the Erdős–Rényi model which exhibits a second order percolation transition at $t_c = 1/2$. Its g-dependent rule regulates growth of large clusters and postpones the percolation transition to a later time $t_c(g) > 1/2$. Resulting transition is discontinuous, in contrast to explosive percolations. The size distribution of finite clusters follows a power law with a g–dependent exponent $2 < \tau(g) < 5/2$. In the following section, the restricted Erdős-Rényi model is discussed in detail.

2.4.4 Restricted Erdős–Rényi model

The restricted Erdős–Rényi model initially ($t = 0$) consists of N isolated nodes. An edge will be added one by one under a certain rule. The time step $t \equiv L/N$ is defined as the total number of edges added per system size. The rule is as follows: The system is divided into two mutually exclusive subsets A and B which have capacity of gN and $(1 - g)N$ nodes. The clusters are sorted by their sizes, where equal sizes are sorted in random order. A (B) is filled maximally to its capacity with the smallest (largest) clusters, avoiding an overfill. Then, if there is a leftover cluster which can neither totally belong to A or B, it is regarded as being in A. Next, select one node from the entire system and the other node from A, and connect the two nodes by an edge unless they are already connected. This process is iterated.

Note the node selection procedure in the two sets is biased. While the nodes in set B has given only the first chance to be selected, the nodes in set A has also been given a second chance. In turn, growth of the large size clusters in set B is globally suppressed. Only the

first two processes are allowed:

$$A + A \to A \text{ or } B \qquad \text{(allowed)}$$

$$A + B \to B \qquad \text{(allowed)}$$

$$B + B \not\to B \qquad \text{(suppressed)}$$

Notice that restricted percolation process involves a systemwide sorting in the A/B classification at every step, and such a suppression rule utilizes a global information on cluster sizes in the system, in contrast to the Achlioptas rules [64]. The order parameter jump of the restricted Erdős–Rényi model is discontinuous, showing a diverging slope in the thermodynamic limit $N \to \infty$ [48]. Moreover, the finite cluster size distribution reaches a power law at the critical point after the order parameter jump [49]. The restricted Erdős–Rényi model is a cluster merging process which exhibits a hybrid phase transition.

Critical exponents are obtained by solving the Smoluchowski rate equation, a mean-field description on the evolution of cluster size distribution $n_s(t)$. It has been found that the critical exponent τ of the finite size cluster distribution and the critical exponent β of the order parameter are continuously varied by the restriction parameter g [49]. The Smoluchowski equation of the restricted Erdős–Rényi model is written as follows.

$$\frac{dn_s}{dt} = \sum_{i+j=k} \frac{in_i jn_j}{g} - \left(1 + \frac{1}{g}\right) kn_s, \quad \text{for } s < s_A \tag{2.71}$$

$$\frac{dn_s}{dt} = \sum_{i+j=k} \frac{in_i jn_j}{g} - kn_s - \left(1 - \sum_{i=1}^{s_A-1} \frac{in_i}{g}\right), \quad \text{for } s = s_A \tag{2.72}$$

$$\frac{dn_s}{dt} = \sum_j \delta_{i+j,k} jn_j \sum_{i=1}^{s_A-1} \frac{in_i}{g} + \sum_j \delta_{s_A+j,k} jn_j \left(1 - \sum_{i=1}^{s_A-1} \frac{in_i}{g}\right) - kn_s, \quad \text{for } s > s_A, \tag{2.73}$$

where $s_A(t)$ is the size of the largest cluster in set A at time t.

It is hard to solve the rate equation exactly at all orders. However, one can instead solve

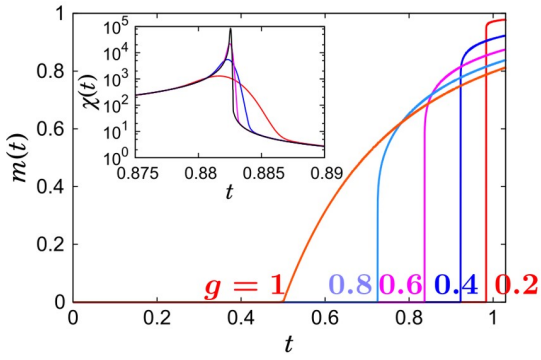

$$m(t) = m_c + a(t - t_c)^{\beta}$$

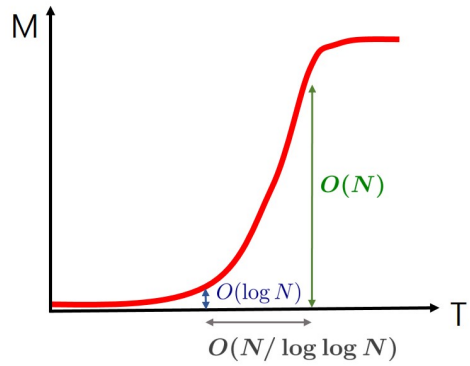

$$\frac{\Delta M}{\Delta T} \to \infty, \text{ as } N \to \infty$$

Figure 2.1: (a) The restricted Erdős–Rényi model consists of two sets which contains gN and $(1-g)N$ nodes belonging to smallest and largest clusters, and which are under normal and suppressed growth, respectively. It exhibits a jump transition, with the suppresion paramter $0 < g < 1$. When $g = 1$, there is only a single set and this model reduces to the Erdős–Rényi model which exhibits a continuous phase transition at $t_c = 0.5$. As g is decreased down to zero, the large cluster set under growth suppresion increases. In turn, the transition $t_c(g)$ is delayed. The figure is from Ref. [49] (b) A schematic figure which explains the nature of transition. At each step, clusters are divided into two sets based on their size ranks. So the model involves a global sorting process which possibly leads to a discontinuous jump of the order parameter characterized by an infinite slope, which has been prooved analytically in Ref. [48].

the rate equation for monomers to obtain $n_1(t)$ and utilize the fact that n_s follows power law at t_c [49]. Given the order parameter jump size $m_0(g)$, the critical exponent $\tau(g)$ of the cluster size distribution is obtained.

$$\dot{n}_1 = \begin{cases} -n_1 - 1, & S_R = 1 \\ -\left(1 + \frac{1}{g}\right) n_1, & S_R \geq 2 \end{cases} \tag{2.74}$$

with initial condition $n_1(0) = 1$. $S_R = 2$ is reached at $t = g$. Assuming $n_s(t_c) = As^{-\tau}$, we

find

$$\sum_s n_s(t_c) = 1 - t_c = A\zeta(\tau) \tag{2.75}$$

$$\sum_s s n_s(t_c) = 1 - m_0 = A\zeta(\tau - 1) \tag{2.76}$$

and hence

$$\frac{\zeta(\tau)}{\zeta(\tau-1)} = \frac{1-t_c}{1-m_0} = \frac{1}{1-m_0}\left(1 - \log\left[\left(\frac{g\zeta(\tau-1)}{1-m_0}\right)^{\frac{g}{1+g}} \frac{2}{g+1}\right]\right). \tag{2.77}$$

Having provided a numerically obtained value of $m_0(g)$, the exponent $\tau(g)$ is obtained by self-consistent solving of the equation (2.77).

Beyond the transition point t_c, size of the giant cluster exceeds the capacity of B. According to the rule, all clusters including the giant cluster are in A (or regarded as being in A), and hence B is emptied. In turn the growth "restriction" is evaded. So the restricted Erdős–Rényi process in the supercritical regime is effectively identical to an Erdős–Rényi process. Nevertheless, this does not necessarily imply that the critical phenomena of the restricted model is identical to those of the ordinary Erdős–Rényi model, because of the presence of a giant much larger than that of a continuous transition. However, the size distribution of finite size clusters follows the scaling form of the Erdős–Rényi model $sn_s(t-t_c) = s^{1-\tau} f(s(t-t_c)^{1/\sigma})$, where $f(x)$ is a scaling function which is analytic. $\sigma(g) = 1$ is obtained in the supercritical regime of the restricted Erdős–Rényi model regardless of the restriction parameter g [49], in stark constrast to the $\sigma = 1/2$ of the ordinary Erdős–Rényi model. This is because the giant cluster size m_0 at the critical point differs significantly in the two models. The restricted model giant attaches leftover finite clusters much more quickly compared to the ordinary model giants. At $t > t_c$, the order parameter $m(t)$ increases continuously after the jump transition.

With the definition of the generating function $H(z,t) \equiv 1 - \sum_s' s n_s(t) e^{-zs}$, notice

$$\dot{H} = 2H\frac{\partial H}{\partial z}, \quad H(z,t_c) = 1 - \sum_s' A s^{1-\tau} e^{-zs} \tag{2.78}$$

$$H(z,t) = 1 - \sum_s' A s^{1-\tau} e^{-(z+2H(z,t)(t-t_c))s} \tag{2.79}$$

and at an *ad hoc* time $\epsilon \equiv t - t_c$ the order parameter is self-consistently written as

$$m(\epsilon) = H(2\epsilon m(\epsilon)). \tag{2.80}$$

At the transition point $\epsilon = 0$,

$$m = 1 - A\zeta(\tau - 1) = m_0. \tag{2.81}$$

Now for the hybrid phase transition $m(\epsilon) = m_0 + r\epsilon^\beta$, we obtain

$$\beta = \tau - 2 \tag{2.82}$$

$$r = \frac{1 - m_0}{\zeta(\tau - 1)} \frac{\Gamma(3-\tau)}{\tau - 2} (2m_0)^{\tau - 2}. \tag{2.83}$$

In contrary if we had used $m(\epsilon) = re^\beta$, relevant to the continuous phase transition $m_0 = 0$, we would have obtained a different $\beta = (\tau - 2)/(3 - \tau)$. The suceptibility, or the second moment of the finite cluster size distribuiton diverges at the supercritical side

$$\chi^+(\epsilon) = \sum_s' s^2 n_s(t) = H'(0,t) \tag{2.84}$$

$$= H(2m\epsilon, t_c)\left(1 + 2\epsilon H'(0,t)\right) \tag{2.85}$$

$$= \frac{H(2m\epsilon, t_c)}{1 - 2\epsilon H(2m\epsilon, t_c)} \tag{2.86}$$

$$= \frac{A\Gamma(3-\tau)(2m\epsilon)^{\tau-3}}{1 - 2A\epsilon\Gamma(3-\tau)(2m\epsilon)^{\tau-3}} \sim \epsilon^{\tau-3}, \tag{2.87}$$

where $H' = \partial H/\partial z$ and the critical exponent of the mean cluster size is $\gamma = 3 - \tau$.

2.4.5 Two diverging length scales of the hybrid percolation transition

Non-self-averaging order parameters were noticed at the hyrid critical point of the k-core percolation [45] and in the restricted percolation [50]. At the hybrid percolation transition point, the sample-to-sample fluctuations of the order parameter $\chi = N(\langle m^2 \rangle - \langle m \rangle^2)$ is wide and it does not vanish even in the thermodynamic limit. In specific, the order parameter distribution is non-gaussian [50]. It yields a critical exponent γ_m which is different from the critical exponent γ_s (or γ_a) obtained from the finite cluster (or avalanche) size distribution. Meanwhile, the hyperscaling relations $2\beta_m + \gamma_m = \bar{\nu}_m$ and $(\tau_s - 1)/\sigma_s = \bar{\nu}_s$ independently hold for sets of exponents related to giant and finite clusters, respectively. Therefore the restricted percolation has two diverging length scales characterized by two different critical exponents $\bar{\nu}_m \neq \bar{\nu}_s$. In contrast, the ordinary percolation had only a single diverging length scale characterized by the critical exponent ν.

Why are there two different exponents in restricted percolation, in contrast to the ordinary percolation? It was further noticed in the two dimensional restricted percolation that the giant cluster at the transition point is very compact, with volume fractal dimension equal to the system's dimensionality [50]. Usually in ordinary percolations, the giant cluster is a fractal, which is characterized by the fractal dimension $d_f = d - \beta/\nu$. However, in the case of restricted 2D model, $d_f \approx d$ and it seems that the effect of discontinuity $\beta = 0, \bar{\nu} = 1, d_f = d$ [100] has already dominated over the effect of the hybrid critical exponent β. Ordinary percolations with a single diverging length scale can be mapped to the $q \to 1$ limit of the q-state Potts spin model [83]. Thus its critical behavior is systematically well understood using the renormalization group theory, where the scaling ansatz is given as $f(t, h) = \ell^{-d} f(\ell^{1/\nu} t, \ell^{d_f} h)$. In the restricted percolation, however, there are two diverging length scales. Also, the finite size clusters are fractal-like in the sense that they show a power-law size distribution, whilst the giant cluster is compact. Hence it is yet unclear how to coarse-grain clusters near the transition point of restricted percolation [45].

It is also remarked that in the cascade class hybrid percolation transition induced by avalanche dynamics, there is an intrinsic scaling relation between the critical exponent γ_a

of mean finite avalanche size and the critical exponent β of the order parameter as $\gamma_a = 1 - \beta_m$ [45]. An analogous scaling relation $\gamma_s = 1 - \beta_m$ holds in the restricted Erdős–Rényi model where $\sigma_s = 1$. However, this relation no longer holds in the low dimensions [46]. On the other hand, in the merging class hybrid percolation transition, three distinct periods are noticed in the subcritical regime: before and after the emergence of a giant cluster, where a powder-keg bump develops and shrinks in the cluster size distribution, and a short period of time very near the critical point, where the restricted process reduces to the Erdős–Renyi process and the cluster size distribution tidy up into a power law. Distinct dynamic organization in the pre-giant and post-giant periods are also noticeable from the interevent time distributions, which obtains two distinct power-law exponents α and α' [51]. Remarkably, $\{\alpha, \alpha'\}$ are directly related to $\{\sigma_s, \tau_s\}$ by two scaling relations, hence they also determine the critical exponents $\{\beta_m, \gamma_s\}$. This matter is discussed in the following section.

Chapter 3

Inter-event time, burst and hybrid percolation transition

Understanding the hybrid percolation transitions induced by cluster coalescence, how the giant cluster reaches a diverging growth rate and how finite clusters reach a power law, is fundamental and intriguing. Here, we uncover the underlying mechanism using the restricted random network model, in which clusters are ranked by size and partitioned into small- and large-cluster sets. As clusters are merged and their rankings are updated, they may move back and forth across the set boundary. The intervals of these crossings exhibit a self-organized critical behavior with two power-law exponents. During this process, a bump is formed and eliminated in the cluster size distribution, resulting a jump of order parameter and organizing a power-law distribution at the critical point. This self-organized critical behavior of the merging class hybrid percolation transition is in contrast to the critical branching process, which governs the avalanche dynamics of the pruning class hybrid percolation transition. Also, the burst of set crossing events near the transition is a warning signal to an upcoming abrupt transition.

3.1 Introduction

Complex systems composed of a large number of interacting components are constantly adapting to the changing environment and sometimes reach critical states [101, 102]. In these states, complex systems may be statistically characterized by power-law distributions [2, 103]. Examples include the number of aftershocks per time step after the main earthquake [104],

nonstationary relaxation after a financial crash [105], the number of fires with a certain area per time step as a function of the area in forest fires [106, 107], and the interevent time distribution in human activities [108]. Such critical phenomena occur in a self-organized manner, but a single framework describing their underlying mechanisms has not yet been established [103,109,110]. In contrast, in critical states of complex systems, a small external perturbation imposed on a system can lead to widespread failure of the system through avalanche dynamics [2]. Examples include blackouts in electric power-grid systems [111–113] and firing in neuronal networks [114, 115] in real-world systems, and k-core percolation [33, 35, 36] and disease contagion models [40,41,43,44] in artificial model systems. In such cascade dynamics, the avalanche sizes of different events form a power-law distribution. These behaviors have been explained by a universal mechanism (the critical branching process), which was also observed in self-organized criticality in the Bak–Tang–Wiesenfeld model [116, 118].

Avalanche dynamics can be clearly observed in k-core percolation. The k core of a network is a subgraph, in which degree of each node is at least k. To obtain a k-core subgraph, once an Erdős–Rényi random network composed of N nodes having links between two nodes with probability p is generated in the supercritical regime, all nodes with degrees less than k are deleted consecutively until no more nodes with degrees less than k remain in the system. The number of nodes deleted during these consecutive pruning processes is considered as the avalanche size. The fraction of nodes remaining in the largest k-core subgraph is defined as the order parameter m, which decreases continuously with decreasing p at criticality. When p is chosen as a transition point p_c, the deletion of a node from an Erdős–Rényi network can lead to collapse of the giant k-core subgraph. Thus, a hybrid percolation transition occurs, which exhibits features of first-order and second-order phase transitions. The avalanche size distribution shows power-law decay as $P_a(s) \sim s^{-\tau_a}$, where $\tau_a = 3/2$ at p_c, similar to that in the Bak–Tang–Wiesenfeld model. Furthermore, there exists a critical avalanche of size $O(N)$, which may correspond to the dragon king often noted in complex systems [103, 119].

In contrast to the hybrid percolation transitions induced by cascading dynamics, hybrid percolation transitions in cluster merging dynamics have received little attention. Here, we

aim to investigate the underlying mechanism of the hybrid percolation transition on a microscopic scale using the restricted Erdős–Rényi network [48, 49]. Then, we set up a theory of the hybrid percolation transition. The model contains a factor that suppresses the growth of large clusters. Accordingly, the type of percolation transition is changed to a discontinuous transition [64], similar to the case in which the $1/r^2$-type long-range interaction changes the transition type to the first-order type in the one-dimensional Ising model [23]. However, this factor alone does not guarantee the occurrence of critical behavior. Here, we uncover underlying mechanism and find a self-organized criticality which determines the critical behavior of the hybrid percolation transition induced by the cluster merging dynamics.

The cluster merging dynamics of the restricted Erdős–Rényi model proceeds in a dichotomous and asymmetric way. Initially, there are N isolated nodes. Clusters are formed as links are connected one-by-one between pairs of unconnected nodes under the rule given below. Clusters are ranked by size and classified into two sets, A and B, which contain a portion gN ($0 < g \leq 1$) of nodes of the smallest clusters and the remaining large clusters, respectively. Two nodes are selected for connection as follows. One node is chosen randomly from set A, and the other is chosen from among all the nodes. They are connected by a link unless they are already connected. Then the classification is updated as the cluster rankings are changed. Time is defined as $t = L/N$, where L is the number of occupied links, and it is the control parameter of the restricted Erdős–Rényi model. This quantity differs from p in k-core percolation in the point that the cluster merging dynamics at a certain time t_1 successively follows the dynamics of previous times, whereas the avalanche dynamics at a certain p_1 may be independent of those at any previous $p > p_1$.

The nodes in set A have twice the opportunity to be linked compared to the nodes in set B; small clusters in set A grow rapidly, and the resulting large clusters may move to B, whereas the smallest clusters among the clusters in set B that have never grown or are growing slowly are evicted to A. Accordingly, cluster coalescence occurs in a dichotomous way, and the growth of large clusters is practically suppressed. The effective suppression becomes global as the portion of the smallest clusters is selected from among clusters of all

sizes. This factor leads to a discontinuous percolation transition.

3.2 Results

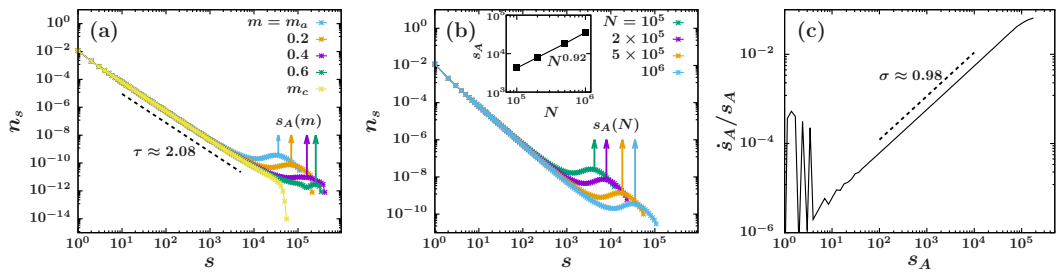

Figure 3.1: (a) Cluster size distributions n_s, which is controlled by the corresponding cluster size cutoff m, at various times. s_A is located around the peak position of the bump for each time. $g = 0.2$ and $N = 10^6$. (b) System size dependence of n_s at m_a. The mean s_A grows with the system size N. Inset: $s_A(m_a)$ depends on N as $\sim N^{0.92}$. (c) To determine the exponent σ' of $s_A(t) \sim (t_g - t)^{-1/\sigma'}$, we plot $\dot{s}_A/s_A$ versus s_A. $\sigma' \approx 0.98$ is obtained. Ensemble average is taken over 10^5 configurations.

We first consider cluster evolution on a macroscopic scale. In the early time regime, the order parameter $m(t)$ (the fraction of nodes belonging to the giant cluster) is $o(N)$, and the cluster size distribution $n_s(t)$ exhibits power-law decay in the small-cluster region, but exponential decay in the large-cluster region. As time proceeds, medium-size clusters accumulate and form a bump in the cluster size distribution $n_s(t)$, as shown in Fig. 3.1(a). Technically, we trace m instead of t in simulations to reduce large sample fluctuations arising around the transition point of the hybrid percolation transition. We estimate a characteristic time t_a, around which a giant cluster of size $m_a N \sim O(N)$ emerges and the bump size becomes maximum. m_a denotes $m(t_a)$. Soon after that, $m(t)$ increases rapidly, as shown in Fig. 3.2(a). t_a is estimated numerically as the intercept of the t-axis and the tangential line of $m(t)$ at the inflection point. m_a is the determined as $m(t_a)$. At t_g, the order parameter $m(t_g)$ (denoted as m_g) is equal to $1 - g$. This means that set B is occupied by the giant cluster alone. Beyond t_g, the giant cluster size exceeds the capacity of set B. In this case, the giant cluster is regarded as belonging to set A, along with all the other clusters [49]. The boundary between

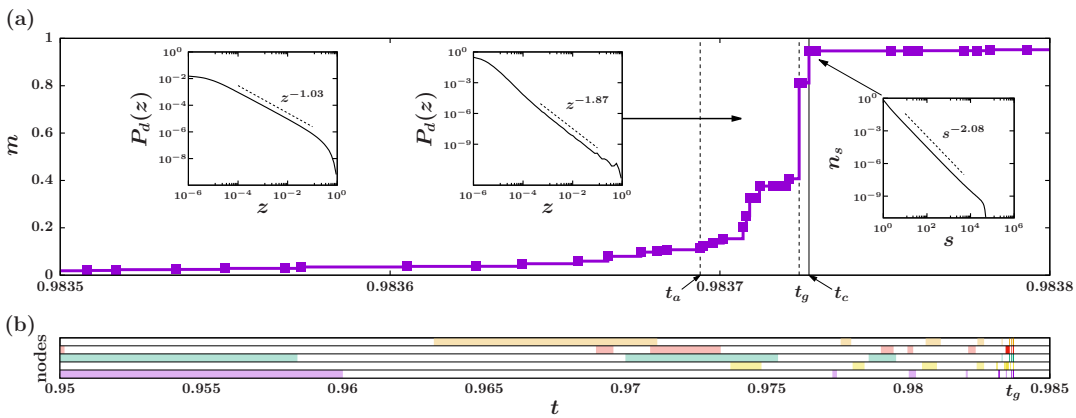

Figure 3.2: Evolution of the giant cluster, interevent time, and burst: (a) Typical staircase growth of the largest cluster size per node $m(t)$ for $g = 0.2$. The giant cluster of size $O(N)$ forms at time t_a and grows rapidly. Soon afterwards, at t_g, it completely fills set B. Subsequently, the system follows Erdős–Rényi dynamics and reaches a transition point t_c, at which $n_s(t_c) \sim s^{-\tau}$ (right inset) for finite clusters. The interevent time distributions $P_d(z)$ are accumulated in the intervals $[0, t_a]$ (left) and $[t_a, t_g]$ (middle), respectively. They exhibit power-law decays with the exponents $\alpha \approx 1.03$ and 1.87, respectively. (b) A succession of inter-set A (colored) $\leftrightarrow$ B (white) switching events demonstrate the bursty nature of this heavy-tailed process.

the two sets is eliminated. Note that this rule was not clearly specified in the original half-restricted model [48]; however, this rule is necessary to reach a critical state at t_c. Therefore, the restricted Erdős–Rényi model reduces to the original Erdős–Rényi model but with the $n_s(t_g)$ of finite clusters and the giant cluster [49]. As time proceeds further to a transition point t_c, the bump disappears completely, and the size distribution of finite clusters n_s exhibits a power-law decay, $n_s(t_c) \sim s^{-\tau}$ (Fig. 3.2(a)), where $\tau(g)$ varies continuously with the parameter g [49]. The order parameter at t_c is denoted as m_c. The interval $[t_a, t_c]$ has been revealed to be $o(1)$ [48]. Therefore, the order parameter is regarded as discontinuous at t_c in the limit $N \to \infty$. For $t > t_c$, the order parameter increases continuously with the critical behavior, $m(t) - m_c \sim (t - t_c)^{\beta}$. A hybrid transition occurs in the order parameter. We divide the time interval $[0, t_g]$ into two windows. In $[0, t_a]$, n_s exhibits power-law decay with an extra bump, whereas during $[t_a, t_g]$, the bump shrinks, and the giant cluster grows drastically. These behaviors clearly indicate that these two intervals need to be considered separately.

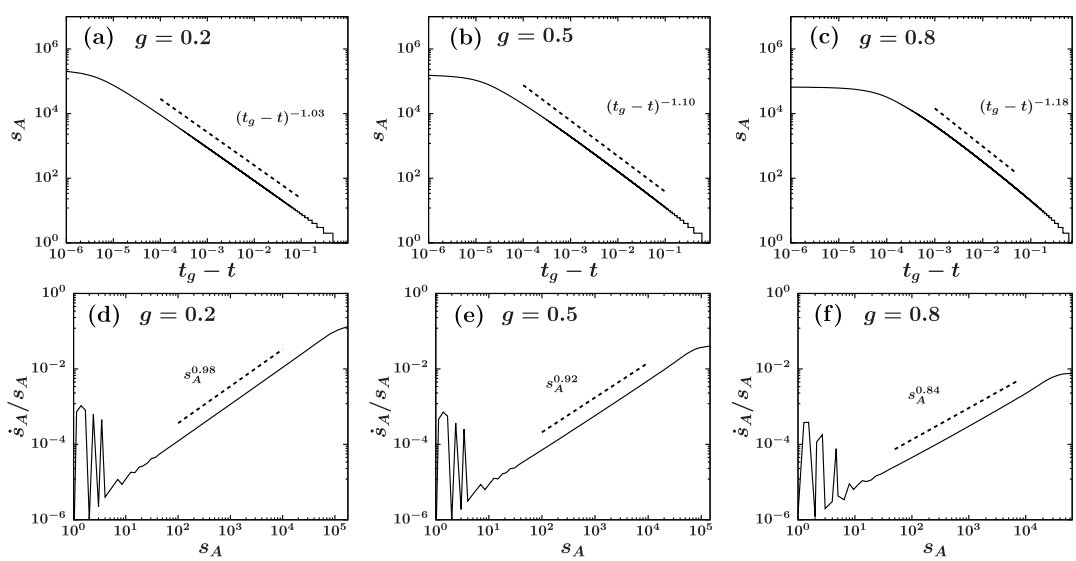

Figure 3.3: (a−c) Dynamic scaling of $s_A \sim (t_g - t)^{-1/\sigma'}$ for different g values. (d−f) $\dot{s}_A/s_A$ versus s_A. The curves were averaged over 10^5 configurations.

Next, we consider cluster evolution microscopically. We check the evolution of the largest

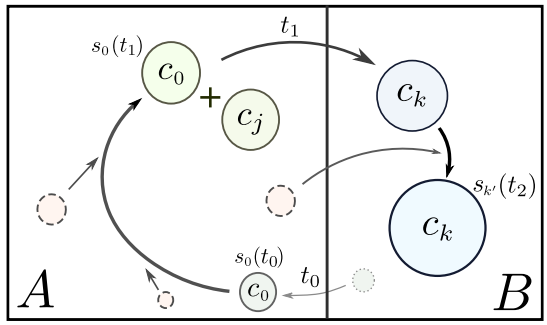

Figure 3.4: Schematic diagram of a typical cluster lifecycle: A cluster is born with size s_0 and grows through coalescence. Each node of a cluster may have a different age (time since its birth). After sufficient growth in set A, a cluster is transferred to set B, where its growth is limited.

cluster size among all the clusters in set A, denoted as $s_A(t)$. We find empirically that $s_A \sim (t_g - t)^{-1/\sigma'}$ for $t \in [0, t_a]$, which is analogous to the relationship used in conventional percolation theory. We measure the exponent σ' directly using the relation $\dot{s}_A/s_A \sim s_A^{\sigma'}$ (Fig. 3.1(c)), where the dot over s_A represents the time derivative. The exponent $\sigma'(g)$ is almost one for $g = 0.2$ but decreases slowly with increasing g, as shown in Fig. 3.3. Note that the value of σ' differs from σ, which is conventionally defined for the characteristic cluster size in the supercritical regime, where $\sigma = 1$ independent of g [49]. Interestingly, $s_A(t)$ is located around the peak position of the bump in $n_s(t)$ for different t but is implemented using the corresponding m value, as shown in Fig. 3.1(a). This behavior appears for different system sizes, as shown in Fig. 3.1(b). The peak at s_A implies that clusters with sizes similar to $s_A(t)$ are abundant in the system although the bump shrinks as t increases beyond t_a.

More specifically, we consider how a cluster c_i of size s_i evolves during the bump formation period $[0, t_a]$. A schematic illustration is presented in Fig. 3.4.

i) Suppose a cluster c_0 is evicted from set B to A at time t_0. If $t_0 = 1$, cluster c_0 has size $s_0 = 1$ in set A. Next, c_0 is merged with other clusters and grows, but it is still small enough that it does not move to B.

ii) Until time t_1, cluster c_0 grows and has size $s_0(t_1)$. At time t_1, cluster coalescence occurs as $c_0 + c_j \to c_k$, and the cluster size changes as $s_k = s_0(t_1) + s_j$, where cluster

c_j is in either set A or set B. We consider the case that the cluster size s_k becomes larger than $s_A(t_1)$, and thus cluster c_k moves to B.

iii) Cluster c_k grows slowly to the size $s_{k'}$ in set B until time t_2. If the size $s_{k'}$ becomes smaller than $s_A(t_2)$ for the first time, then cluster c_k is evicted to A. Then the evolution returns to step i).

This cycle is a prototypical pattern of cluster evolution up to the time t_a. During this cycle, small clusters (e.g., c_0) in set A have more opportunities to grow, whereas the growth of large clusters in set B (e.g., c_k) is suppressed. Accordingly, clusters of medium size become abundant and form a bump around $s_A(t)$, as shown in Fig. 3.1(a).

During the interval $t_a < t < t_g$, a non-negligible amount of cluster coalescence occurs between a large cluster in set A and another large cluster in set A or the giant cluster in set B. In this case, step iii) must also include the following event.

iii′) Cluster c_k of size $s_{k'}$ grows further by merging with clusters in set A, and $s_{k'}(t) \leq s_A(t)$ never occurs through t_g.

The cycle of steps i)–iii) is analyzed in terms of the duration time [108], how long a node remains in one set before switching to the other. Whenever a node i switches from one set to the other, its duration time is reset to zero. In Fig. 3.2(b), the horizontal axis denotes time, and the boundary between two domains (indicated by alternating use of color) represents an event in which a cluster of a given node i moves from one set to the other set. The interval between two consecutive boundaries is called the interevent time of node i and is denoted as z_i. Each node i can mark multiple set-crossing events and duration times on the timeline. The interevent time distribution $P_d(z)$ is constructed by accumulating these duration times over all nodes during a given time interval, for instance, $[0, t_g]$. We find that the interevent time distribution exhibits power-law decay as $P_d(z) \sim z^{-\alpha}$ (inset of Fig. 3.2(a)). The exponent α depends on the time window. For $[0, t_a]$, α is measured to be approximately one for $g = 0.2$, being insensitive to g as long as g is not close to one. This exponent value is also insensitive

to the set-crossing type (either from A to B or from B to A). During the window $[t_a, t_g]$, the exponent α, alternatively denoted as α', is found to be $\alpha' = 4 - \tau$ for the type $A \to B$, and is less than two. However, for the type $B \to A$, we obtain $\alpha' > 2$. We note that in the latter case, the duration times that were reset to zero before t_a remain, even though they are measured during the window $[t_a, t_g]$. Because the interevent time distribution for the window $[t_a, t_g]$ decays rapidly, the exponent α measured during the entire period $[0, t_g]$ is governed by the values measured during the window $[0, t_a]$, and thus, the exponent α is close to one.

3.3 Analytic calculation of interevent time distribution

We obtain the interevent time distribution analytically. Let us consider the case in which a cluster c_0 of size s_0 is evicted from B to A at time $t_0 > 0$. A node belonging to cluster c_0 has more opportunity to be selected. Thus, cluster c_0 grows rapidly in set A, and it returns to B for the first time at a time $t_1 = t_0 + z$, at which its size becomes larger than $s_A(t_1)$. Then all s_0 nodes that belonged to the original cluster c_0 at time t_0 have duration time z, which is accumulated in the interevent time distribution. The probability $P_d^{A\to B}(z)$ that such events happen during the interval $[0, t_g]$ is calculated as

$$P_d^{A\to B}(z) = \int_0^{t_g} dt_0 \; s_0 q_1(s_0; t_0) \Bigg[\prod_{t=1/N}^{z-1/N} q(s_{t_0+t}; t_0 + t) \Bigg] \big[1 - q(s_{t_0+z}; t_0 + z)\big], \quad (3.1)$$

where $q_1(s_0; t_0)$ is the probability that a cluster of size $s_0 = s_A(t_0)$ in set B is evicted to set A at t_0 by an event in which a cluster larger than s_0 moves from A to B at t_0. Further, $q(s_{t_0+t}; t_0 + t)$ is the probability that cluster c_0 remains in set A with size s_{t_0+t} at time $t_0 + t$. Next, we use the relation $s_A/\dot{s}_A = \sigma' s_A^{-\sigma'}$ and regard n_s as $\sim s^{-\tau}/(1 - s_A^{2-\tau})$ for $s \leq s_A$. Then we obtain $P_d(z) \sim z^{-(4-\tau-\sigma')}$. A detailed derivation of the above equation is presented in [51].

Next, we calculate the interevent time distribution $P_d(z)$ in $[t_a, t_g]$, which is composed of duration times that terminate in the interval $[t_a, t_g]$. During this short interval, the probability

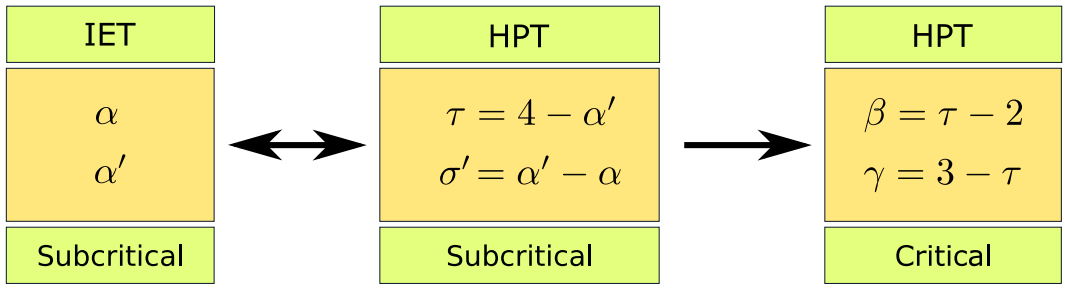

Figure 3.5: The interevent time exponents α and α' determined in subcritical regime are related to the critical exponents τ and σ' of the cluster size distribution. And then, the exponent τ determines the critical exponents β and γ of the order parameter and susceptibility.

of selecting a cluster of size s may be regarded as $sn_s(t_g) \propto s^{1-\tau}e^{-s/s^*(t_g)}$, where $s^*(t_g)$ is constant, and thus $\sigma' = 0$. In this case, $P_d(z) = s \cdot sn_s \left|\partial s/\partial\langle z\rangle\right| \sim z^{-(4-\tau)}$. The exponent $\alpha' = 4 - \tau$ is in reasonable agreement with numerical results for the process $A \to B$. Note that the two relations, $\alpha = 4 - (\tau + \sigma') = 1$ for $[0, t_a]$ (and even for $[0, t_g]$) and $\alpha' = 4 - \tau$ for $[t_a, t_g]$, enable us to determine the static exponents τ and σ' for the cluster size distribution, once we have measured the dynamic exponents α and α'. Furthermore, the exponent τ determines the critical exponents β and γ associated with the order parameter and the susceptibility as $\beta = \tau - 2$ and $\gamma = 3 - \tau$, respectively [49]. Therefore, the interevent time exponents α and α' characterize the critical behavior of the hybrid percolation transition induced by cluster coalescence. We summarize these relationships in Fig. 3.5.

Overall, we find that cluster inter-set crossing events occur more frequently as time passes, as shown in Fig. 3.2(b). We examine the number of crossing events, denoted as $N_{\text{event}}(t)$, as a function of time by counting the number of nodes that switch from one set to the other at a given time t. We argue that $N_{\text{event}}(t) \sim 1/\langle z\rangle_s \sim s^*(t) \sim (t_g - t)^{-1}$ with some cutoff. Thus, a burst occurs in the inter-set crossing as the time approaches t_g. The burst may signal the upcoming hybrid percolation transition. We also find a Devil's staircase pattern during a short time period $[t_a, t_c]$ [120]. For more details, see [51].

3.4 Summary

In summary, we have investigated the underlying mechanism of the hybrid percolation transition induced by cluster merging dynamics using the restricted Erdős–Rényi model, finding that the interevent times between two consecutive set-crossing times have two distributions with power-law decays. This implies that there exists a self-organized critical behavior previously unrecognized in the hybrid percolation transition. We established a theoretical framework for the hybrid percolation transition, analogous to the conventional percolation theory, and showed that the exponents of the interevent time distributions determine the critical behavior of the hybrid percolation transition.

Chapter 4

Synchronization

Synchronization is self-organization of a collective rhythm among individuals whose beating rates are originally independent. When fully synchronized, the rhythmic motions of the individuals are in unison. They are entrained into a common frequency and become coherent to one another. Examples include flickering of the fireflies [121], applause at the concert hall [122], electrical frequency of the power grid [123, 124], synchronization among chaotic oscillators [125], and so on [66–71].

4.1 Kuramoto model

A theoretical formulation of synchronization phenomena begins by regarding each individual as an oscillator. Each oscillator is described by a single angular variable, which abstractly represents the phase of its self-sustained and rhythmic limit cycle motion. Any interaction should also respect this built-in 2π-periodicity of phase variables, which can be in turn series represented by a fundamental sine function and its harmonics. It is assumed that the interaction is weak, in the sense that the limit cycle character of individual oscillators is not destroyed although the rhythmic motions are slightly altered.

Kuramoto model is a simple phase oscillator model which exhibits synchronization phase transition. It incorporates just the fundamental sinusoidal mode in the interaction term. The model is written as follows.

$$\dot{\theta}_i(t) = \omega_i + \frac{K}{N}\sum_{j=1}^{N}\sin(\theta_j - \theta_i), \tag{4.1}$$

where $\theta_i(t)$ denotes the phase of an oscillator i, ω_i is the natural frequency, and K is the coupling constant. The coupling constant K is usually set positive, so that the sinusoidal interaction term tends to attract the oscillator phases towards synchrony. The natural frequency term, on the other hand, represents an intrinsic disorder present in the system which disturbs synchronization. This intrinsic disorder is characterized by a distribution function $g(\omega)$. For simplicity, we assume a symmetric distribution $g(\omega) = g(-\omega)$ so that the mean natural frequency of the system is zero $\bar{\omega} = 0$ and mean angular rotation of the system is zero $\bar{\dot{\theta}} = 0$.

4.2 Synchronization phase transition

In the Kuramoto model, individual disordered rhythmic nature of oscillators are encoded by the intrinsic frequencies $\{\omega_i\}$. In the non-interacting or weakly interacting limit $K \ll \omega$, each oscillator run independently at its own period and the oscillator motions are incoherent. On the other hand, in the limit of strong interaction $K \gg \omega$, the oscillators approach a perfect synchrony $\theta_i \simeq \theta_j$. Therefore, we expect a phase transition somewhere in between. As a natural measure of synchronization a complex order parameter $Z(t)$ is introduced as followed.

$$Z(t) \equiv R(t)e^{i\psi(t)} \equiv \frac{1}{N}\sum_{j=1}^{N} e^{i\theta_j(t)}. \tag{4.2}$$

The magnitude $R(t)$ signifies the coherence and $\psi(t)$ represents an overall collective phase. The coherence R becomes zero when oscillators are uniformly distributed around the phase circle and it becomes unity unity when oscillators are perfectly aligned at a same phase. With this definition of the order parameter (4.2) it is possible to rewrite the equation (4.1) as

$$\dot{\theta}_i = \omega_i - KR\sin(\theta_i - \psi). \tag{4.3}$$

Each Kuramoto oscillator can thus be understood as being attracted towards the collective phase $\psi(t)$ by an effective sine interaction, which has a strength proportional to both coupling

strength K and coherence R.

It should be noted that $R(t)$ in equation (4.3) is also time dependent. Remarkably exact solution can be obtained for identical oscillators $\omega_i = \omega$ [126, 127] or for a Lorentzian $g(\omega)$ distribution [128, 129]. In those cases, N dimensional phase dynamics $\{\theta_i(t)\}$ can be reduced to a low dimensional dynamics which involves the order parameter $R(t)$, and the exact bifurcation of the dynamic system can be investigated (for more details, see Appendix B). However, an exact solution for general distribution $g(\omega)$ remains elusive. In the continuous synchronization transition the time averaged order parameter $\langle R(t;K)\rangle = R(K)$ exhibits critical behavior in the vicinity of the transition point K_c in the thermodynamic limit $N \to \infty$ as

$$R(K) = \begin{cases} 0 & K < K_c \\ A(K - K_c)^{\beta} & K \geq K_c \end{cases} \tag{4.4}$$

where A is a constant. The temporal fluctuations of the order parameter [130] diverges near the transition point as (see Appendix C)

$$\chi \equiv N\left\langle \left| Z(t;K) - \langle Z(t;K)\rangle \right|^2 \right\rangle \sim |K - K_c|^{-\gamma}. \tag{4.5}$$

The angular brackets denote temporal mean. Multiplication factor N should be noted, which compensates the usual $O(1/\sqrt{N})$ decrease of the fluctuations. Temporal fluctuations of the order parameter is a finite size effect which vanishes in the thermodynamic limit $N \to \infty$. There is a controversy on the value of the critical exponent γ of the temporal fluctuations of the order parameter. Daido's analytic calculation [130] had obtained distinct exponents in the subcritical regime ($\gamma' = 1$) and in the supercritcal regime ($\gamma = 1/4$). However, the recent finite size scaling analysis of Gaussian $g(\omega)$ [131] and the analytic calculations of Lorentzian $g(\omega)$ [132] both suggest that the subcritical and supercritical exponents are the same $\gamma' = \gamma = 1$ [130, 131, 133].

4.3 The mean field theory of Kuramoto

We are now interested in the time averaged order parameter value in the steady state. In the steady state, the order parameter will fluctuate around a mean value $R(t) = \langle R \rangle + \delta R(t)$. Fluctuations are usually very small in the thermodynamic limit $O(N^{-1/2})$. Let us assume a stationary order parameter $R(t) = \langle R \rangle = R$. Then it is noted that the oscillator population divides into two groups: locked and drifting. An oscillator having a natural frequency in the range $-KR \leq \omega \leq KR$ will become stationary after reaching an angle

$$\theta^* = \psi + \arcsin\left(\frac{\omega}{KR}\right). \tag{4.6}$$

The position $\theta^* + \pi$ is also stationary but unstable. So small fluctuations which we neglected here should actually lead the oscillator towards the stable position θ^*. On the other hand, $|\omega| > KR$ oscillator will undergo a periodic motion with period (see appendix D)

$$T = \int_0^{2\pi} d\theta \frac{\theta}{|\dot{\theta}|} = \frac{2\pi}{\sqrt{\omega^2 - K^2R^2}}. \tag{4.7}$$

We let $\psi = 0$ without loss of generality. It follows from the definition of the order parameter that

$$R = \frac{1}{N}\sum_{j=1}^{N} \Theta\left(KR - |\omega_j|\right) e^{i\theta^*(\omega_j)} + \frac{1}{N}\sum_{j=1}^{N} \Theta\left(|\omega_j| - KR\right) \left\langle e^{i\theta(t)} \right\rangle. \tag{4.8}$$

The angular bracket represents a temporal average. Having that a drifting oscillator only gives a purely imaginary contribution to the average order parameter (see appendix D), the real part of the previous equation is written as

$$R = \frac{1}{N}\sum_{|\omega_j| \leq KR} \cos(\theta^*(\omega_j)) = \frac{1}{N}\sum_{|\omega_j| \leq KR} \sqrt{1 - \frac{\omega_j^2}{K^2R^2}}, \tag{4.9}$$

and the imaginary part of the equation should be vanished, for the consistency of the "temporal mean" of the order parameter. The equation (4.9) is called the self-consistency equation [8]. For a distribution $g(\omega)$ the equation is written in the integral form as

$$R = KR\int_{-\pi/2}^{\pi/2} d\theta g(KR\sin\theta)\cos^2\theta = \int_{-KR}^{KR} d\omega g(\omega)\sqrt{1-\frac{\omega^2}{K^2R^2}}. \tag{4.10}$$

unimodal For a unimodal distribution of $g(\omega)$, it is Taylor expanded as

$$g(\omega) = \sum_{n=0}^{\infty} g^{(n)}(0)\frac{\omega^n}{n!} \tag{4.11}$$

where $g'(0) = 0$ and $g''(0) < 0$ is assumed. Plugging in the above series to the self-consistency equation (4.10) results an algebraic equation as followed.

$$R = \int_{-KR}^{KR} d\omega \sum_{n=0}^{\infty} \frac{g^{(n)}(0)}{n!}\omega^n\sqrt{1-\frac{\omega^2}{K^2R^2}} \tag{4.12}$$

$$= \sum_{n=0}^{\infty} \frac{g^n(0)}{n!} I_n (KR)^{n+1} \tag{4.13}$$

$$= g(0)I_0 KR + \frac{g''(0)}{2!}I_2(KR)^3 + \frac{g^{(4)}(0)}{4!}I_4(KR)^5 + \cdots, \tag{4.14}$$

where $I_{2n} \equiv \int_{-1}^{1} dx x^{2n}(1-x^2)^{1/2} = \beta(\frac{3}{2}, \frac{2n+1}{2}), I_0 = \pi/2, I_2 = \pi/8, I_4 = \pi/16$ (see appendix D). It results a supercritical Hopf bifurcation. A partial synchronization solution ($R \neq 0$) emerges at

$$K_c = \frac{2}{\pi g(0)}, \tag{4.15}$$

and the order parameter follows the scaling law

$$R \sim \sqrt{\frac{16(K-K_c)}{\pi K_c^4 |g''(0)|}}, \quad \text{as } K \to K_c^+. \tag{4.16}$$

Therefore, for unimodal $g(\omega)$ with nonvanishing and negative $g''(0)$, we find a continuous synchronization transition with critical exponent $\beta = 1/2$. This scaling law applies to a variety of natural frequency distributions including Lorentzian and Gaussian distributions.

bimodal For a bimodal distribution $g''(0) > 0$ and $g^{(4)} < 0$. Thus we expect a subcritical Hopf bifurcation, suggesting a discontinuous transition with hysteresis. However, an exact analysis of the bi-Lorentzian case through Ott-Antonsen reduction [10] has revealed a much richer bifurcation diagram. The bifurcation diagram of the bi-Lorentzian case includes for example a standing wave phase, which involves two synchronized frequency clusters whose behavior is not fully captured by a single global order parameter R.

4.4 Remarks on self-consistency method and exact theories

The self consistency equation solutions are only candidate solutions of the steady state. Some unstable solutions among them may not be realized. Thus some further analytic or numerical examinations are required to determine either the solution's local [134–136] or global stability [61]. For some frequency distributions, the self-consistency method alone is insufficient to fully characterize the rich higher dimensional dynamics [10]. This "failure" is largely because the system is not characterized by a uniform circular motion of a single complex order parameter. The self-consistency equation solutions of the assumed form of steady states may not include all possible steady states of the system. At worst, none of the self-consistency solutions might be an actual steady state. We remark that the bifurcation diagram of a Kuramoto system can become far more complex than the phase diagram given by a simple order parameter analysis, in contrary to simple unimodal cases where the two diagrams are identical. In this regard, such a "failure" in the analysis is primarily due to the false assumption on the form of steady state.

If a steady state of the system follows the simplest form $Z(t) \sim Re^{i\Omega t}$, with R and Ω being regarded as constants, the usual self-consistency equation can be written on the order parameter Z. However, in principle, there may be a variety of far more complicated

steady states, considering the high dimensionality of the oscillator system. To the best of my knowledge, self-consistency method on a non-simple steady state has not been reported. It is because steady states with more than 3 parameters is in general not determined by a single complex self-consistency equation which only gives two independent real equations at most.

It is remarked that exact theories are available for identical oscillators and a family of Lorentzian distributions. In these theories, the order parameter dynamics can be fully determined; therefore both transient and steady states are exactly calculable [127–129, 132]. We provide a brief review of them in Appendix B. Theoretically, it is motivating to study those exact reduction methods. However, the limitations are in the narrow practical applicability. Kuramoto's self-consistency theory, on the other hand, can be written on first-hand at any frequency distributions, and it obtains candidate steady state solutions which bears the simplest form $Z(t) \sim Re^{i\Omega t}$, although it is not sufficient to yield the full solutions of the multimodal frequency distributions [10]. We remark that the self-consistency method is also applicable to finite-size systems in contrary to the Ott-Antonsen method which assumes infinitely many oscillators. It is also remarked that Ott-Antonsen theory yields the equation identical to the self-consistency equation under the assumption of a simple steady state $Z(t) \sim Re^{i\Omega t}$ (see Appendix B). Thus it is fair to say that for infinite system with and when no further reduction is possible, both approaches are identical. In turn, Kuramoto's theory still remains as a quick and powerful analyzing tool. For example, the self-consistency method gave a universal critical exponent $\beta = 1/2$ of the order parameter, for any unimodal frequency distributions. And for any flat distributions appended by power-law tails, which is to be discussed in the next section, it yields the hybrid critical exponent $\beta = 2/5$.

In the next chapters we apply this method to Kuramoto model with flat topped frequency distributions, neither concave (unimodal) or convex (bimodal) at the center. This marginal case therefore lies in between the continuous and discontinuous phase transitions. Moreover, it turns out to exhibit hybrid characters of both transitions. We find that the self-consistency method provides a valid analysis on hybrid synchronization transitions, which we discuss in the following chapters.

Chapter 5

Hybrid synchronization transition

Kuramoto model exhibits hybrid synchronization transition when the natural frequency distribution becomes flat-topped. In this chapter we review the uniform distribution case and present some new results in the case of modified uniform distribution with long-range tails appended.

5.1 From Lorentzian to uniform

Consider a family of distributions

$$g_m(\omega) \equiv \frac{c_m}{\omega^{2m} + \gamma^{2m}} \tag{5.1}$$

where the normalization constant is calculated as $c_m = \frac{m \sin(\pi/2m)}{\pi \gamma^{2m-1}}$ (see appendix D). A uniform distribution is obatined in the $m \to \infty$ limit.

$$g(\omega) = \lim_{m\to\infty} g_m(\omega) = \frac{1}{2\gamma}\Theta(\gamma - |\omega|), \tag{5.2}$$

where Θ is Heaviside step function.

Now for a finite m, series expand $g_m(\omega)$.

$$g_m(\omega) = \frac{c_m}{\gamma^{2m}}\left(1 - \frac{\omega^{2m}}{\gamma^{2m}} + \frac{\omega^{4m}}{\gamma^{4m}} - \cdots\right). \tag{5.3}$$

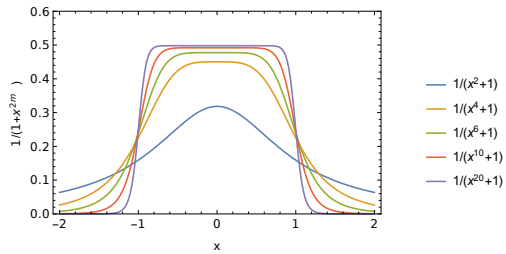

Figure 5.1: The distribution $g_m(\omega)$. $m = 1$ corresponds to a Lorentzian distribution. A uniform distribution is appraoched in the limit $m \to \infty$.

Plugging this into the self consistency equation gives

$$R = \int_{-KR}^{KR} g_m(\omega)\sqrt{1-\frac{\omega^2}{K^2R^2}} \tag{5.4}$$

$$= \frac{c_m}{\gamma^{2m}}\int_{-KR}^{KR}\left(1-\frac{\omega^{2m}}{\gamma^{2m}}+\frac{\omega^{4m}}{\gamma^{4m}}-\cdots\right)\sqrt{1-\frac{\omega^2}{K^2R^2}} \tag{5.5}$$

$$= g(0)KR\big(I_0-(KR/\gamma)^{2m}I_2+(KR/\gamma)^{4m}I_4-\cdots\big) \tag{5.6}$$

$$= \frac{\pi g(0)}{2}KR\left(1-\frac{(2m-1)!!}{2^m(m+1)!}\frac{K^{2m}R^{2m}}{\gamma^{2m}}+\cdots\right). \tag{5.7}$$

where $I_{2n} = \int_{-1}^{1} dx x^{2n}\sqrt{1-x^2} = \beta(\frac{3}{2}, \frac{2n+1}{2})$ are some constants (see appendix D). For a finite m and in the thermodynamic limit $N \to \infty$ a continuous synchronization phase transition occurs at

$$K_c = \frac{2}{\pi g(0)}, \tag{5.8}$$

beyond which the coherence order parameter grows continuously from zero, and with the critical exponent

$$\beta = \frac{1}{2m}. \tag{5.9}$$

If we take the limit $m \to \infty$, this β vanishes to zero; which is a signature of a discontinuous transition. In this limit, the distribution becomes flat as in Fig. 5.1. However, the limiting value of $\beta \to 0$ is different from the hybrid critical exponent $\beta = 2/3$ of the uniform distribution case ($m = \infty$). For the such flat distributions, the series expansion of the self consistency equation yields only the zeroth order term while the remaining higher orders vanishes. Such an expansion cannot obtain the nontrivial solution branch or the hybrid critical exponent β.

5.2 Uniform

The uniform natural frequency distribution allows exact integration. A discontinuous transition with $\beta = 2/3$ has been discovered [11]. It should be noted that this β is defined in the supercritical regime and that it is a non-integer. Roughly speaking, the system undergoes two consecutive transitions at the same transition point; a continuous transition is followed after the discontinuous transition. For the description of this later continuous transition, an order parameter similar to that of the Bragg-Williams theory can be adopted; offset by the jump size R_c from the usual order parameter. Alltogether, hybrid phase transition is described by the following order parameter curve

$$R = \begin{cases} 0 & K < K_c \\ R_c + A(K - K_c)^\beta & K \geq K_c \end{cases} \tag{5.10}$$

where R_c is size of the discontinuous jump in the order parameter R at the transition point K_c. The term $\propto (K - K_c)^\beta$ after the jump is nonanalytic if β takes a non-integer value. The curve is singular. The singularity lies at the top of the jump. This β is the critical exponent of the order parameter in the hybrid phase transition. In the following Pazó's solution [11] is reproduced.

$$R = \frac{1}{2\gamma} \int_{-KR}^{KR} \Theta(\gamma - |\omega|) \sqrt{1 - \frac{\omega^2}{K^2 R^2}} \tag{5.11}$$

$$= \begin{cases} \frac{\pi KR}{4\gamma}, & KR \leq \gamma \\ \frac{KR}{2\gamma}\sin^{-1}\frac{\gamma}{KR} + \frac{1}{2}\sqrt{1-\left(\frac{\gamma}{KR}\right)^2}, & KR \geq \gamma \end{cases} \tag{5.12}$$

The synchronization transition occurs when $K_c R_c = \gamma$ where the oscillator with the largest natural frequency becomes phase locked. Beyond the transition all oscillators are locked into a single frequency cluster. We denote the phase of the largest natural frequency oscillator as $\theta_M = \arcsin(\gamma/KR)$ and expand near the critical point (K_c, R_c) as $K = K_c + \delta K, R = R_c + \delta R, \theta_M = \frac{\pi}{2} - \delta\theta$.

$$\gamma = Kr\sin\theta_M = (K_c + \delta K)(r_c + \delta r)\sin\left(\frac{\pi}{2} - \delta\theta\right) \tag{5.13}$$

$$\frac{\gamma}{2}(\delta\theta)^2 \sim K_c\delta r + r_c\delta K \tag{5.14}$$

For nontrivial R the self consistency equation is written

$$1 = K\int_{-\theta_M}^{\theta_M} d\theta\cos^2\theta g(KR\sin\theta) \tag{5.15}$$

$$= \frac{K_c + \delta K}{2\gamma}\left(\frac{\pi}{2} - \delta\theta + \frac{1}{2}\sin(\pi - 2\delta\theta)\right) \tag{5.16}$$

$$= \frac{\pi K_c}{4\gamma} - \frac{2K_c}{3\gamma}(\delta\theta)^3 + \cdots \tag{5.17}$$

which gives the transition point

$$K_c = \frac{4\gamma}{\pi} \tag{5.18}$$

and scalings $\delta\theta \sim (\delta K)^{1/3}, \delta R \sim A(\delta\theta)^2 - B\delta K \sim (\delta K)^\beta$ and thus the leading order is $\beta = 2/3$. It is remarked that the the formula for the transition point (5.8) of unimodal distribution also applies to the transition point of the uniform distribution case. In summary, the Kuramoto model with uniform natural frequency distribution exhibits a hybrid synchronization transition with critical exponent $\beta = 2/3$.

5.3 Lorentzian vs uniform : clustering picture

When two oscillators are synchronized they rotate together at a same angular velocity, i.e. phase-locked. In the coherent phase of the unimodal/uniform cases, there exists a finite fraction of phase-locked population at an entrainment frequency. We shall call them the giant cluster. We have seen in the previous chapter (the mean field theory of Kuramoto) that only the giant cluster contributes to the coherence R. The order parameter R grows by an acquirement of additional oscillators to the giant cluster. However, it is remarked that coherence R can also be improved without an acquirement. For example, the order parameter still increases after the full phase locking of the hybrid synchronization transition. In Fig. 5.2 we compare frequency clustering of the continuous synchronization transition and that of the hybrid synchronization transition. Frequency clusters are characterized by time averaged oscillator angular velocities at each given coupling strength K. So the clustering occurs along with increase in K. The temporal clustering, or the clustering dynamics, at a given fixed K is presented in Fig. 5.3.

5.4 Flat top with tails appended

What are the ingredients of the hybrid synchronization transition? Can the hybrid critical exponent β be varied? What other distributions result hybrid synchronization transition? Motivated by these questions, we study the Kuramoto model with natural frequency distributions with slight modifications from the uniform distribution.

Trimmed Lorentzian Consider a trimmed Lorentzian natural frequency distribution defined as

$$g(\omega) = \begin{cases} \frac{1}{\mathcal{N}} \frac{\gamma/\pi}{\gamma^2+\alpha^2} & |\omega| \leq \alpha \\ \frac{1}{\mathcal{N}} \frac{\gamma/\pi}{\gamma^2+\omega^2} & |\omega| > \alpha \end{cases} \tag{5.19}$$

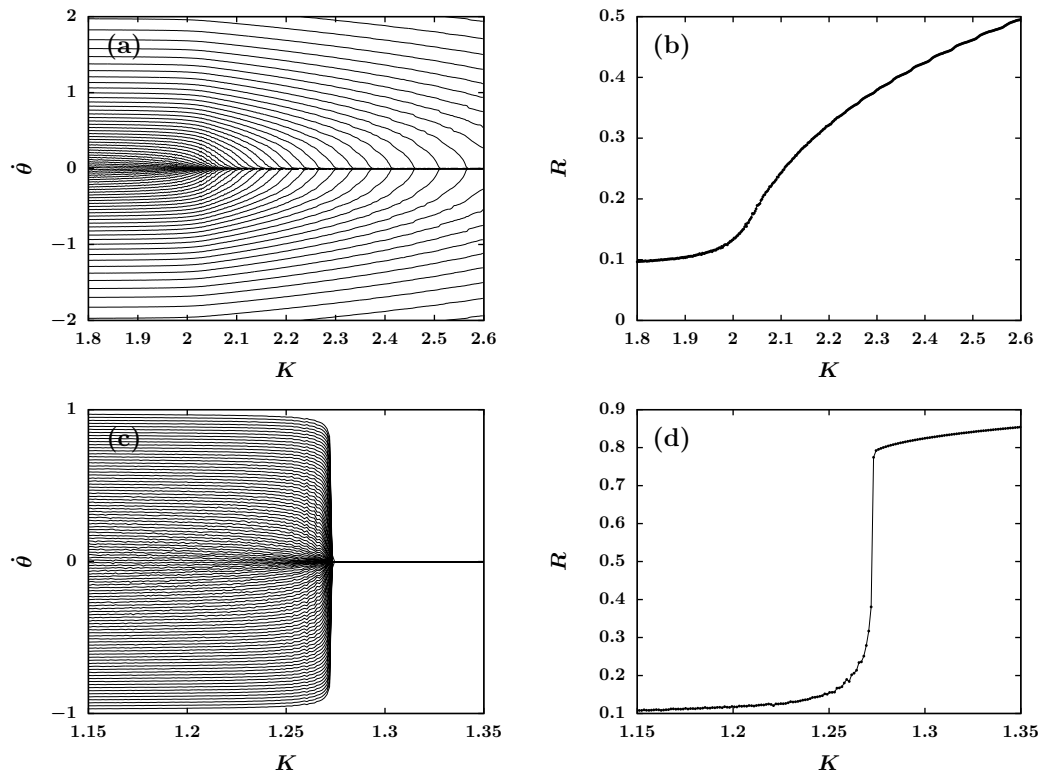

Figure 5.2: Frequency clustering and order parameter curve $R(K)$ in a finite size ($N = 100$) Kuramoto model with Lorentzian natural frequency distribution $g(\omega) = 1/(\pi(1+\omega^2))$ and uniform natural frequency distribution $g(\omega) = (1/2)\Theta(1-|\omega|)$. (a) In the Lorentzian case, the giant frequency cluster at $\dot{\theta} = 0$ grows gradually by sequential acquirement of oscillators. (b) Correspondingly, the order parameter grows continuously. (c) In the uniform case, all oscillators suddenly merge together, forming a single giant cluster of size N at the hybrid critical point. The locked phases distribute roughly on a semicircle $\theta_i^* = \arcsin(\omega_i/K_cR_c) \in [-\pi/2, \pi/2]$, which results a jump height $R_c \simeq \pi/4$.

where the normalization is calculated as $\mathcal{N} = 1 - (2/\pi)\arctan(\alpha/\gamma) + 2\gamma\alpha/(\pi(\gamma^2+\alpha^2))$. $g(\omega)$ is thus flat in $(-\alpha, \alpha)$ and has a decaying tail $\sim |\omega|^{-2}$ at each side. By solving the self-consistency equation numerically, we obtain $\beta = 2/5$. In fact, we find that for any flat distribution with decaying tails $\sim |\omega|^{-m}$ and with a finite $m > 0$, $\beta = 2/5$ is obtained in contrast to $\beta = 2/3$ of the Pazó model.

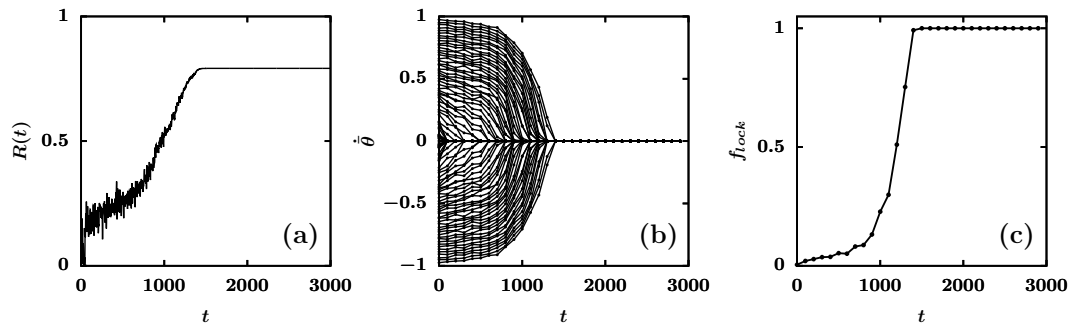

Figure 5.3: Order parameter dynamics and the dynamic cluster formation at a supercritical K of a finite-size Kuramoto model with uniform natural frequency distribution. $N = 3200$. (a) shows the order parameter trajectory $R(t)$. Locking dynamics is noticed from the (b) interval-averaged angular velocity trajectories $\dot{\bar{\theta}}$ of some oscillators, which has been coarse-grained at sliding time window of $100s$. The oscillators are eventually fully locked and reaches a monolithic state where the dynamic fluctuations is totally absent. Corresponding variations in the locking fraction f_{lock} is plotted in (c).

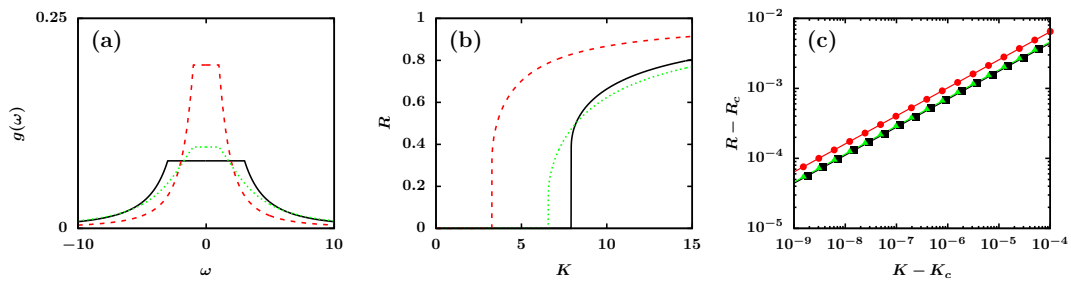

Figure 5.4: (a) Trimmed Lorentzian distribution with various values of (γ, α); solid $(1, 3)$, dashed $(1, 1)$, and dotted $(3, 1)$. (b) The order parameter curve obtained by the self-consistency equation. (c) $\beta = 0.40$ is measured for all cases.

Flat with tails Now, consider natural frequency distribution which is flat in the interval $[-\alpha, \alpha]$ and having tails $\sim |\omega|^{-m}$ $(m > 1)$

$$g(\omega) = \begin{cases} g(0), & |\omega| \leq \alpha \\ \frac{g(0)\alpha^m}{|\omega|^m}, & |\omega| > \alpha \end{cases} \tag{5.20}$$

where

$$g(0) = \frac{m-1}{2\alpha m} \tag{5.21}$$

by the normalization condition $\int g(\omega)d\omega = 1$. For $KR \geq \alpha$, the self consistency equation is written as

$$R = KRg(0)\int_{-\alpha/(KR)}^{\alpha/(KR)} dx\sqrt{1-x^2} + \frac{2g(0)\alpha^m}{(KR)^{m-1}}\int_{\alpha/(KR)}^{1} x^{-m}\sqrt{1-x^2}dx \tag{5.22}$$

$$= 2KRg(0)\int_0^{\theta_0} d\theta\cos^2\theta + \frac{2g(0)\alpha^m}{(KR)^{m-1}}\int_{\sin^2\theta_0}^{1}\frac{1}{2}y^{-\frac{m+1}{2}}(1-y)^{\frac{1}{2}}dy \tag{5.23}$$

where we have let $\frac{\alpha}{KR} = \sin\theta_0$. Notice at $\theta_0 = \pi/2$, the self consistency equation gives

$$K_c = \frac{2}{\pi g(0)}, \quad R_c = \frac{\pi g(0)\alpha}{2}. \tag{5.24}$$

Now look for a $R \neq 0$ solution at $K = K_c + \delta K$ and $\theta_0 = \frac{\pi}{2} - \delta\theta$.

$$1 = 2Kg(0)\int_0^{\theta_0} d\theta\cos^2\theta + \frac{2g(0)\alpha^m}{K^{m-1}R^m}\int_{\sin^2\theta_0}^{1}\frac{1}{2}y^{-\frac{m+1}{2}}(1-y)^{\frac{1}{2}}dy \tag{5.25}$$

$$= Kg(0)\Bigg[\int_0^{\theta_0}\Big(1-\cos(2\theta)\Big)d\theta + \sin^m\theta_0\int_{\sin^2\theta_0}^{1} y^{-\frac{m+1}{2}}(1-y)^{\frac{1}{2}}dy\Bigg] \tag{5.26}$$

$$= Kg(0)\Bigg[\theta_0 + \frac{1}{2}\sin(2\theta_0) + \sin^m\theta_0\int_0^{1-\sin^2\theta_0}(1-y)^{-\frac{m+1}{2}}y^{\frac{1}{2}}dy\Bigg] \tag{5.27}$$

$$\simeq (K_c+\delta K)g(0)\Bigg[\frac{\pi}{2} - \frac{2}{3}(\delta\theta)^3 + \frac{2}{15}(\delta\theta)^5 + \Big(1 - m\frac{(\delta\theta)^2}{2}\Big) \times\left(\frac{2}{3}\Big((\delta\theta)^2\Big)^{3/2} + \frac{m+1}{2}\frac{2}{5}\Big((\delta\theta)^2\Big)^{5/2}\right)\Bigg]. \tag{5.28}$$

Thus one finds $\delta K \simeq \frac{4mK_c}{15\pi}(\delta\theta)^5$. Meanwhile,

$$\alpha = (K_c+\delta K)(R_c+\delta R)\sin\Big(\frac{\pi}{2} - \delta\theta\Big) \tag{5.29}$$

$$(\delta\theta)^2 \simeq \frac{2}{\alpha}(K_c\delta R + R_c\delta K) \tag{5.30}$$

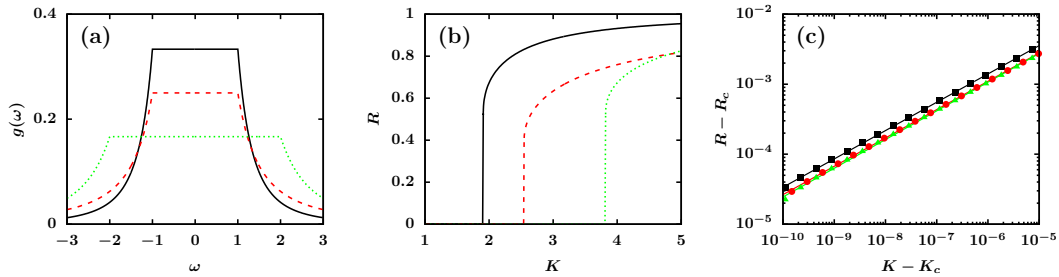

Figure 5.5: (a) Flat-with-tails distribution with various values of (α, m); solid $(1, 3)$, dashed $(1, 2)$, and dotted $(2, 3)$. (b) The order parameter curve obtained by the self-consistency equation. The transition point and jump height is determined by the relations $K_c = 2/\pi g(0)$ and $R_c = \pi g(0)\alpha/2$. (c) $\beta = 0.40$ is measured for all cases.

Finally,

$$\delta R \simeq \frac{\alpha}{2K_c}(\delta\theta)^2 - \frac{R_c}{K_c}\delta K \tag{5.31}$$

$$= \frac{\alpha}{2K_c}\left(\frac{15\pi}{4mK_c}\right)^{2/5}(\delta K)^{2/5} - \frac{R_c}{K_c}\delta K \tag{5.32}$$

$$\propto (\delta K)^{2/5}. \tag{5.33}$$

Therefore with the flat distribution of $g(\omega)$ appended by long tails, we find $\beta = 2/5$ regardless of the exponent m.

Limiting case $m \to \infty$ Notice in the limit $m \to \infty$, $\sin^m\theta_0 \to 0$, since $\sin\theta_0 = \sin\left(\frac{\pi}{2} - \delta\theta\right) < 1$. Thus (5.26) becomes

$$1 = Kg(0)\int_0^{\theta_0}\big(1 - \cos(2\theta)\big)d\theta \tag{5.34}$$

$$\simeq (K_c + \delta K)g(0)\left[\frac{\pi}{2} - \frac{2}{3}(\delta\theta)^3\right]. \tag{5.35}$$

and therefore $\delta K \sim (\delta\theta)^3$ and $\beta = 2/3$ are recovered. We remark that our results are different from the results of Refs. [12,55], which shows a continuously varying hybrid critical exponent β. There the flat distribution had tails attached, but the distribution was truncated in

order to satisfy the normalization condition, i.e. it had a finite support in contrast to the long range tail.

5.5 Any hybrid critical phenomena?

So far, we have seen that the hybrid phase transitions of the Kuramoto models can exhibit a unique bifurcation with hybrid critical exponent such as $\beta = 2/3$ or $\beta = 2/5$. It is in contrast to the saddle-node bifurcation of the order parameter curves in the hybrid percolation transitions, for example, where $\beta = 1/2$. Such a singularity in the order parameter characterized by the critical exponent β means that the slope of the order parameter curve becomes divergent at the transition point, as it is approached from the supercritical side. Thus the system is highly responsive near this singularity, and there may be some related critical phenomena. For instance, the hybrid percolation transition point is not only characterized by the singularity of the order parameter curve, but also by a power-law in the size distribution of finite-size clusters.

So, what are the related critical phenomena to the hybrid synchronization transition? In Ref. [7] it was claimed that the Kuramoto model with uniform frequency distribution exhibits a jump of the order parameter as in a first-order phase transition and also with strong critical fluctuations as in a continuous phase transition. So precisely, what is the quantity being critical? In the continuous synchronization transition, Daido fluctuations was a diverging quantity [130]. However, this is not a good candidate for the hybrid critical phenomena of the Kuramoto model with uniform frequency distribution, where a complete phase-locked coherent state state emerges suddenly from the phase incoherent state. This monolithic state can be viewed as a single giant frequency cluster of the system size N. Hence, in the supercritical regime beyond the hybrid transition point of Kuramoto model with flat frequency distributions, Daido fluctuations is totally absent. Although it is remarked that a restricted synchronization can have non-vanishing fluctuations after a jump transition (See chapter 7).

In particular, the possibility of an avalanche of frequency splittings triggered upon some small perturbation was suggested [7]. It is very tempting to mention about the possibility of

an analogous power law, in retrospect of the power-law distribution of avalanches over some size S follows a power-law $P(s) \propto s^{-\sigma}$ of the hybrid percolation transitions. However, then, the definition of the avalanche size S should quite differ from the ordinary sense. In contrast to a cascade process in percolation which eventually comes to an end, at least in the finite system. Instead of a quiescent stationary state, synchronization dynamics reaches some steady state. Quite often, synchronization dynamics obtains very few (usually no more than one or two are considered by many literatures) steady states at the given parameter values.

Pazó had investigated on the bifurcations of frequency clusters in the hybrid synchronization [11]. For a finite population, indeed, a cascade of frequency splitting had occurred during some interval $[K_s, K_c]$. However, to be congruent with the discontinuous transition predicted in the thermodynamic limit, he claimed that all the splittings should accumulate at the transition point $K_s \to K_c$ as $N \to \infty$. Hence the possibility of finding a distribution of steady states upon some small perturbations, change in the value of $\{\theta_i\}$, remains precisely at the transition point.

It is because the bifurcation of the hybrid synchronization is quite unique. In comparison to the hybrid percolation transition, hybrid synchronization transition point is more responsive; the vertical jump consists of infinitely many metastable states and infinitely many unstable states. Such a character is deduced from the self-consistency solutions of the finite-size systems, which in the thermodynamic limit results a line of solutions (a countably infinite number of solutions, to be more precise) at the transition point. For example, see Fig. 5.6. As a consequence, the dynamic transition precisely at the hybrid critical point is highly nontrivial. Remarkably, instead of having just one of the infinitely many self-consistency solutions as a steady state, a mixture state is noticed. A critical slowdown in the jump time is noted, and there is a non-trivial finite-size scaling in the collective incoherent steady state, which is characterized by a distribution of order parameter values $P(R)$ rather than by taking a single value R [56]. Such a statistical state involves more complex order parameter dynamics, which is beyond the usual steady state form assumed by the self-consistency mean-field theory.

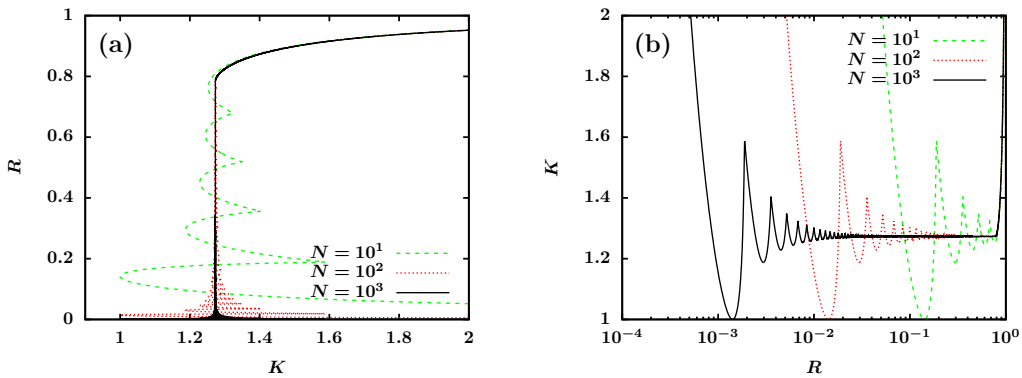

Figure 5.6: (a) Finite-size self-consistency solutions of the Kuramoto model with uniform $g(\omega)$ in range $[-1, 1]$, and for sizes $N = 10, 10^2, 10^3$. The number of solutions at the transition point $K_c(N)$ increases in proportion to the system size. In the thermodynamic limit $N \to \infty$ the transition point is at $K_c = 4/\pi$, where we find a line of infinitely many solutions. Approximately half of them are linearly stable, and the other half are linearly unstable, since the linear stability alternates. (b) The same curves are drawn in the semi-log scale. To be precise, the base part maintains a constant wide range in K, but its range in R shrinks in the thermodynamic limit.

It is remarked that the order parameter dynamics at the hybrid critical point of a competing Kuramoto model with mixed signs of couplings can become even more complex, where a traveling-wave ordered state is also possible. There are basins of attractions characterized by saddle fixed points and stable/unstable fixed points, and the system exhibits metastabiltiy [20]. Also, subcritical and supercritical hybrid bifurcations were noticed, depending on the relative strength of competing-sign couplings $Q \equiv |K_1|/K_2$ [20]. See chapter 6.2 for further details.

Therefore, further general studies are necessary in order to understand the synchronization dynamics at the hybrid transition point. A possible road of thinking might be viewing the complex nonlinear dynamical system from a perturbation and response perspective. In chapter 6.4, we propose a possible way of perturbation which results a dynamic cascade of cluster splittings phenomenon, in contrast to the static bifurcations of cluster splittings studied by Maistrenko [137] and Pazo [11].

5.6 Explosive synchronization and hybrid synchronization

On a scale-free network, synchronization phase transition is characterized by the vanishing threshold [57]. Hubs take the lead in synchronization clustering [58]. Gómez-Gardeñes et al. [59] invented a degree-frequency correlated synchronization model. The correlation of intrinsic and structural disorders generates an explosive synchronization dynamics in the networked oscillators. The correlations balances the frequency term and the interaction term of the Kuramoto model, i.e. the acquired strengths are proportional to each other. In consequence the transition is delayed and also discontinuous [58, 59]. In parallel to the explosive percolation studies, this novel transition was studied extensively and several viewpoints have been followed [61–63]. In particular, Ref. [62] has concisely pointed the suppressive aspect of the correlated model, and Ref. [63] compiled the analogous aspects of the explosive synchronization and the explosive percolation. In contrast to the explosive percolation transition, it is remarked that the synchronization transition is truly discontinuous. Furthermore, forward and backward hysteresis is noticed as in the usual first-order transitions. The hysteresis regime is hence multistable. Depending on the initial condition, oscillators may reach either coherent or incoherent steady state. Further detailed self-consistency analysis of the explosive synchronization on a scale-free network [7] has discovered an interesting marginal case of the scale-free degree exponent being $\gamma = 3$, whereat the forward and backward transition points coincide. This particular case with absence of hysteresis corresponds to a hybrid transition with critical exponent $\beta = 2/3$ [7], a value which had also appeared previously in the hybrid synchronization of the Kuramoto model with uniform natural frequency distribution.

In the correlated Kuramoto model, the degree-frequency correlation is, for example, given as follows:

$$\omega_i = k_i. \tag{5.36}$$

Now, consider the correlated Kuramoto model on a scale-free network with degree distribu-

tion $P_d(k) \sim k^{-\gamma}$, which is written as

$$\dot{\theta}_i = \omega_i + \sum_{j=1}^{N} K_{ij} a_{ij} \sin(\theta_j - \theta_i), \tag{5.37}$$

where a_{ij} is the adjacency matrix, $K_{ij} = K$ is the coupling between node i and j. The structural inhomogeneity is mean-field approximated by an annealed network

$$a_{ij} = \frac{k_i k_j}{N\langle k \rangle}. \tag{5.38}$$

Together with the definition of the degree-weighted synchronization order parameter

$$Z = Re^{i\Psi} \equiv \frac{\sum_j k_j e^{i\theta_j}}{\sum_j k_j} = \frac{1}{N\langle k \rangle} \sum_j k_j e^{i\theta_j}, \tag{5.39}$$

the equation is simplified as

$$\dot{\theta}_i = \omega_i - K k_i R \sin(\theta_i - \Psi). \tag{5.40}$$

Asymmetry in the intrinsic frequency distribution should be noted, since it is now identical to the power-law degree distribution. Let the entrained frequency be Ω. The locked population is in the range

$$-k_i K R \leq k_i - \Omega \leq k_i K R, \tag{5.41}$$

or equivalently, in the frequency (or degree) range

$$\frac{\Omega}{1 + KR} \leq \omega_i \leq \frac{\Omega}{1 - KR}. \tag{5.42}$$

Kuramoto's self consistency equation for the stationary solution is written as

$$R = \frac{1}{N\langle k\rangle}\sum_{j=1}^{N} k_j e^{i(\theta_j - \Psi)} \tag{5.43}$$

In the thermodynamic limit $N \to \infty$ [7],

$$R = \int_1^\infty dk k P_d(k)\sqrt{1-\frac{(k-\Omega)^2}{(kKR)^2}}\,\Theta\left(1-\left|\frac{k-\Omega}{kKr}\right|\right) + i\int_1^\infty dk P_d(k)\frac{k-\Omega}{KR}$$
$$- i\int_1^\infty dk k P_d(k)\sqrt{\frac{(k-\Omega)^2}{(kKR)^2}-1}\,\Theta\left(\left|\frac{k-\Omega}{kKR}\right|-1\right) \tag{5.44}$$

where $\Theta(x)$ is the heaviside step function. The real and imaginary parts of the above complex self consistency equation may be solved simultaneously to obtain the solution as in Fig. 5.7. Both continuous transition and discontinuous transition are possible, depending on the degree

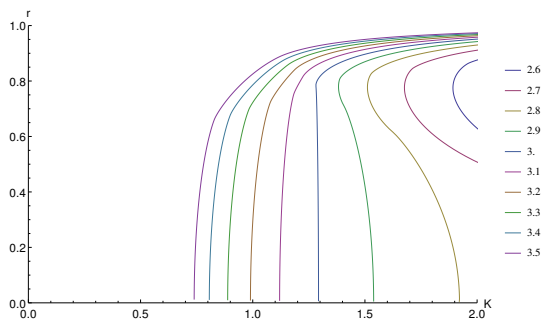

Figure 5.7: The order parameter curve of the degree-frequency correlated ($\omega_i = k_i$) Kuramoto model on scale free networks $P_d(k) \sim k^{-\lambda}$ for several values of degree exponent λ. For continuous, hybrid, and discontinuous transitions occur for $\lambda > 3, \lambda = 3$, and $\lambda < 3$, respectively. For $5/2 < \lambda < 3$, first-order (explosive) synchronization transition occurs. Ordinary Kuramoto oscillators on highly heterogeneous structure has vanishing synchronization threshold and can easily synchronize by attaching to hubs [57, 58]. However, for degree-frequency correlated oscillators, structural heterogeneity delays the transition and induces an explosive jump. There is also a hysteresis regime as in the usual first-order phase transition, and the forward transition point diverges as $\lambda \to 5/2$ is approached. Precisely at $\lambda = 3$, hysteresis is absent. Order parameter jumps and exhibits a hybrid critical exponent $\beta = 2/3$ [7].

of structural heterogeneity introduced by λ. On the border of continuous and discontinuous

transitions, which happens particularly when the scale-free degree exponent is $\lambda = 3$, hybrid phase transition occurs with critical exponent $\beta = 2/3$ (for more details refer to [7]). It should be noticed that in the ordinary scale-free Kuramoto model without degree-frequency correlations, hub oscillators with dense connections would have easily reached the locking condition $|\omega| < kKR$, thus it may perform the role as a seed node in the clustering process. The transition is continuous with vanishing thresholds [57]. For degree-frequency correlated model, however, role of hubs is degraded and first-order transition is possible [57–60]. In the next section we discuss how the oscillators of explosive models and hybrid synchronization models exhibit abrupt transitions.

5.7 Jump mechanisms of explosive synchronization and hybrid synchronization

Zhang et al. [62] pointed out that introduction of correlation is analogous to having suppressive rule in explosive percolation. Their argument is simple. The link synchrony between the two correlated Kuramoto oscillators i and j

$$R_{ij} = \left| \lim_{T\to\infty} \frac{1}{T} \int_0^T e^{i(\theta_i(t)-\theta_j(t))} dt \right| \tag{5.45}$$

is obtained by the phase locking

$$\Delta\dot{\theta}_{ij} = (\omega_i - K|\omega_i|R\sin\theta_i) - (\omega_j - K|\omega_j|R\sin\theta_j) = 0 \tag{5.46}$$

which is satisfied if

$$\frac{|\omega_i - \omega_j|}{|\omega_i| + |\omega_j|} \leq KR. \tag{5.47}$$

The presence of the denominator, in contrast to the pairwise locking condition $|\omega_i - \omega_j| \leq KR$ of the ordinary synchronization, modifies the rule of competition between segregation

and aggregation. Segregation is relatively small for the oscillator pair with same sign in ω, while for the opposite sign ω the value is unity, which is a maximum possible value. Hence, it is a kind of rule which suppresses the formation of a large synchronization cluster.

In the explosive synchronization, a modified rule of synchronization clustering leads to a sudden frequency locking. In the ordinary Kuramoto model where such suppression is absent, the hub nodes with large degrees become the seeds of synchronization clustering [58]. Correspondingly, the synchronization cluster grow from the dense core of the network and extend to the periphery. The suppression factor degrades such a role of hubs, and hence a system-wide distributed clustering may occurs, which leads to an abrupt emergence of giant synchronization cluster [59].

On the other hand, in the hybrid synchronization of the ordinary Kuramoto model, the abrupt clustering origins solely from the flatness of the natural frequency distribution. It also occurs without having a structural heterogeneity. Unimodal or bimodal distribution has presence of a mode(s) under which oscillators with small frequency mismatches are crowded. Hence in the fully-connected ordinary Kuramoto model with unimodal natural frequency distributions, a small seed population locks first and grows continuously beyond the transition point. With bimodal distribution, there may be two synchronization seeds, generating standing wave synchronization [10]. However, for flat distributions, frequencies are evenly dispersed. Instead of having a single preferred seed node, there is a maximal competition in the synchronization clustering. Hence it is intuitive that at some threshold point, locking condition can be met simultaneously by a macroscopic $O(N)$ number of oscillators. With flat distributions, oscillators are suddenly locked together at the transition point and a giant frequency cluster emerges discontinuously at the transition point.

In summary, hybrid synchronization transition occurs in the Kuramoto models with flat natural frequency distributions, where the oscillators are in maximal competition to each other in reaching synchrony and there is an abrupt frequency clustering. Explosive synchronization also exhibits similar phenomena, but by a different reason; by correlation of the two disorders [63]. In the reverse transition, a small decrement of coupling below the threshold

value detaches the oscillator one by one from the extreme sides of the natural frequency distribution, which leads to consecutive desynchronization of oscillators and the cascade destruction of giant frequency cluster. As a consequence, hysteresis is absent. Such a feature distinguishes the hybrid synchronization transition from explosive synchronization. In the restricted synchronization of Chapter 7, we discuss an interesting hybrid synchronization transition characterized by an emergent giant cluster of size less than the system size N, but still of $O(N)$, and its persistent growth beyond the transition point by continued attachment of oscillators.

Chapter 6

Competing Kuramoto model

In this chapter hybrid phase transition of the Kuramoto models with competing signs of couplings is studied. In short, they are called as competing Kuramoto models. General description of the synchronization process under presence of such competing disorders in the coupling strengths can be very complex and complicated, owing to its glassy aspect. In this regard, restricted class of solvable competing models have been studied. Namely, they include Sherrington-Kirkpatrick, actively competing and passively competing types.

6.1 Mixed signs of couplings

Inspired by spin glass systems and neural networks with competing signs of interactions, generalizations of Kuramoto model have been made [14–20, 138, 145, 146]. One most precedent suggested by Daido [14, 15] is written as

$$\dot{\theta}_i = \omega_i + \frac{1}{\sqrt{N}} \sum_{j=1}^{N} K_{ij} \sin(\theta_j - \theta_i), \tag{6.1}$$

where K_{ij} is of Sherrington-Kirkpatrick type, which is Gaussian distributed about zero mean, and is assumed symmetric $K_{ij} = K_{ji}$. Daido questioned the possibility of an oscillator glass under such competing interactions [14]. It was revealed that in this model the frequency entrainment occurs but the phase-locking does not. The oscillator phases show a diffusive motion and therefore the initial coherence is always lost in the long time. Discovery of non-exponential relaxation of coherence in supercritical control parameter regime suggested the

presence of potential glassy oscillators; yet it still remains as an inconclusive problem [15]. A critical phenomenon, the so-called volcano transition, was found regarding the motion of local fields in the complex plane. The volcano transition point has been calculated only recently [16].

Hong and Strogatz [19, 138] considered simplified Kuramoto models with competing interactions based on nodes instead of edges. One can immediately notice that two generalizations are possible: $K_{ij} = K_i$ (active) or K_j (passive). In the actively competing Kuramoto model, $K_{ij} = K_i$ is given as a competing mixture of attractive and repulsive signs. K_i can be pulled outside the sum. In this case the synchronization order parameter is defined in a similar manner to that of the ordinary Kuramoto model, but each oscillator i has a distinct and active response to the conventional order parameter $Z = Re^{i\Psi}$, depending on the value of coupling K_i. An actively competing model can be written as

$$\dot{\theta}_i = \omega_i + K_i R \sin(\Psi - \theta_i), \tag{6.2}$$

where K_i follows a distribution $f(K)$ and takes either a positive or negative value. For simplicity, $f(K)$ is set as a mixture of two node species $f(K) = (1-p)\delta(K-K_1)+p\delta(K-K_2)$, where p $(1-p)$ is the mixing fraction of positive (negative) coupling constant K_2 (K_1) oscillators. It is remarked Ref. [18] instead considered frustrated coupling of identical oscillators $\omega_i = \omega$, with a mixture of two link species; K_{ij} being either $-w$ or unity. In the actively competing model, depending on the sign of K_i, the stability of an oscillator at the velocity-balancing position is reversed and becomes either attractive or repulsive to the mean ordering $Z = Re^{i\Psi}$. Therefore, the oscillators are clustered in the phase circle into two groups that are separated roughly by an angle π. They can be either static or traveling. This leads to a rich phase transition diagram involving three different phases, namely incoherent, π and traveling wave phases [19, 20].

The passively competing Kuramoto model is written as

$$\dot{\theta}_i = \omega_i + \frac{1}{N}\sum_{j=1}^{N} K_j \sin(\theta_j - \theta_i), \tag{6.3}$$

where K_j follows the same distribution $f(K)$. Varying p from zero to unity linearly interpolates the mean coupling constant $\langle K \rangle$ between $K_1 < 0$ and $K_2 > 0$. At $p = 0$ all oscillators are repulsive, while at $p = 1$ all oscillators are attractive. The intrinsic frequency distribution $g(\omega)$ is assumed to be symmetric about zero. In this interaction form, each oscillator i interacts with the weighted (antiferromagnetic) influence of other oscillators. In this regard we call this model the passively competing Kuramoto model. For the passively competing Kuramoto model, it is more convenient and natural to define the weighted mean field order parameter [14, 138] as follows:

$$W(t) \equiv S(t)e^{i\Phi(t)} \equiv \frac{1}{N}\sum_{j=1}^{N} K_j e^{i\theta_j(t)}, \tag{6.4}$$

At this stage, it is remarked that the staggered order parameter and the conventional order parameter are in fact related to each other (6.42). The use of the staggered order parameter W transforms eq. (6.3) into the decoupled form.

$$\dot{\theta}_i = \omega_i + S(t)\sin(\Phi(t) - \theta_i), \tag{6.5}$$

where $S(t)$ is the magnitude of the staggered field and $\Phi(t)$ is the average phase of the order parameter $W(t)$. Notice that all oscillators are under a common mean field interaction strength $S(t)$, where the effect of competing disorder K_j is collectively coarse-grained. Particularly, the sign of effective interaction S is no longer directly proportional to the individual coupling K_j. This is in contrast to the actively competing model, where individual coupling K_i has a direct individual effect to the oscillator motion (6.2). Hence tiered synchronization patterns such as π or traveling wave is absent in the passively competing synchrnization. In case when $g(\omega)$ is unimodal, a previous study [138] showed that a continuous phase transi-

tion occurs when the mean coupling constant $\langle K \rangle \equiv \frac{1}{N}\sum_j K_j$ of the mixture reaches the value of the critical coupling strength K_c of the corresponding Kuramoto model. The onset of order $S(t)$ coincides with the onset of order $R(t)$. Therefore, a phase transition from the incoherent to coherent phase in the passively competing systems was characterized solely by the order parameter S. For such reasons, it was concluded in [138] that the passively competing generalization is rather a monotonous extension to the Kuramoto model. However, in particular for the hybrid critical behavior, distinct finite-size crossovers are noticed from the two models [13].

In the following sections, we consider actively competing and passively competing Kuramoto models with uniform natural frequency distribution $g(\omega)$, which undergo hybrid phase transition. Hereafter, we call our model the competing Winfree–Pazó model [9, 11, 17, 19]. Natural frequency ω and coupling constant K of an oscillator follow the probability distribution

$$g(\omega, K) = \frac{1}{2\gamma}\Theta(\gamma - |\omega|)\big[(1-p)\delta(K-K_1) + p\delta(K-K_2)\big], \tag{6.6}$$

where Θ represents the Heaviside step function.

6.2 Hybrid phase transition of actively competing model

A hybrid phase transition is a discontinuous transition that accompanies critical phenomena. Recent hybrid percolation model studies [22,34–36,43] have discovered that the system stays at a long-lasting metastable preparatory step on the way to an explosive transition, during which the so-called powder keg is accumulated [52]. In this regard, one may wonder if there exists a similar metastable state in a synchronization transition. However, the presence of a metastable state has been rarely highlighted in synchronization problems [60]. Here, we reveal that such an intermediate metastable state indeed exists on the way to a discontinuous synchronization transition near the hybrid critical point. Moreover, we show that this long-lasting metastable step can be understood as persisting circulation inside a metastable basin,

characterized by balancing between saddle points and stable fixed points.

The actively competing Kuramoto equation is written as

$$\dot{\theta}_i = \omega_i + \frac{K_i}{N}\sum_{j=1}^{N}\sin(\theta_j - \theta_i), \quad i = 1, 2, \cdots, N. \tag{6.7}$$

The synchronization transition is characterized by a complex order parameter

$$Z(t) \equiv R(t)e^{i\Psi(t)} \equiv \frac{1}{N}\sum_{j=1}^{N} e^{i\theta_j(t)}, \tag{6.8}$$

where R is the coherence of oscillators and ψ is the average phase. Plugging the definition of the complex order parameter into the Kuramoto equation leads to an effective decoupling of oscillators,

$$\dot{\theta}_i = \omega_i + K_i R\sin\left(\Psi - \theta_i\right), \quad i = 1, 2, \cdots, N. \tag{6.9}$$

After a suffciently long time, the system falls into a steady state, in which $Z(t) \simeq Re^{i\Omega t}$ with constant $R(t) = R$ and $\Omega(t) = \Omega = \Psi/t$. The synchronization order parameter R distinguishes coherent and incoherent phases. The coherent steady state of the competing model is characterized by a tiered synchronization of two groups of oscillators, the inhibitory and excitatory populations, separated by an angle Δ on the phase circle. When $\Delta = \pi$ (π–state), the two groups are balanced and the steady-state rotation $\Omega = \Psi/t$ is zero. When $\Delta \neq \pi$, the traveling wave order with $\Omega \neq 0$ emerges (see Fig. 6.1). Hence the C phase of the competing model is further distinguished into π and traveling wave phases by the traveling wave order parameter Ω. Overall, three phases are possible: incoherent ($R = 0$), π ($R \neq 0, \Omega = 0$), and traveling wave ($R \neq 0, \Omega \neq 0$) phases.

Notice stability of an oscillator at the velocity-balancing position of equation 6.9 relates to the sign of coupling constant K_i. A positive coupling $K_2 > 0$ oscillator is attracted towards the average phase ψ, while a negative coupling $K_1 < 0$ oscillator is drawn towards the antipod $\psi + \pi$ (Fig. 6.1). As a consequence, oscillators are tiered into two groups, each of which consists of K_1 or K_2 oscillators. The K_1 group in general is more widespread in angle,

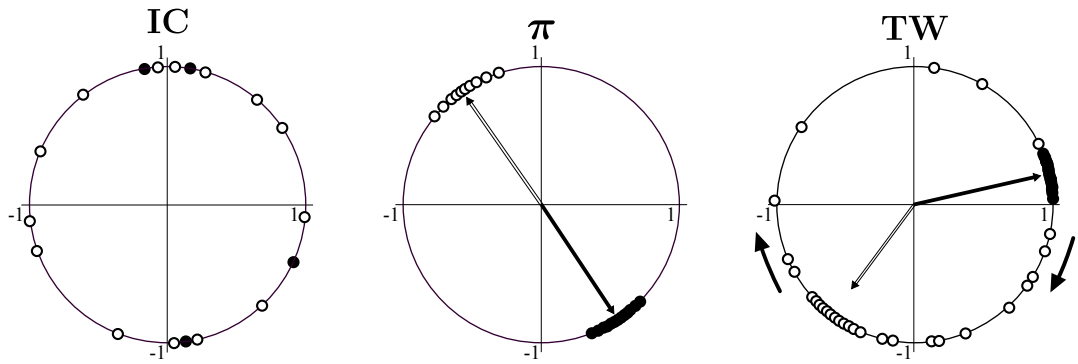

Figure 6.1: Schematic illustration of the incoherent, π, and traveling-wave states. Oscillators are plotted around the phase circle. Depending on the sign of coupling constant K_i, the stability of oscillator i at a force-balancing position is reversed. Each oscillator with $K_2 > 0$ denoted by $\bullet$ is attracted towards the mean phase ψ, while each oscillator with $K_1 < 0$ denoted by $\circ$ is attracted towards the antipod $\psi + \pi$. Hence, the oscillators are tiered into two groups in the π and traveling wave phases.

compared to the K_2 group, because each K_1 (or K_2) oscillator repulses (or attracts) all other oscillators.

In the π phase, the two groups are balanced at a separation angle π and stay fixed on the phase circle. In the traveling wave phase, a separation less than π is maintained, where the attractive K_2 group tries to catch up with the K_1 group while the repulsive K_1 group tries to keep the distance with the K_2 group. As a result, the two groups co-rotate at a common angular speed Ω.

Recall that the net interaction between every pair of ordinary Kuramoto oscillators was zero. It is a kind of action-reaction principle of the two-body interaction. Between a pair of K_1 and K_2 oscillators in the competing model, however, such principle does not hold. Not only the interaction strengths are different, but also the pull is in the same direction. In consequence, both K_1 and K_2 can run in the same direction. A nonvanishing net interaction, does not necessarily lead to a traveling wave, however. The traveling wave phase can emerge only if $Q \equiv |K_1|/K_2 < 1$, when the attraction of the K_2 group is larger than the repulsion of the K_1 group, otherwise a separation less than π is not maintainable. A mean field theory is followed as a first attempt to understand the emergence of traveling wave.

6.2.1 Emergence of the mean angular speed

In the traveling wave phase, the system also rotates at a nonzero mean angular speed $\langle\dot{\theta}\rangle$, although Ω is different from $\langle\dot{\theta}\rangle$. The mean angular speed of the two groups K_1 and K_2 and that of the total system are calculated as follows:

$$
\begin{aligned}
v_1 &\equiv \langle\dot{\theta}_j\rangle_1 \equiv \frac{1}{N_1}\sum_{j\in K_1}\left[\omega_j + \frac{K_1}{N}\sum_{k=1}^{N}\sin(\theta_k-\theta_j)\right] = p|K_1|R_1R_2\sin\Delta \\
v_2 &\equiv \langle\dot{\theta}_j\rangle_2 \equiv \frac{1}{N_2}\sum_{j\in K_2}\left[\omega_j + \frac{K_2}{N}\sum_{k=1}^{N}\sin(\theta_k-\theta_j)\right] = (1-p)K_2R_1R_2\sin\Delta \\
v &= pv_2 + (1-p)v_1 = p(1-p)(|K_1|+K_2)R_1R_2\sin\Delta
\end{aligned}
\tag{6.10}
$$

where $\langle e^{i\theta_j}\rangle_\alpha \equiv R_\alpha e^{i\Psi_\alpha}$ is the complex order parameter of each group $\alpha = 1, 2$, and $\Psi_1 - \Psi_2 \equiv \Delta$ is the group separation. $\langle\omega_j\rangle_1 = \langle\omega_j\rangle_2 = 0$ for $g(\omega)$ with even symmetry. Also $\langle\sin\theta_{12}\rangle \equiv \frac{1}{N_1N_2}\sum_{j\in K_1}\sum_{k\in K_2}\sin(\theta_j-\theta_k) = R_1R_2\sin(\psi_1-\psi_2) = R_1R_2\sin\Delta$. The summation counts only for inter-group interactions because the intra-group interactions pairwisely cancel up to zero. When $\Delta = \pi$, $\sin\Delta$ is zero and therefore $v_1 = v_2 = v = 0$. However, in the traveling wave phase, Δ is less than π and the angular speed v is nonzero. Now for each group,

$$
\psi_\alpha = \arctan\left[\frac{\langle\sin\theta_i\rangle_\alpha}{\langle\cos\theta_i\rangle_\alpha}\right] = \arctan\left[\frac{\langle\theta_i\rangle_\alpha - \langle\theta_i^3\rangle_\alpha/3! + \cdots}{1 - \langle\theta_i^2\rangle_\alpha/2! + \cdots}\right]. \tag{6.11}
$$

As a mean field approximation, we let $\Delta \approx \langle\theta_{12}\rangle \equiv \frac{1}{N_1N_2}\sum_{j\in 1}\sum_{k\in 2}(\theta_j-\theta_k)$ and $\psi_\alpha \approx \langle\theta_i\rangle_\alpha(1+(\langle\theta_i^2\rangle_\alpha - \langle\theta_i\rangle_\alpha^2)/2!) \approx \langle\theta_i\rangle_\alpha$ for each group, i.e., $R_1 \approx R_2 \approx 1$. The approximation is valid as long as the distribution angle of each group is small. Let $\Delta \equiv \pi - \delta$. Assuming that the amplitude parts are stable, the phase dynamics of δ is given as

$$
\dot{\delta} \approx -\langle\dot{\theta}_{12}\rangle = -(V_1 - V_2) = -(p-p_u)(|K_1|+K_2)R_1R_2\sin\delta, \tag{6.12}
$$

where $p_u = 1/(Q+1)$. Notice that for $p > p_u$, the π state ($\delta = 0$) is a stable solution. The stability of the π state is lost at $p = p_u$ as p is decreased, suggesting that a new solution with $\Delta \neq \pi$ (traveling wave) can possibly emerge for $p < p_u$. Using the self-consistency equation, it is found that the traveling wave solution indeed exists in some interval $[p_\ell, p_u]$. However, this lower bound p_ℓ is not determined from the mean field calculation.

6.2.2 Self-consistency equation

Now we construct the self-consistency equation of the actively competing Kuramoto model and obtain the steady-state order parameter solutions (R, Ω). Also the solutions are compared with the numerical simulations results. Unexpectedly, a rich phase diagram involving the hybrid synchronization transition is obtained, as shown in Fig. 6.5. The self-consistency equation is written as follows [21, 139]:

$$R = \int_{-\infty}^{\infty} dK d\omega g(K,\omega) \overline{e^{\mathrm{i}\phi}} \tag{6.13}$$

$$= \int_{-\infty}^{\infty} dK \int_{\Omega-|K|R}^{\Omega+|K|R} d\omega g(K,\omega)\ \mathrm{sgn}(K) \sqrt{1-\left(\frac{\omega-\Omega}{KR}\right)^2}$$

$$+ \mathrm{i} \int_{-\infty}^{\infty} dK \int_{\text{drifting}} d\omega \frac{g(K,\omega)}{KR} \left[\omega - \Omega - \mathrm{sgn}(\omega-\Omega)\sqrt{(\omega-\Omega)^2 - (KR)^2}\right], \tag{6.14}$$

where $g(K,\omega)$ is the distribution of disorders of the actively competing Kuramoto model, and $\mathrm{sgn}(x)$ denotes the sign $\pm$ of the argument x. The imaginary part on the right hand side of the complex self-consistency equation (6.14) has to vanish, because R in the left hand side is real-valued. Usually in the ordinary Kuramoto model with symmetric $g(\omega)$, Ω is given as the mean intrinsic frequency of the system and the traveling wave order is absent. In that case only the real part of the equation is needed to be solved. Indeed, for symmetric g with respect to $\omega = \Omega$, one can easily check that the integrand of the imaginary part becomes odd in $\omega - \Omega$ and hence it vanishes to zero. To obtain a traveling wave solution, however, both real and imaginary parts of the equation (6.14) must be solved simultaneously for R and Ω.

6.2.3 Incoherent and π solutions

Notice if $\Omega = 0$, equation (6.14) has vanishing imaginary parts and hence it is greatly simplified as

$$R = -(1-p)\int_{-|K_1|R}^{|K_1|R} d\omega g(\omega)\sqrt{1-\left(\frac{\omega}{|K_1|R}\right)^2} + p\int_{-K_2R}^{K_2R} d\omega g(\omega)\sqrt{1-\left(\frac{\omega}{K_2R}\right)^2}, \tag{6.15}$$

where $g(\omega) = \frac{1}{2\gamma}\theta(\gamma - |\omega|)$. The vanishment is owing to the oddity of integrand in ω. Equation (6.15) corresponds to the real part of the complex equation (6.14) and it solves all incoherent and π states, which are $\Omega = 0$. Moreover, (6.15) is now analytically solvable and it can be used to characterize incoherent to π transition.

In the following, analytic solutions of Eq. (6.15) are obtained for different parameter values. Note that the integration is evaluated differently depending on the relative sizes of $|K_1|R$, K_2R and γ. i) For $Q \equiv |K_1|/K_2 < 1$, γ can fall in one of the three ranges $(0, |K_1|R]$, $(|K_1|R, K_2R]$, and (K_2R, ∞). ii) For $Q > 1$, γ can fall in one of the three ranges $(0, K_2R]$, $(K_2R, |K_1|R]$, and $(\,|K_1|R, \infty)$.

6.2.4 The self-consistency solution for incoherent and π states

Depending on the relative coupling strength of the two competing species $Q = |K_1|/K_2$, we find a supercritical type hybrid phase transition ($Q < 1$) or a subcritical type hybrid phase transition ($Q > 1$) as illustrated schematically in Fig. 6.2.

6.2.5 Supercritical hybrid phase transition

The integration of Eq. (6.15) when $Q < 1$ leads to

$$R = \begin{cases} -\frac{1-p}{2\gamma}\frac{\pi}{2}|K_1|R + \frac{p}{2\gamma}\frac{\pi}{2}K_2 R & \text{for } R < \frac{\gamma}{K_2} < \frac{\gamma}{|K_1|}, \\ -\frac{1-p}{2\gamma}\frac{\pi}{2}|K_1|R + p\Big(\frac{K_2 R}{2\gamma}\arcsin\frac{\gamma}{K_2 R} + \frac{1}{2}\sqrt{1-\big(\frac{\omega}{K_2 R}\big)^2}\Big) & \text{for } \frac{\gamma}{K_2} < R < \frac{\gamma}{|K_1|}, \\ -(1-p)\Big(\frac{|K_1|R}{2\gamma}\arcsin\frac{\gamma}{|K_1|R} + \frac{1}{2}\sqrt{1-\big(\frac{\omega}{|K_1|R}\big)^2}\Big) & \\ \quad + p\Big(\frac{K_2 R}{2\gamma}\arcsin\frac{\gamma}{K_2 R} + \frac{1}{2}\sqrt{1-\big(\frac{\omega}{K_2 R}\big)^2}\Big) & \text{for } \frac{\gamma}{K_2} < \frac{\gamma}{|K_1|} < R. \end{cases} \tag{6.16}$$

Note the incoherent ($R = 0$) state is a trivial solution of the above self-consistency equation. The remaining nontrivial solutions correspond to π states. After inverting the above equations and solving for p, we obtain the inverse function of the order parameter curve $p(R)$ as

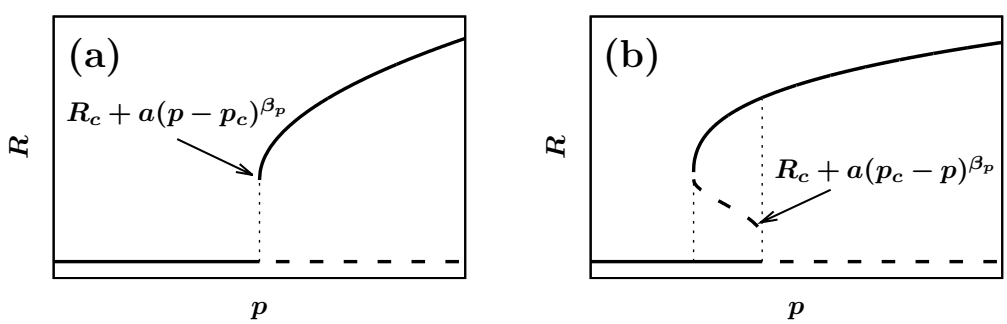

Figure 6.2: Schematic plots of the hybrid phase transition and the first-order transition with hysteresis: (a) a hybrid phase transition with $\beta_p = 2/3$ occurs for $Q < 1$, while (b) a first-order transition with hysteresis occurs for $Q > 1$, in which an unstable hybrid phase transition with $\beta_p = 2/3$ is hidden. Thick solid and dashed lines denote stable and unstable self-consistency solutions, and the thin dotted vertical lines denote jumps at the transition points.

follows:

$$p=\begin{cases}\frac{|K_1|+4\gamma/\pi}{|K_1|+K_2} & \text{for } 0<R<\frac{\gamma}{K_2},\\ \frac{(\pi|K_1|+4\gamma)R}{\pi|K_1|R+2\gamma\sqrt{1-(\frac{\gamma}{K_2R})^2}+2K_2R\arcsin(\frac{\gamma}{K_2R})} & \text{for } \frac{\gamma}{K_2}<R<\frac{\gamma}{|K_1|},\\ \frac{\gamma\sqrt{1-(\gamma/|K_1|R)^2}+|K_1|R\arcsin\left(\frac{\gamma}{|K_1|R}\right)+2\gamma R}{\gamma\sqrt{1-(\frac{\gamma}{|K_1|R})^2}+|K_1|R\arcsin\left(\frac{\gamma}{|K_1|r}\right)+\gamma\sqrt{1-(\frac{\gamma}{K_2R})^2}+K_2R\arcsin\left(\frac{\gamma}{K_2R}\right)} & \text{for } \frac{\gamma}{K_2}<\frac{\gamma}{|K_1|}<R.\end{cases} \tag{6.17}$$

Numerical solutions of $R(p)$ from the self-consistency equations are represented as solid and dashed curves in Fig 6.3. Solid (dashed) curves are stable (unstable) through the linear stability analysis [139], which will be discussed later. The order parameter curve $R(p)$ shows a discontinuous jump of size R_c at the critical point p_c.

$$\begin{aligned}p_c&=\frac{|K_1|+4\gamma/\pi}{|K_1|+K_2}=\frac{Q+\frac{4\gamma}{\pi K_2}}{Q+1},\\ R_c&=\gamma/K_2.\end{aligned} \tag{6.18}$$

Expanding the intermediate branch $\frac{\gamma}{|K_1|}<R<\frac{\gamma}{K_2}$ in powers of $\epsilon\equiv(R-R_c)/R_c$ after the jump gives:

$$\begin{aligned}p&=\frac{(\pi|K_1|+4\gamma)R}{\pi|K_1|R+2\gamma\sqrt{1-\left(\frac{\gamma}{K_2R}\right)^2}+2K_2R\arcsin\left(\frac{\gamma}{K_2R}\right)}\\ &\approx\frac{(\pi|K_1|+4\gamma)R_c(1+\epsilon)}{\pi|K_1|R_c(1+\epsilon)+2\gamma\left(\sqrt{2\epsilon}-\frac{3\epsilon^{3/2}}{2\sqrt{2}}+O(\epsilon^{5/2})\right)+2\gamma(1+\epsilon)\left(\frac{\pi}{2}-\sqrt{2\epsilon}+\frac{5\epsilon^{3/2}}{6\sqrt{2}}+O(\epsilon^{5/2})\right)}\\ &\approx p_c+\frac{8\sqrt{2}}{3\pi}\frac{p_c}{(Q+1)}\epsilon^{3/2}+O(\epsilon^{5/2}).\end{aligned} \tag{6.19}$$

Hence when $Q<1$, a supercritical hybrid phase transition occurs, for which the behavior of the order parameter is expressed near the hybrid critical point $p_c=[Q+4\gamma/(\pi K_2)]/(Q+1)$

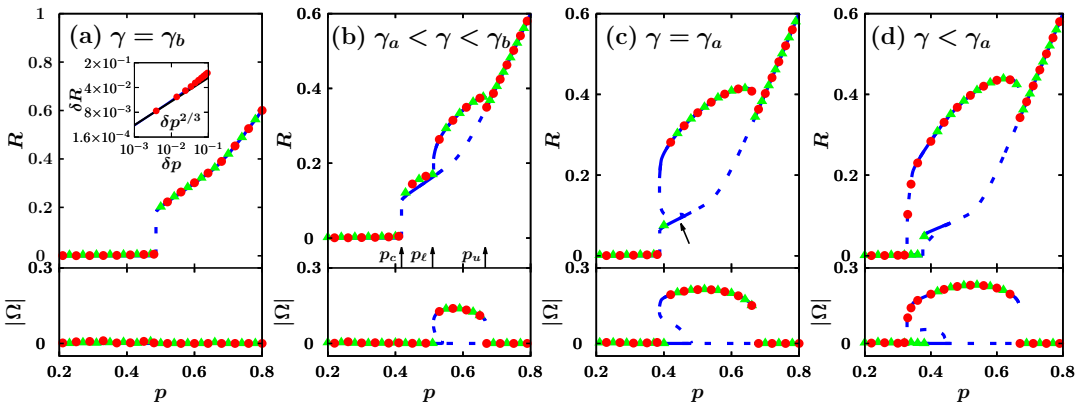

Figure 6.3: Diverse types of synchronization transitions for $Q = 0.5$ and various γ. Green triangles and red circles denote data points of $R(p)$ and $|\Omega(p)|$ obtained from simulations starting from the incoherent (IC) and coherent (C) initial states, respectively. Solid (dashed) blue curves are self-consistency solutions representing stable(unstable) states, according to the stability criterion presented in the main text. In (a), a hybrid phase transition occurs with the critical exponent $\beta_p = 2/3$ at p_c. A close check of the exponent value is shown in the inset. The black line guides a slope of $2/3$. (b) The traveling wave (TW) phase emerges at γ_b and exists in the range $[p_\ell, p_u]$. When $\gamma_a < \gamma < \gamma_b$, IC $\rightsquigarrow \pi \rightarrow$ TW $\rightarrow \pi$ occur with increasing p. (c) At $\gamma = \gamma_a, p_c = p_\ell$; thus, IC $\dashrightarrow$ TW $\rightarrow \pi$ occur. The part of the π line (indicated by arrow) that is stable according to the criterion is actually metastable. (d) When $\gamma < \gamma_a$ ($\gamma = 0.05$), $p_\ell < p_c < p_u$. R jumps from the IC state to the TW state, and a hysteresis occurs between the IC and TW states at $[p_\ell, p_c]$, where IC $\dashrightarrow$ TW $\rightarrow \pi$ occurs. Different types of arrows distinguish the types of phase transitions: continuous ($\rightarrow$), discontinuous ($\dashrightarrow$), and hybrid ($\rightsquigarrow$). A hysteresis behavior appears in (d), while it does not in (b) and (c).

as

$$R(p) = \begin{cases} 0 & \text{for } p < p_c \\ R_c + a(p - p_c)^{\beta_p} & \text{for } p \geq p_c \end{cases} \tag{6.20}$$

where $R_c = \gamma/K_2$ and with a noninteger exponent $\beta_p = 2/3$. Notice at p_c, the competing system has a mean coupling strength

$$\langle K \rangle_c = (1 - p_c)K_1 + p_c K_2 = \frac{4\gamma}{\pi}, \tag{6.21}$$

which is equivalent to the critical coupling strength $K_c = 2/\pi g(0) = 4\gamma/\pi$ for the ordinary Kuramoto model phase transition [9, 11]. Also the coincidence with the critical exponent value $\beta_K = 2/3$ should be noticed. This is rather natural because the ordinary Kuramoto model corresponds to a particular case of the competing Kuramoto model with $p = 1$.

Thus far, the incoherent (IC) and π states and the transitions between the two phases are obtained exactly for when $Q < 1$. Traveling wave (TW) solutions, however, could not be obtained in a closed form. Instead we solve the complex self-consistency equation numerically. Solving the real and imaginary parts of the self-consistency equation simultaneously (6.14), we obtain $R(p)$ and $\Omega(p)$. Numerical solutions of $R(p)$ and $|\Omega(p)|$ are shown in Fig. 6.3. There exist two characteristic values γ_a and γ_b. i) For $\gamma \geq \gamma_b$, the transition IC $\rightsquigarrow$ π state at p_c as shown in Fig. 6.3(a). ii) For $\gamma \leq \gamma_b$, Traveling wave phase appears in the range $[p_\ell, p_u]$ in Fig. 6.3(b)$-$Fig. 6.3(d). iii) Particularly when $\gamma_a < \gamma < \gamma_b$, the transitions IC $\rightsquigarrow$ π $\rightarrow$ TW $\rightarrow$ π occur successively with increasing p (Fig. 6.3(b)). Here we use the symbols ($\rightarrow$), (- - $\rightarrow$), and ($\rightsquigarrow$) to represent continuous, discontinuous and hybrid types of synchronization transition. iv) At $\gamma = \gamma_a, p_c = p_\ell$; thus, IC - - $\rightarrow$ TW $\rightarrow$ π occur successively (Fig. 6.3(c)). v) When $\gamma < \gamma_a$, $p_\ell < p_c < p_u$. R jumps from incoherent to traveling wave state, and a hysteresis occurs between the incoherent and traveling wave states in the interval $[p_\ell, p_c]$, where IC - - $\rightarrow$ TW $\rightarrow$ π occurs (Fig. 6.3(d)). The presence of traveling wave order can be recognized from the plot in the bottom row of Fig. 6.3, in which the order parameter $|\Omega(p)|$ of traveling wave state is plot as a function of p.

6.2.6 Subcritical hybrid bifurcation

When $Q > 1$, the critical exponent β_p remains the same while the post-jump branch has the opposite direction and becomes unstable (Fig 6.3(a)). The transition from incoherent phase to π phase is first-order and exhibits a hysteresis curve in the region between p_c and $p_{c,b}$. Notice that this subcritical hybrid phase transition (bifurcation) is different from the usual subcritical Hopf bifurcation. The unstable lines in Fig. 6.4 does not continuously decrease to zero at p_c, but instead has a drop of size $\gamma/|K_1|$.

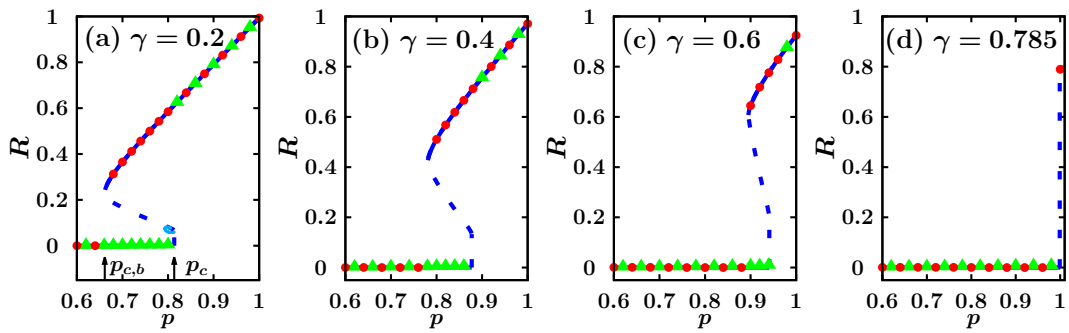

Figure 6.4: Plot of the order parameter versus p for $Q = 3$ and various γ: (a) $\gamma = 0.2$, (b) $\gamma = 0.4$, (c) $\gamma = 0.6$, and (d) $\gamma_h = \pi K_2/4 \approx 0.785$. A first-order transition and hysteresis occur between p_c and $p_{c,b}$. As γ is increased, $p_{c,b}$ and p_c are increased at different rates and hysteresis range is reduced. The unstable solution contains a discontinuous jump and a hidden hybrid critical exponent $\beta_p = 2/3$. Notice also that in (d) at $\gamma = \gamma_h = \pi K_2/4 \approx 0.785$, $p_c^b = p_c = 1$ and $R_c = \gamma/K_2$. At $p = 1$, the competing model reduces to the ordinary Kuramoto model [9, 11]. For larger values of γ beyond γ_h, the system is incoherent because the value of K_2 is subcritical i.e. $K_2 < K_c \equiv 4\gamma/\pi$, where K_c is the critical coupling strength of the ordinary Kuramoto model.

Integration of Eq. (6.15) when $Q > 1$ leads to

$$R = \begin{cases} -\frac{1-p}{2\gamma}\frac{\pi}{2}|K_1|R + \frac{p}{2\gamma}\frac{\pi}{2}K_2 R & \text{for } R < \frac{\gamma}{|K_1|} < \frac{\gamma}{K_2} \\ -(1-p)\left(\frac{|K_1|R}{2\gamma}\arcsin\frac{\gamma}{|K_1|R} + \frac{1}{2}\sqrt{1-\left(\frac{\omega}{|K_1|r}\right)^2}\right) + \frac{p}{2\gamma}\frac{\pi}{2}K_2 R & \text{for } \frac{\gamma}{|K_1|} < R < \frac{\gamma}{K_2} \\ -(1-p)\left(\frac{|K_1|R}{2\gamma}\arcsin\frac{\gamma}{|K_1|R} + \frac{1}{2}\sqrt{1-\left(\frac{\omega}{|K_1|R}\right)^2}\right) & \\ \quad + p\left(\frac{K_2 R}{2\gamma}\arcsin\frac{\gamma}{K_2 R} + \frac{1}{2}\sqrt{1-\left(\frac{\omega}{K_2 R}\right)^2}\right) & \text{for } \frac{\gamma}{|K_1|} < \frac{\gamma}{K_2} < R. \end{cases} \tag{6.22}$$

Taking a similar step, we obtain that

$$p = \begin{cases} \frac{|K_1|+4\gamma/\pi}{|K_1|+K_2} & \text{for } 0 < R < \frac{\gamma}{|K_1|} \\ \frac{2R\gamma+\gamma\sqrt{1-(\frac{\gamma}{|K_1|R})^2}+|K_1|R\arcsin\left(\frac{\gamma}{|K_1|R}\right)}{\frac{\pi K_2 R}{2}+\gamma\sqrt{1-(\frac{\gamma}{|K_1|R})^2}+|K_1|R\arcsin\left(\frac{\gamma}{|K_1|R}\right)} & \text{for } \frac{\gamma}{|K_1|} < R < \frac{\gamma}{K_2} \\ \frac{\gamma\sqrt{1-(\frac{\gamma}{|K_1|R})^2}+|K_1|R\arcsin\left(\frac{\gamma}{|K_1|R}\right)+2\gamma R}{\gamma\sqrt{1-(\frac{\gamma}{|K_1|R})^2}+|K_1|R\arcsin\left(\frac{\gamma}{|K_1|R}\right)+\gamma\sqrt{1-(\frac{\gamma}{K_2 R})^2}+K_2 R\arcsin\left(\frac{\gamma}{K_2 R}\right)} & \text{for } \frac{\gamma}{|K_1|} < \frac{\gamma}{K_2} < R. \end{cases} \tag{6.23}$$

As $R \to R_c = \gamma/|K_1|$, with $\epsilon = (R_c - R)/R_c$

$$\begin{aligned} p &= \frac{2R\gamma + \gamma\sqrt{1-(\frac{\gamma}{|K_1|R})^2} + |K_1|R\arcsin\left(\frac{\gamma}{|K_1|R}\right)}{\frac{\pi K_2 R}{2} + \gamma\sqrt{1-(\frac{\gamma}{|K_1|R})^2} + |K_1|R\arcsin\left(\frac{\gamma}{|K_1|R}\right)} \\ &\approx \frac{2\gamma R_c(1+\epsilon) + \gamma\left(\sqrt{2\epsilon} - \frac{3\epsilon^{3/2}}{2\sqrt{2}} + \frac{23\epsilon^{5/2}}{16\sqrt{2}} + \cdots\right) + \gamma(1+\epsilon)\left(\frac{\pi}{2} - \sqrt{2\epsilon} + \frac{5\epsilon^{3/2}}{6\sqrt{2}} - \frac{43\epsilon^{5/2}}{80\sqrt{2}} + \cdots\right)}{\frac{\pi K_2}{2}R_c(1+\epsilon) + \gamma\left(\sqrt{2\epsilon} - \frac{3\epsilon^{3/2}}{2\sqrt{2}} + \frac{23\epsilon^{5/2}}{16\sqrt{2}} + \cdots\right) + \gamma(1+\epsilon)\left(\frac{\pi}{2} - \sqrt{2\epsilon} + \frac{5\epsilon^{3/2}}{6\sqrt{2}} - \frac{43\epsilon^{5/2}}{80\sqrt{2}} + \cdots\right)} \\ &\approx \frac{\pi|K_1| + 4\gamma}{\pi|K_1| + \pi K_2} - \frac{8\sqrt{2}(\pi K_2 - 4\gamma)\gamma R_c}{3\pi^2(K_2 R_c + \gamma)^2}\epsilon^{3/2} + O(\epsilon^{5/2}). \end{aligned} \tag{6.24}$$

We remark that our result for the transition from incoherent to π when $Q > 1$ contains a discontinuous gap between the incoherent and an unstable solution as shown in Fig. 6.4. Here the unstable solution follows $(R - R_c) \sim (p_c - p)^{2/3}$, which gives the same exponent $\beta_p = 2/3$. However, notice it has a reversed direction, towards $p < p_c$. This $Q > 1$ hybrid transition is not noticed in the simulations, because it corresponds to an unstable branch. The discontinuous transition for $Q > 1$ shows a hysteresis curve which starts at $p_{c,f} = p_c$ in the forward direction and at $p_{c,b}$ in the backward direction, where $p_{c,f}$ is given as

$$p_{c,f} = \frac{|K_1| + 4\gamma/\pi}{|K_1| + K_2} = \frac{Q + \frac{4\gamma}{\pi K_2}}{Q+1} = p_c, \tag{6.25}$$

and $p_{c,b}$ and $R_{c,b}$ are determined numerically from the equation, $dp/dR = 0$, i.e.

$$\frac{d}{dR}\left(\frac{\gamma\sqrt{1-(\frac{\gamma}{|K_1|R})^2}+|K_1|R\arcsin\left(\frac{\gamma}{|K_1|R}\right)+2\gamma R}{\gamma\sqrt{1-(\frac{\gamma}{|K_1|R})^2}+|K_1|R\arcsin\left(\frac{\gamma}{|K_1|R}\right)+\gamma\sqrt{1-(\frac{\gamma}{K_2R})^2}+K_2R\arcsin\left(\frac{\gamma}{K_2R}\right)}\right)=0. \tag{6.26}$$

6.2.7 Phase diagram involves three phases

Phase diagrams of synchronization transitions in the (p,γ) plane for various Q values are presented in Fig. 6.5. In Fig. 6.5 (a$-$b), we consider the case $Q > 1$. The phase diagrams contain IC and π phases, and the hysteresis zone **H** of the two phases. Both types of dashed lines represent discontinuous transitions, but the forward transition from IC to π phase is hybrid. At $Q = 1$ in Fig. 6.5 (b), the hysteresis vanishes. The $p = 1$ line corresponds to the phase diagram of the WP model, and a hybrid synchronization transition occurs at $\gamma_h \approx 0.78$ (denoted by $\bullet$) of the WP model [9,11]. In Fig. 6.5 (c$-$f), we consider the case $Q < 1$. Part of the region of π state is occupied by the TW phase. The hysteresis region reappears between IC and TW. As the ratio Q is decreased, the interval $[p_\ell, p_u]$ of TW state becomes broader. It is remarked that our result for the actively competing Kuramoto model with uniform intrinsic frequency distribution is in stark contrast to the Lorentzian case, which exhibits continuous transition or discontinuous transition with absence of critical behaviors or long-lasting metastable states [19].

6.2.8 Linear stability of the self-consistency solutions

It is intriguing to check the stability of the self-consistency solution. To perform this task, the so-called empirical stability criterion proposed in Ref. [139] was checked on the competing

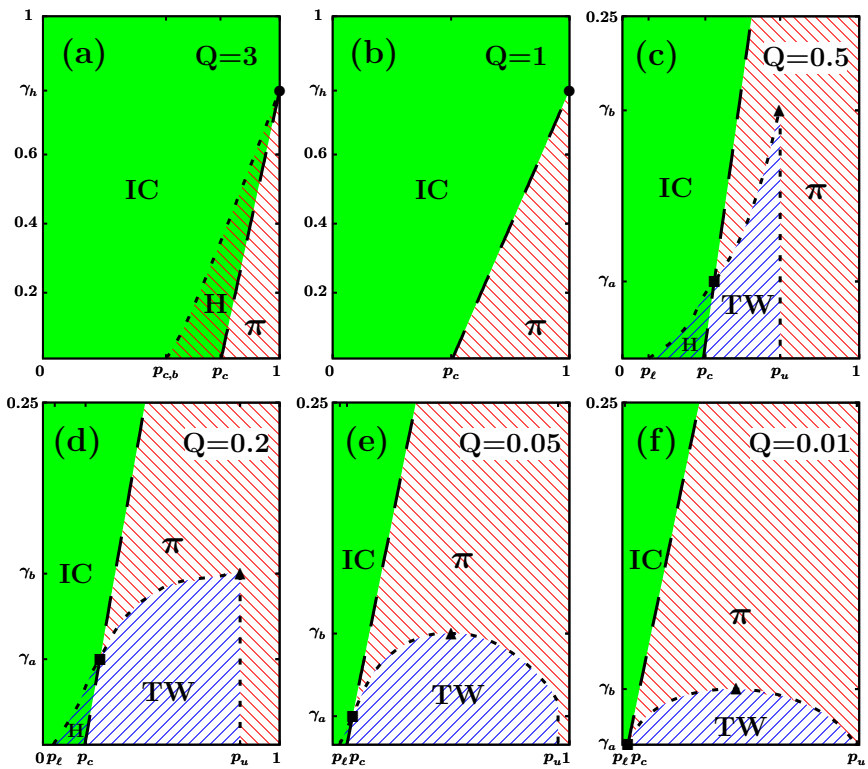

Figure 6.5: Phase diagram of synchronization transitions in the (p, γ) plane for various Q. p is the fraction of oscillators with positive coupling K_2 and γ is the half width of the uniform distribution $g(\omega)$. (a)$-$(b) When $Q > 1$, the phase diagrams contain IC and π phases, and the hysteresis zone **H** of the two phases. Both types of dashed lines represent discontinuous transitions, but the forward transition from incoherent (IC) to π phase is hybrid. At $Q = 1$, the hysteresis vanishes. The $p = 1$ line corresponds to the phase diagram of the WP model, and the symbol $\bullet$ at $\gamma_h = \pi K_2/4 \approx 0.78$ denotes the hybrid critical synchronization transition point for $K_2 = 1$ [9, 11]. (c)$-$(f) When $Q < 1$, some part of π state is replaced by traveling wave (TW) phase. The hysteresis region reappears between IC and TW. The symbols $\blacktriangle$ and $\blacksquare$ represent critical points across which different types of phases or phase transitions emerge.

model. The stability matrix $\hat{S}$ of Ref. [139] is reproduced as follows:

$$\begin{aligned}\begin{pmatrix}\dot{\delta R}\\ \dot{\delta\psi}\end{pmatrix} &= A\begin{pmatrix}(\partial_R F_R)-1 & R^2\partial_\Omega F_R\\ R^{-1}\partial_R F_\Omega & R\partial_\Omega F_\Omega\end{pmatrix}\begin{pmatrix}\delta R\\ \delta\psi\end{pmatrix}\\ &\equiv A\hat{S}\begin{pmatrix}\delta R\\ \delta\psi\end{pmatrix} \qquad (6.27)\end{aligned}$$

$$\begin{aligned}F_R(R,\Omega) &\equiv \int_{\text{locked}} dK d\omega g(\omega,K)\sqrt{1-(\omega/KR)^2}\\ F_\Omega(R,\Omega) &\equiv \int_{\text{drifting}} dK d\omega g(\omega,K)\sqrt{(\omega/KR)^2-1} \qquad (6.28)\end{aligned}$$

where F_R and F_Ω correspond to the real and imaginary parts of the self-consistent order parameter. The system is (empirically) stable if and only if $\text{tr}(\hat{S}) < 0$ and $\det(\hat{S}) > 0$. The result is presented by the blue solid (stable) and dashed (unstable) curves in Figs. 6.3. Our numerical result suggests that this linear stability criterion is partly fulfilled; some portions of the "stable" π curve are not covered by the simulation data points in the long-time limit. Interestingly, the order parameter stays for quite a long time at these uncovered parts, before it finally settles down in the stable stationary line occupied by the symbols in Figs. 6.3(d)–6.3(e). These parts uncovered by simulation data are not stable but metastable. Fig. 6.6(a) shows the dynamic phase transition just above the hybrid critical point p_c; a tiered synchronization transition occurs from the incoherent phase to the traveling wave phase through a long-lasting metastable π phase. The order parameter R exhibits large temporal and sample-to-sample fluctuations in this metastable interval. As p is increased further, the fluctuations decrease and the metastable period becomes shorter (Figs. 6.6(c) and (d)). Subsequently, the metastability is lost and the synchronization transition to the traveling wave state occurs directly. These behaviors terminate at p_u.

6.2.9 Metastable state en route to traveling-wave synchronization state

The empirical linear flows given by Eq. (6.28) around each of the steady-state solutions (R,Ω) are shown in Figs. 6.7(b)–6.7(d). We remark that all traveling wave (TW) solutions

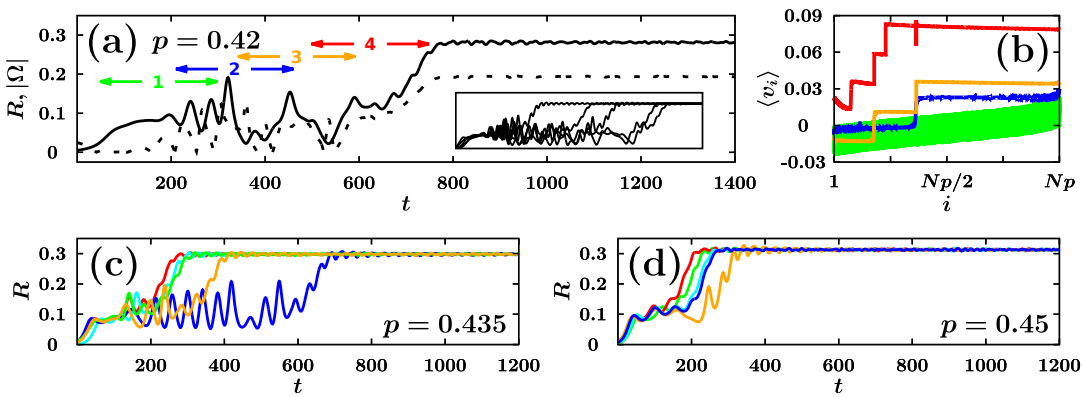

Figure 6.6: Tiered synchronization transition from the incoherent state to traveling wave state through the metastable π state. $R(t)$ was obtained at various p for the system size $N = 25\,600$, $Q = 0.5$, and $\gamma = 0.064$. (a) At $p = 0.42$, the traveling wave state appears as the steady state, and the state does as metastable. The solid and dashed lines correspond to $R(t)$ and $|\Omega(t)|$, respectively. Note that both the temporal and sample-to-sample (inset) fluctuations of R are large during the metastable period. In (b), the velocities of K_2 oscillators are averaged over each specified time interval, as indicated by the corresponding colors and cluster numbers in (a). The oscillators are indexed in ascending order of the intrinsic frequencies. We find several intermediate states with different numbers of clusters composed of oscillators with similar velocities. The number of clusters increases as the stages proceed. In (a), (c), and (d), as p is increased, the metastable period becomes shorter. Subsequently, the traveling wave state is reached shortly.

in Figs. 6.7(b) and 6.7(c) exist in pairs owing to the symmetry $\Omega \leftrightarrow -\Omega$. The red circle in Fig. 6.7(b) represents a TW stable point, the green circle in Fig. 6.7(c) represents a TW saddle point, and the red circle in Fig. 6.7(d) represents a π state with neutral stability. In Fig. 6.7(d), the eigenvalue in the Ω direction is extremely small compared with that of the R direction. Thus, the corresponding eigenvector in the vertical Ω direction can be effectively understood as a $\dot{\Omega} \approx 0$ nullcline. The dotted blue line in Fig. 6.7(a) and the blue line in Fig. 6.7(e) correspond to a trajectory $(R(t), \Omega(t))$ realized from simulation. In Fig. 6.7(e), the system passes by the π state of Fig. 6.7(d) and is then attracted by the saddle point of Fig. 6.7(c), forming unstable oscillations. It stays for a long time in the metastable basin bounded by the Ω nullclines and the saddle point. After escaping from the region, the dynamics flows immediately into the stable TW point. We remark that this trajectory is in fact a two-dimensional projection of a higher-dimensional dynamics and all other degrees of freedom do not vanish, inducing dynamic noise, until the stable steady TW is finally reached posterior to the escapement.

Numerical simulations are performed using the fourth-order Runge–Kutta method with $\Delta t = 0.01$. The number of oscillators is $N = 25\,600$ and total runtimes are over $t = 10^4$ s, sufficiently longer than the transient periods. Fluctuations in R and Ω at the stationary state were averaged out over the last 10% of total runtime. The stationary state may additionally depend on the initial coherence, especially in the hysteresis zone. Oscillator phases are randomly assigned either in the range $[0, 2\pi]$ or $[0, \pi/100]$, corresponding to the initially coherent or incoherent state. Natural frequencies of oscillators with $K_1 < 0$ and $K_2 > 0$ are regularly sampled between $[-\gamma, \gamma]$. K_2 is set to unity for convenience, leading to $K_1 = -Q$.

The two-step jump transition of Figs. 6.6 and 6.7(a) near the hybrid critical point (p_c, γ_t) closely resembles those observed in the percolation on interdependent networks [22, 34], k-core percolation [35, 36] and the two-step contagion model [43] near the critical point of the hybrid percolation transition. In those systems, the order parameters also show a long-lasting plateau with large fluctuations, as we observed in the metastable states of the competing Kuramoto model. During this lengthy period, the system accumulates a so-called powder

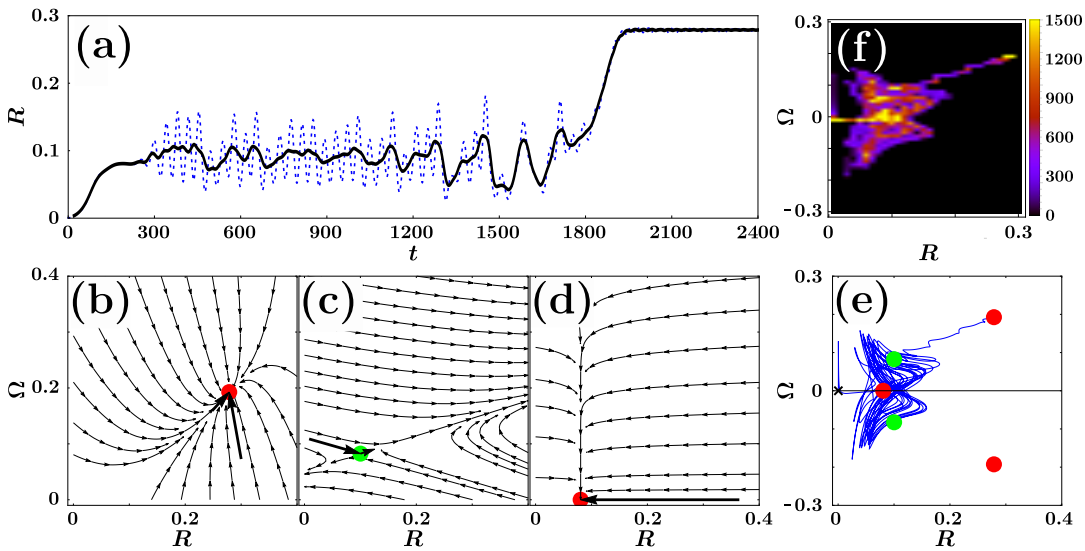

Figure 6.7: The flow of the order parameter in the two-step synchronization transition. (a) Plot of blue dotted curve $R(t)$ vs t at $p = 0.418$. The time-averaged black curve $\langle R \rangle$ is obtained using a sliding 40-s time window centered at each t with a window step of 1 s. (b)–(d) The linearized flow in the (R, Ω) plane. Two stable points of π and TW states are represented by red circles, and a saddle point of the TW state is shown in green. (e) An actual flow is obtained from simulations. $\boldsymbol{x}$ represents the starting point. (f) Frequencies of the dynamic flow passing through each state in the phase space. A few states (yellow) are active throughout the flow.

keg for the later explosive transition [43, 52]. This feature is also similar to the accumulation of similar-size clusters near the transition point of the restricted percolation model [49, 51]. During the metastable period of the competing Kuramoto model, the excitatory K_2 oscillators form a number of velocity clusters, i.e., clusters with similar velocities, when averaged over short time intervals, as shown in Fig. 6.6(b). The number of clusters discretely increases as the dynamics proceeds. However, the divisions into small K_2 clusters are transient. Eventually, those clusters merge into the largest cluster and become monolithic in the traveling wave state, whereas the inhibitory K_1 clusters break off and become liquid. It would be interesting to find out whether those K_2 clusters play an equivalent role as a time bomb that sets off an abrupt escapement of the metastable basin.

6.2.10 A potential application to brain

The competing synchronization model may have potential applications to the recovery dynamics of human consciousness from anesthetic-induced unconsciousness [140, 141]. Inhibitory anesthetics such as γ-aminobutyric acid hinder cortical synchronization and the brain in turn loses its ability to integrate information, vigilance, and responsiveness [140]. Recent electroencephalogram (EEG) experiments have revealed that the power spectrum of the cortical local field potentials during the conscious state peak at a certain intrinsic frequency [141]. This feature may be interpreted as an indicator of the traveling wave synchronization in the competing model. The consciousness recovery dynamics of the anesthetic-induced brain passes through a sequence of several discrete activity states. Moreover, transitions between those metastable states are abrupt [141]. A series of studies have previously modeled the anesthetic recovery using Kuramoto-type synchronization models [142, 143]. However, our model further involves the metastable dynamic restoration of coherence by the discrete merging of velocity clusters. More interestingly, it deals with excitatory and inhibitory neural interactions through a controllable parameter p and the recovery period is reduced by increasing p beyond a threshold p_c, corresponding to the clinical findings that the recovery time is reduced with lesser anesthetic concentration. We remark that reducing the

inhibitory anesthetic concentration also corresponds to increasing p of our model. Moreover, our analysis not only provides a visualization scheme but also opportunities to manipulate the metastable terrain directly by controlling the saddle-point position in the phase space.

6.2.11 Summary

In summary, we found that near the critical point of the hybrid phase transition, a tiered synchronization occurs from the incoherent state to the traveling wave state through the intermediate π state. The dynamic process in the metastable state was explained as the circulating flow through a few active states in the phase space, which exhibits large temporal and sample-to-sample fluctuations. We discussed that such a tiered synchronization transition can be a potential model for the process by which the brain recovers from pathological states to the awake state.

6.3 Hybrid phase transition of passively competing model

The passively competing Winfree-Pazó model (6.3) also exhibits a hybrid phase transition with the critical exponent $\beta = 2/3$. In this section we calculate a subleading scaling $\beta' = 1$ for the order parameter R, keeping finite systems in mind. That is,

$$R = \begin{cases} 0 & \big(K < K_c\big) \\ R_c + a\big(K - K_c\big)^{\beta} + b\big(K - K_c\big)^{\beta'} & \big(K > K_c\big) \end{cases}, \tag{6.29}$$

where R_c is the jump size of the order parameter R at K_c, and a and b are some constants. We also obtain $\beta' = 1$ for the scaling of the order parameter R. Similarly leading exponent β and subleading exponent β' can be defined from the asymptotic behavior of the order parameter S near the transition point:

$$S = \begin{cases} 0 & \big(\langle K\rangle < \langle K\rangle_c\big) \\ S_c + a\big(\langle K\rangle - \langle K\rangle_c\big)^{\beta} + b\big(\langle K\rangle - \langle K\rangle_c\big)^{\beta'} & \big(\langle K\rangle > \langle K\rangle_c\big) \end{cases}, \tag{6.30}$$

where S_c is the jump size of the order parameter S at $\langle K\rangle_c$, and a and b are again some constants. Interestingly, for the order parameter S we obtain a different subleading hybrid scaling behavior $\beta' = 4/3$.

We find that in case of the passively competing Kuramoto model with uniform $g(\omega)$ the subleading scaling exponent depends on which order parameter (R or S) is in use. For the passively competing Kuramoto model with unimodal frequency distribution, however, the leading exponent β and the subleading exponent β' are the same for both order parameters R and S.

The self-consistency equation The self-consistency equation of the passively competing model is written as [138]

$$\begin{aligned} S &= \int dK f(K) \int d\omega g(\omega) K \cos\theta \\ &= \int dK f(K) \int d\omega g(\omega) K \sqrt{1-\left(\frac{\omega}{S}\right)^2} \\ &= \langle K\rangle \int_{-S}^{S} d\omega g(\omega) \sqrt{1-\left(\frac{\omega}{S}\right)^2}. \end{aligned} \tag{6.31}$$

6.3.1 Uniform

Let us consider a uniform distribution of $g(\omega)$ ranging $[-\gamma, \gamma]$. In this case, the transition is hybrid. Integration in the self consistency equation can be performed exactly as follows:

$$\begin{aligned} S &= \frac{\langle K\rangle}{2\gamma} \int_{-\gamma}^{\gamma} d\omega \sqrt{1-\left(\frac{\omega}{S}\right)^2} \\ &= \frac{\langle K\rangle S}{2\gamma} \left[\arcsin\frac{\gamma}{S} + \frac{\gamma}{S}\sqrt{1-\left(\frac{\gamma}{S}\right)^2} \right]. \end{aligned} \tag{6.32}$$

The transition point, denoted by the subscript c, occurs when $S_c = \gamma$ and is determined as

$$\langle K\rangle_c = \frac{4\gamma}{\pi} = \frac{2}{\pi g(0)}. \tag{6.33}$$

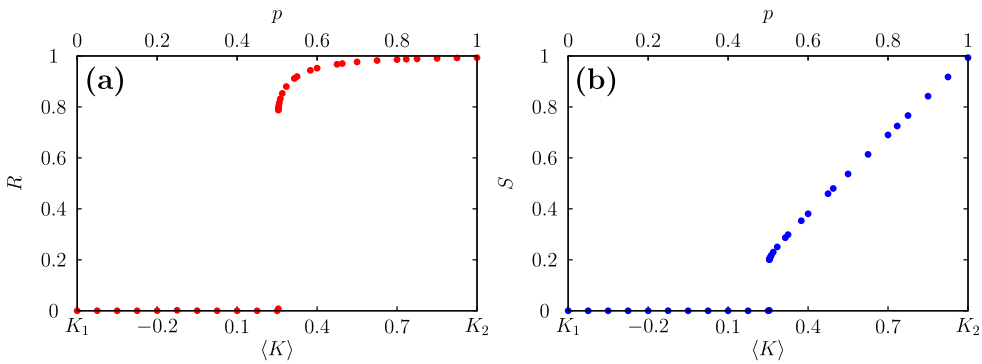

Figure 6.8: Plots of the order parameters (a) R and (b) S of the Kuramoto model with the passively competing coupling constants K_1 and K_2 with the probability $1-p$ and p, respectively. The intrinsic frequency distribution is uniform in the range $[-\gamma, \gamma]$. Data points are obtained by simulations for $N = 25600, K_1 = -0.5, K_2 = 1$, and $\gamma = 0.2$. The data points are obtained by taking average over the last ten percent of the total runtime $t = 10^5 s$. Both order parameters show a discontinuous jump at the transition point $\langle K\rangle_c = 4\gamma/\pi = 0.255$.

We remark that beyond this transition point all oscillators are phase locked with an angular spread less than or equal to π on the phase circle beyond this transition point [11]. Thus the temporal fluctuations of the order parameters are totally absent in the synchronized phase after reaching a steady state, although the value of transition point may involve some finite size corrections as in Ref. [11]. In Fig. 6.8, we check that both order parameters R and S capture the discontinuous synchronization transition at the same $\langle K\rangle_c$. A S-ordered state shows the coherence to R and is stable beyond the transition point.

Now for scaling analysis we take a supercritical point $\langle K\rangle = \langle K\rangle_c + \delta\langle K\rangle$ near the transition point. The angular spread of locked phases is characterized by $\theta_m \equiv \arcsin(\gamma/S)$, which becomes slightly less than $\pi/2$. Let $\theta_m \equiv \frac{\pi}{2} - \delta\theta$. From the self consistency equation $S = \frac{\langle K\rangle S}{2\gamma}\int_{-\theta_m}^{\theta_m}\left(\frac{1+\cos 2\theta}{2}\right)d\theta$, the ordered state is given by

$$
\begin{aligned}
1 &= \frac{\langle K\rangle_c + \delta\langle K\rangle}{2\gamma}\left[\frac{\pi}{2} - \delta\theta + \frac{1}{2}\sin(\pi - 2\delta\theta)\right] \\
&= \left(\langle K\rangle_c + \delta\langle K\rangle\right)\left[\frac{1}{\langle K\rangle_c} - \frac{\delta\theta}{2\gamma} + \frac{1}{4\gamma}\left(2\delta\theta - \frac{(2\delta\theta)^3}{3!}\right)\right] \\
&= \left(\langle K\rangle_c + \delta\langle K\rangle\right)\left[\frac{1}{\langle K\rangle_c} - \frac{(\delta\theta)^3}{3\gamma}\right],
\end{aligned}
\tag{6.34}
$$

where truncation is up to the lowest order in $\delta\theta$. Thus,

$$\delta\langle K\rangle = \frac{\langle K\rangle_c^2}{3\gamma}(\delta\theta)^3. \tag{6.35}$$

From $\gamma = S\sin\theta_m$, we have

$$\begin{aligned}\gamma &= (S_c + \delta S)\sin\left(\frac{\pi}{2} - \delta\theta\right) \\ &= (\gamma + \delta S)\left(1 - \frac{(\delta\theta)^2}{2}\right)\end{aligned} \tag{6.36}$$

and therefore,

$$\begin{aligned}\delta S &= \frac{\gamma}{2}(\delta\theta)^2 \\ &= \frac{\gamma}{2}\left(\frac{3\pi^2}{16\gamma}\right)^{2/3}\delta\langle K\rangle^{2/3}.\end{aligned} \tag{6.37}$$

Note that the leading order calculation gives the critical exponent $\beta = 2/3$, which is also verified from the simulations as shown in Fig. 6.9(a). Therefore, the synchronization transition of the passively competing Kuramoto model with uniform frequency distribution falls into the category of the HPT of the non-competing Kuramoto model with a uniform $g(\omega)$.

Up to the next order we find,

$$\delta\langle K\rangle = \frac{\langle K\rangle_c^2}{3\gamma}(\delta\theta)^3 - \frac{\langle K\rangle_c^2}{15\gamma}(\delta\theta)^5 + O\big(\delta\theta^6\big) \tag{6.38}$$

and reversing the above series gives

$$\delta\theta = \left(\frac{3\gamma}{\langle K\rangle_c^2}\delta\langle K\rangle\right)^{1/3} + \frac{\gamma}{5\langle K\rangle_c^2}\delta\langle K\rangle. \tag{6.39}$$

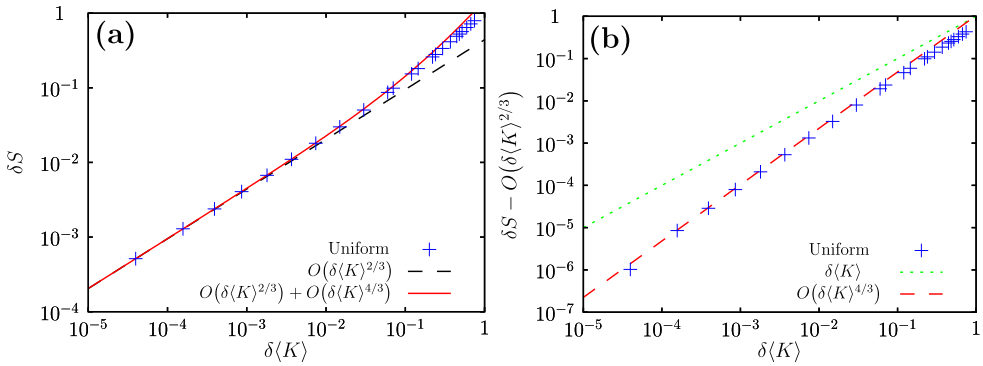

Figure 6.9: (a) Plot of δS versus $\delta\langle K\rangle$ for the uniform $g(\omega)$. The black dashed line denotes the leading order δS of Eq. (6.40) and the critical exponent $\beta = 2/3$ is clearly noticed. The red solid line counts up to the next leading order of Eq. (6.40). Data points are obtained by simulations with $N = 25600, K_1 = -0.5, K_2 = 1$, and $\gamma = 0.2$. We used time averaged values during the last ten percent of the total runtime $t = 10^5 s$. For larger values of $\langle K\rangle$ beyond the critical point, a small deviation is noticed. (b) Plot of the subleading correction values versus $\delta\langle K\rangle$ to check the exponent of the subleading order $\beta' = 4/3$. Red dashed line denotes the subleading correction of Eq. (6.40). The dotted green line with slope one is drawn for comparison, which represents the subleading correction for the Pazó model.

Therefore,

$$\begin{aligned}\delta S &= \frac{\gamma(1-\cos\delta\theta)}{\cos\delta\theta} = \frac{\gamma}{2}(\delta\theta)^2 + \frac{5\gamma}{24}(\delta\theta)^4 \\ &= \left(\frac{9\pi^4\gamma}{2048}\right)^{1/3}\delta\langle K\rangle^{2/3} + \frac{289\pi^2}{5760}\left(\frac{3\pi^2}{16\gamma}\right)^{1/3}\delta\langle K\rangle^{4/3}. \end{aligned} \tag{6.40}$$

This subleading term gives a non-integer exponent $\beta' = 4/3$ for the order parameter S, which is well noticed in Fig. 6.9(b).

Finally we consider the conventional order parameter $R = \left|\frac{1}{N}\sum_j e^{i\theta_j}\right|$ in the passively competing Kuramoto model. R is obtained as

$$R = \int d\omega g(\omega)\sqrt{1-\left(\frac{\omega}{S}\right)^2}. \tag{6.41}$$

From Eqs. (6.31) and (6.41), we observe that the two order parameters are related to each

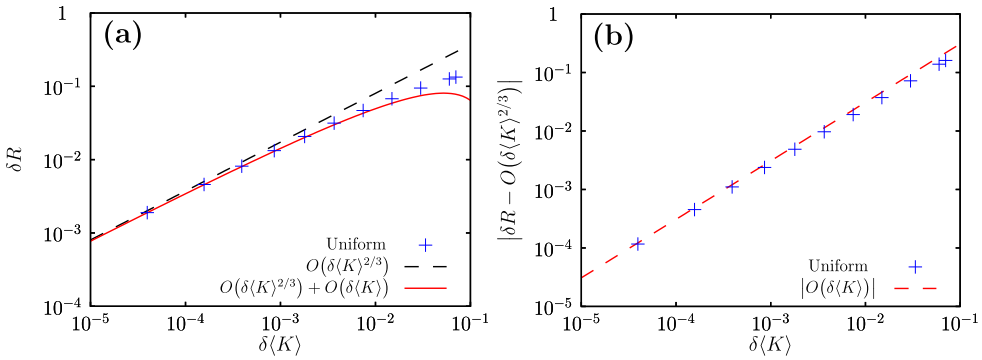

Figure 6.10: (a) Plot of δR versus $\delta\langle K\rangle$ for the uniform $g(\omega)$. Scaling of δR is governed by the same hybrid critical exponent $\beta = 2/3$. The black dashed line represents the leading order of Eq. (6.44), while the red solid line counts up to the next leading order of Eq. (6.44). (b) Plot of the magnitudes of the subleading correction values versus $\delta\langle K\rangle$ to check the exponent of the subleading order $\beta' = 1$. The dashed red line denotes the absolute value of the subleading correction of Eq. (6.44), which is linear in $\delta\langle K\rangle$. The data points are obtained by simulations.

other by

$$S = \langle K\rangle R \tag{6.42}$$

as long as the coupling constant K and the intrinsic frequency ω are uncorrelated. Indeed it is checked from Fig. 6.8 that the jump sizes R_c and S_c at the transition point differ by the factor $\langle K\rangle_c$. This relation between the two order parameters can be expanded above the transition point $S_c = \langle K\rangle_c R_c$, giving

$$\delta S = \delta\langle K\rangle R_c + \langle K\rangle_c \delta R + \text{higher order}. \tag{6.43}$$

From Eqs. (6.40) and (6.43), we find the scaling of δR as

$$\begin{aligned}\delta R &= \frac{\gamma}{2\langle K\rangle_c}\left(\frac{\langle K\rangle_c^2}{3\gamma}\right)^{2/3}\delta\langle K\rangle^{2/3} - \frac{R_c}{\langle K\rangle_c}\delta\langle K\rangle \\ &= \frac{\pi}{8}\left(\frac{3\pi^2}{16\gamma}\right)^{2/3}\delta\langle K\rangle^{2/3} - \frac{\pi^2}{16\gamma}\delta\langle K\rangle,\end{aligned} \tag{6.44}$$

where we used $R_c = \pi/4 = S_c/\langle K\rangle_c$ in the last line. This scaling of δR is the same as the one obtained by Pazó [11], except that the coupling constant K has been replaced by the mean coupling $\langle K\rangle$. The obtained scaling of δR above the critical point coincides exactly with the numerical simulation results (Fig. 6.10).

We notice in Eqs. (6.40) and (6.44) that δS and δR scale with the same critical exponent $\beta = 2/3$ in leading order. However, the subleading terms have different exponent values. Infact, the subleading exponent $\beta' = 1$ is non-critical, for the order parameter R [11]. The exponent $4/3$ will appear instead in the next order term. We remark that the linear term with exponent 1 will intervene in the scaling of δR, generally if the transition is discontinuous $R_c \neq 0$, which is derived from the r.h.s. first term of Eq. (6.43).

It is also noticed that if the leading scaling exponent of δS were $\beta = 1$ or $\beta = 1/2$, which is frequently the case of first-order phase transitions with our definitions of β in equations (6.29) and (6.30), the leading or subleading exponent would have been unity anyway and therefore the difference in the scaling exponents for δR and δS would not have arisen. Here, the difference is owing to an abnormal exponent $\beta = 2/3$.

At this stage, we need to compare our result for the sub-leading scaling behaviors of S and R in the case of uniform $g(\omega)$ with those in the case of unimodal $g(\omega)$.

6.3.2 Lorentzian

Here we take a Lorentzian distribution for $g(\omega)$ as a unimodal distribution, for which the self consistency equation is exactly integrable. The order parameter S is derived as follows:

$$\begin{aligned} S &= \langle K\rangle \int_{-S}^{S} d\omega \frac{\gamma/\pi}{\omega^2+\gamma^2}\sqrt{1-\frac{\omega^2}{S^2}} \\ &= \langle K\rangle \Big(\sqrt{1+\Big(\frac{\gamma}{S}\Big)^2} - \frac{\gamma}{S}\Big). \end{aligned} \tag{6.45}$$

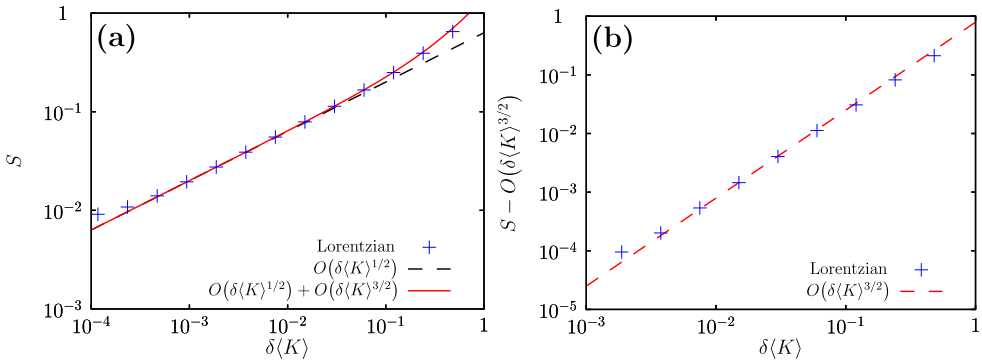

Figure 6.11: (a) Plot of S versus $\delta\langle K\rangle$ for the Lorentzian $g(\omega)$. The black dashed line denotes the leading order S of Eq. (6.46) and the critical exponent $\beta = 1/2$ is noticed. The red solid curve includes up to the next order of Eq. (6.46). Simulations are performed with the Lorentzian distribution $g(\omega) = (\gamma/\pi)/(\omega^2 + \gamma^2)$ for $N = 102400, K_1 = -0.5, K_2 = 1$, and $\gamma = 0.2$. Time average is taken during the last fifty percent of the total runtime $t = 10^4 s$. The error bar denotes temporal fluctuations of the order parameter S. The deviation near the critical point is due to finite-size effect. (b) Plot of the subleading correction values versus $\delta\langle K\rangle$ to check the exponent of the subleading order $\beta' = 3/2$. Red dashed line denotes the subleading correction of Eq. (6.46).

Therefore,

$$\delta S = \sqrt{2\gamma}\delta\langle K\rangle^{1/2} + \frac{1}{\sqrt{8\gamma}}\delta\langle K\rangle^{3/2} + O\big(\delta\langle K\rangle^{5/2}\big). \tag{6.46}$$

Comparison of the above scaling for S with the simulation results are presented in Fig. 6.11. For the continuous transition of Lorentzian case, jump is absent. Instead, plugging in $\langle K\rangle = \langle K\rangle_c + \delta\langle K\rangle$ directly to Eq. (6.42) yields

$$\delta R = \frac{1}{\sqrt{2\gamma}}\delta\langle K\rangle^{1/2} - \frac{1}{4\gamma\sqrt{2\gamma}}\delta\langle K\rangle^{3/2}. \tag{6.47}$$

Notice here that the exponents $\beta = 1/2$ and $\beta' = 3/2$ are the same for both order parameters R and S. Furthermore, one can check that any symmetric unimodal $g(\omega)$ leads to the same exponents $\beta = 1/2$ and $\beta' = 3/2$, where the integral of the self consistency Eq. (6.45) can be solved after inserting the Taylor series of g at zero.

Therefore, for the case of unimodal $g(\omega)$, β and β' are not changed, regardless of using

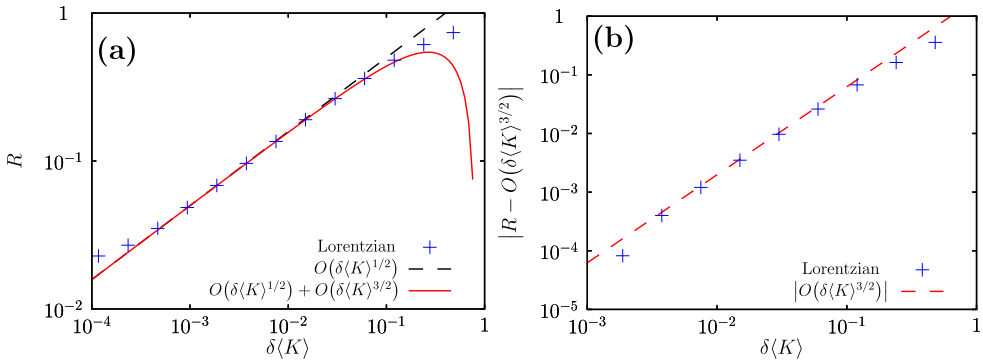

Figure 6.12: (a) Plot of R versus $\delta\langle K\rangle$ for the Lorentzian $g(\omega)$. The black dashed line denotes the leading order R of Eq. (6.47) and the critical exponent $\beta = 1/2$ is noticed. The red solid curve includes up to the subleading order of Eq. (6.47). The data points are from the same simulation as that of Fig. 6.11. (b) Plot of the subleading correction values versus $\delta\langle K\rangle$ to check the exponent of the subleading order $\beta' = 3/2$. Red dashed line denotes the subleading correction of Eq. (6.47).

R or S. In contrast, the subleading exponents β' for the uniform $g(\omega)$ depends on which of the order parameter, R or S, is in use. This is owing to the jump of the order parameters at the transition point and the abnormal exponent β.

6.4 An avalanche of frequency splittings: a hybrid critical phenomenon?

Finally, we revisit the problem of critical phenomenon of the hybrid synchronization transition. We consider the dynamic cascade phenomenon of the passively competing Kuramoto model. Although Pazó and Maistrenko had considered a frequency bifurcation phenomenon [11, 137], their investigations largely considered static splittings, i.e. time averaged frequencies of clusters in the domain of the coupling constant. Here, we consider the splittings in the time domain, induced by a quench event.

In Fig. 6.13, finite system with $N = 8$ oscillators are initially under a supercritical coupling strength and thus settled to a completely phase locked monolithic state. The mean frequency of the oscaillators to zero. Initially, a positive coupling strength $K_2 = 1$ is set for all

oscillators. In the mean time, a single oscillator's coupling strength is changed to a negative value $K_1 = -2$, hence the average coupling strength becomes smaller. This sudden quench of a coupling triggers an avalanche of cluster segregations, which eventually leads to a complete destruction of a single giant frequency cluster into $N = 8$ separate frequency clusters. We remark that in finite size systems the number of segregated clusters, i.e. the avalanche size, may depend on which oscillator is being quenched. Depending on the value of K_1 it may require more than a single quench. However, in the thermodynamic limit, this length of quench sequence required for a complete breakup of the giant cluster should be of $o(N)$, considering that the transition is discontinuous. It is remarked, on the other hand, frequency splitting had occurred gradually for unimodal frequency distribution (recall Fig. 5.2). Such a difference in the frequency clustering pattern results in a continuous transition or a discontinuous transition at the critical point, in the thermodynamic limit. In Fig. 6.14, we compare the effect of (a) homogeneous decrease in coupling strengths to (b-d) replacement of a single

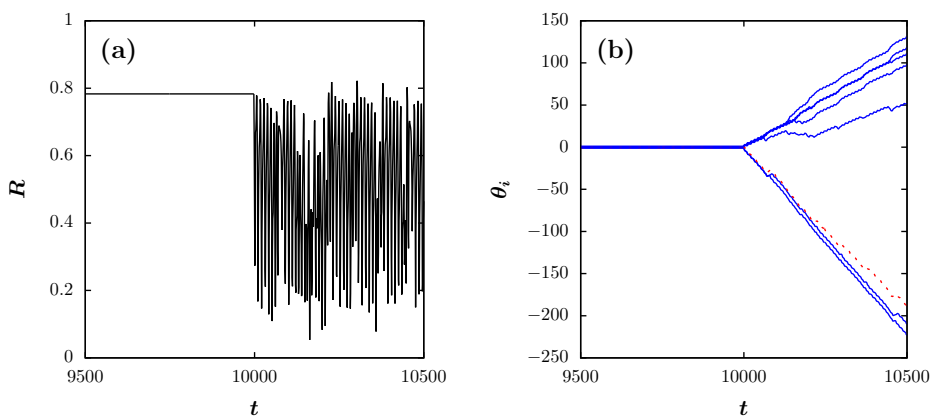

Figure 6.13: Quench dynamics of the passively competing Kuramoto model with nearly uniform natural frequency distribution. The oscillators have roughly distribution of frequencies $\omega = -0.7, -0.5, -0.3, -0.1, 0.11, 0.28, 0.51, 0.7$, and a single positive passive coupling strength $K_2 = 1$ initially. Critical coupling strength is roughly $K_c \approx 0.9$ and the oscillators settle at fixed phases, before the quench. At time $t = 10^4$, one of the oscillator's coupling strength is modified to $K_2 = -2$ (denoted by the dotted red trajectory). This triggers (b) an avalanche of cluster segregations and (a) a sudden drop of coherence. We remark in (b) that after a long time each oscillators reaches a different slope, which is the frequency splitting characteristics of the Pazó model [11].

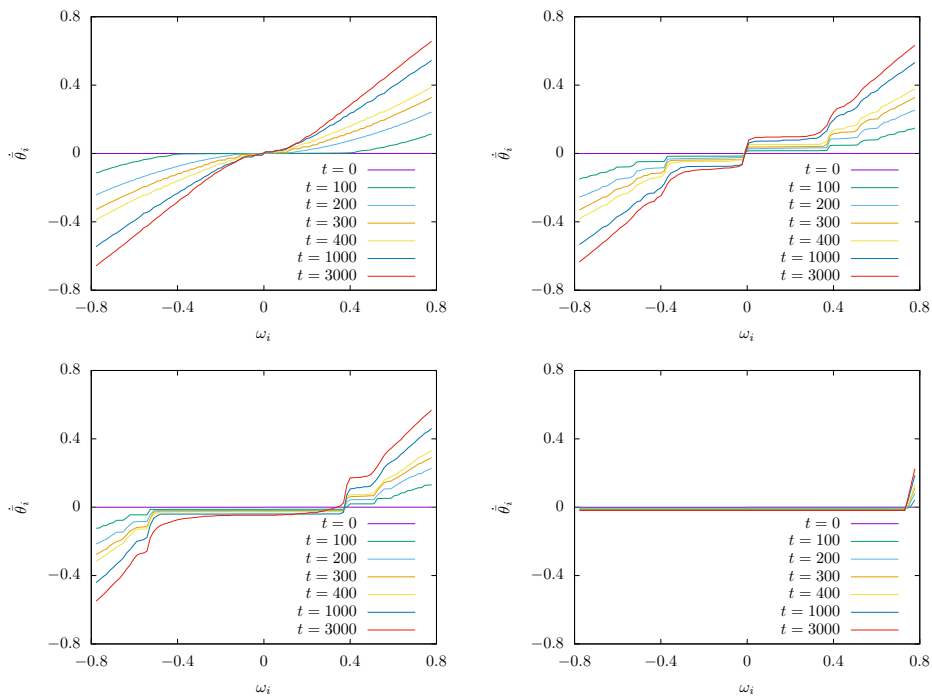

Figure 6.14: Equally spaced natural frequencies. $N = 100$, $\gamma = \pi/4$. All oscillators are set to a positive coupling constant $K_2 = 1$ initially. (a) Homogeneous decrease of K_2 to 0.99 (homogeneous). (b-d) A highly heterogeneous variation. A single oscillator's coupling constant is replaced from $K_2 = 1 \rightarrow K_1 = -2$, while remaining oscillators' coupling strengths are unchanged $K_2 = 1$. The cascade further depends on the precise position of the replacement. (b) center (c) quarter or (d) end in the axis of natural frequency.

oscillator coupling strength. In contrast to the homogeneous variation, a single replacement may not lead to a complete breakdown of the giant frequency cluster, although change in the system's mean coupling strength is the same. As for such highly heterogeneous perturbation, we find that attacking an oscillator in the middle of the frequency distribution is more effective in resulting the frequency splitting cascade.

It is remarked in association to the avalanche collapse and a power law suggested by Ref. [7], that here the total number of frequency clusters generated in the steady state follows a *distribution* of values which depends on the *details* of the quench. Hence, it can be interpreted as the size of avalanche s which may potentially give a power law $P(s) \sim s^{-\sigma}$ upon some random quench. Also, Fig. 6.13 gives an impression that time series statistics of the splitting events, e.g. interevent time distribution, might be considerable instead.

6.5 Remarks on the Ott–Antonsen method

The Ott–Antonsen method has been quite successful in the bifurcation analysis of Kuramoto model including the Lorentzian and bi-Lorentzian $g(\omega)$, where $N \to \infty$ continuum oscillator degrees of freedom are reduced to few coupled modes [10, 128, 129]. An exact low dimensional reduced system is also known for the Kuramoto oscillators with identical frequency [127, 136, 137, 144, 145] (see Appendix B for more details).

Especially in the hybrid synchronization case of uniform $g(\omega)$, the previous reduction methods lead to an integral that is difficult to evaluate analytically and therefore the bifurcation analysis is not feasible. For such a reason, the exact hybrid synchronization dynamics remains veiled. Instead, one can investigate the phase transition from the stationary self-consistency solutions. This method is applicable to the current passively competing Kuramoto models. It turned out that, in contrast to the actively competing Kuramoto models, which can exhibit π clustering patterns, traveling wave dynamics [19], hysteresis, and metastability [20], the passively competing Kuramoto models exhibit a rather simple transition pattern from incoherent to coherent phase. We remark however that this method is applicable to a general intrinsic frequency distribution $g(\omega)$. We also remark that the self-

consistency equation is obtained just by assuming stationarity, regardless of the use of the Ott–Antonsen ansatz. Stability of the self consistency solutions can be checked by numerical simulations, or one can use an empirical linear stability criterion [139] instead. However, the validity of the empirical linear stability criterion remains subtle; for example our previous analysis have shown that the linear stability becomes incomplete for uniform $g(\omega)$, a case which gives metastable solutions with neutral or weakly stable linear stability [20].

Kuramoto's self consistency method [8] is still a general powerful tool for studying phase transition of the Kuramoto oscillator system. This mean field theory is applicable to many other types of intrinsic frequency distributions $g(\omega)$ other than Lorentzian or uniform distributions. It is also useful when analyzing phase transitions of finite size systems. On the contrary, the Ott–Antonsen method provides a bifurcation for limited types of distributions, and it is not suitable for calculations on finite size systems. Finite size effects are important. For example, Daido's discovery on the divergence of temporal fluctuations at the transition point is an important critical phenomenon, an aspect which is analogous to the divergence of susceptibility in second order phase transitions in thermodynamics [130]. Therefore, the self consistency method can be used complementarily to the Ott–Antonsen method.

6.6 Summary

We investigated the synchronization transition of the Kuramoto model with passively competing interactions and a uniform intrinsic frequency distribution, which was compared with that of the corresponding Kuramoto model with a unimodal intrinsic frequency distribution. A common feature between the two results is that the transition point $\langle K \rangle_c$ of the mean coupling constant of the competing mixture plays a similar role as K_c of the ordinary Kuramoto model. The order parameter S representing the weighted coherence was useful in analyzing the phase transition of passively competing Kuramoto models. We have unexpectedly found a novel exponent $\beta' = 4/3$ for δS in the subleading order for the passively competing Kuramoto model with uniform frequency distribution, although $\beta' = 1$ for δR remains the same as in the Pazó model. We found that this difference is attributed by the jump of the order

parameter at the hybrid synchronization transition with an abnormal exponent $\beta = 2/3$ in the leading order. This suggests that further interesting features are to be expected from the hybrid synchronization transition of the passively competing generalization of the Kuramoto model beyond the model we considered. Although the subleading correction itself is not a finite size effect, a correct understanding of the subleading order in the scaling of the order parameter is requested in finite systems, because the leading order term governs only near the transition point, which is generally not accessible with small-size systems. We also observed the avalanche collapse of synchronization at the hybrid critical point of the passively competing model. A single quench of an oscillator's coupling constant slightly decreases the system's mean coupling constant, which in turn results cascade of segregation of frequency clusters. The giant frequency cluster completely dissolves into smaller clusters at independent running frequencies.

Chapter 7

The restricted Kuramoto model

Global restriction is a necessary ingredient to build a discontinuous percolation transition [64]. Recently we discovered a dichotomous cluster merging process, namely the restricted percolation model, which organizes criticality at the discontinuous transition has been discovered [48–51]. Such a transition which exhibits characters of both continuous and discontinuous transitions is called a hybrid transition [11, 13, 20, 22, 33, 41, 46, 48–51].

In the restricted Erdős–Rényi (r-ER) model [48, 49], dichotomous cluster merging process self-organizes a power-law cluster size distribution and develops a power-law interevent time distribution [49, 51]. It is remarked that hybrid percolation transiiton also occurs in a class of percolation models, which includes k-core percolation [33], cascade failure of interdependent networks [22], and generalized epidemic spreadings [40, 41]. A universal mechanism has been found in this type of hybrid phase transition, which is induced by prunning processes [46]. In contrast, the hybrid percolation transition of the restricted percolation is induced by cluster merging process [48–51]. And it has a different mechanism [51].

Inspired by the global restriction idea of hybrid percolation which leads to an abrupt jump accompanied by critical phenomena, we consider a restricted synchronization model composed of two groups of oscillators: leader and follower. The leader group oscillators interact only with the follower group oscillators, while the follower oscillators interacts with all oscillators. The leader group and follower group is divided every time based on rankings of the angular velocity.

The interaction strength between a leader-follower pair is asymmetric. In consequence, a follower oscillator may take over a leader oscillator and become a leader. In average, the

leader group is draged by the follower group, while the follower group is pulled by the leader group. However, the attraction strength also depends on the phase gap between the two groups. If too close to each other, intrinsic disorder in the natural frequency dominates the oscillator motions and hence they become dispersed. Macroscopically, leader and follower groups are separated by a phase gap, but their microscopic compositions are continuously altered by exchange of oscillators based on the velocity rankings.

Group switching of an oscillator depends on its intrinsic frequency and also on the phase values of other oscillators. Switching is frequent for an oscillator with intermediate values of frequencies, while it takes a long time for ones with extreme values of intrinsic frequencies. The switching intervals can span a broad range of values and we find a power-law tail in the interevent time distribution. Remarkably, restricted interaction together with such a dynamic reorganization of the two groups by ranking based oscillator exchange leads to a hybrid synchronization transition.

Here, we attempt to understand this novel type of collective behavior. Due to the asymmetric interaction, traveling wave synchronization may occur; the leader and follower populations are separated by a constant phase and co-rotate at a nontrivial angular speed [20]. To obtain such a steady state solution of the restricted synchronization model, we setup and simultaneously solve the three complex self-consistency equations on the leader, follower, and the whole. We find that the theory successfully captures the transition points and yields the order parameter curves which are similar to those obtained by simulation, but some discrepancy is also noticed. The current self-consistency theory fixes the leader/follower classification based on natural frequencies of the oscillators, and hence it is insufficient to capture the detailed dynamic switchings in the leader/follower. It is a limitation of a mean field theory.

The leader-follower role switching is important in real life, for instance, in speed skating and flight of birds. Team pursuit in speed skating is a Winter Olympics sports which a team of three skaters compete with another team, starting on opposite side of the rink. The team's time is taken from the third skater to cross the finish line. The team pursuit is technically demanding; skaters in a team run as a unit, following each other closely in line to minimize

the drag, and they push from back to front and shuffle from front to back in attempt to synchronize their pace and to keep the freshest leader doing the pull. As in the speed skate team, the role of a leader is also important for an effective flight of the bird flocks [147, 148]. Leader-follower hierarchy is also present in the pigeons [147].

Traditional Vicsek model studies provide understandings on the emergent flocking behavior of birds [147, 149]. Vicsek model and Kuramoto model are similar in that they both characterize an individual's state with an angular variable. Also, greater interaction leads to a incoherent-to-coherent phase transition of the angular states, generating a collective synchronous movement. However, the intricate reclassification or shuffling dynamics of our model, a real-time role-switching adaptively to the change in ranking, has yet not been considered in the previous models, to the best of our knowledge.

Our results conceptually extends our previous line of hybrid phase transition studies on the restricted percolation [48–51] to synchronization. Both in the restricted percolation and the restricted synchronization we find: ranking based restrictions can yield discontinuity and criticality. A strong implication is that the hybrid phase transition can be in general induced by a ranking based restriction rule.

7.1 model

At each time step, the oscillators are divided into two groups: leader group L and follower group F. Oscillators are sorted by angular velocities. F consists the slowest g fraction while L consists the fastest $1-g$ fraction of the total N oscillators. Interaction among the leader oscillators is suppressed. The leader group oscillators interact only with the follower group oscillators, while the follower group oscillators interact with all other oscillators.

$$\dot{\theta}_i = \begin{cases} \omega_i + \frac{K}{N} \sum_{j=1}^{N} \sin(\theta_j - \theta_i), & i \in F \\ \omega_i + \frac{K}{gN} \sum_{j \in F}^{gN} \sin(\theta_j - \theta_i), & i \in L. \end{cases} \tag{7.1}$$

Order parameters are defined as

$$
\begin{aligned}
Z_F = R_F e^{i\psi_F} &\equiv \frac{1}{gN}\sum_{i\in F}^{gN} e^{i\theta_i}, \\
Z_L = R_L e^{i\psi_L} &\equiv \frac{1}{(1-g)N}\sum_{i\in L}^{(1-g)N} e^{i\theta_i}, \\
Z = Re^{i\psi} &\equiv \frac{1}{N}\sum_{i=1}^{N} e^{i\theta_i},
\end{aligned} \tag{7.2}
$$

which are related by an identity $Z = (1-g)Z_L + gZ_F$.

7.2 self consistency equation

By the definitions of the order parameters (7.2) the model (7.1) is rewritten as

$$
\begin{aligned}
\dot{\theta}_i &= \omega_i - KR\sin(\theta_i - \psi) \quad \text{for } i \in F, \\
\dot{\theta}_i &= \omega_i - KR_F\sin(\theta_i - \psi_F) \quad \text{for } i \in L.
\end{aligned} \tag{7.3}
$$

The synchronized state $R \neq 0, R_L \neq 0, R_F \neq 0$ can be a traveling wave. In the steady state $R(t) \simeq R, R_F(t) \simeq R_F, R_L(t) \simeq R_L, \psi(t) \simeq \psi_0 + \Omega t, \psi_F(t) \simeq \psi_{0F} + \Omega t, \psi_L(t) \simeq \psi_{0L} + \Omega t$, rotating frame variables $\phi_i \equiv \theta_i - \Omega t$ are introduced.

$$
\begin{aligned}
\dot{\phi}_i^F &= \omega_i^F - \Omega - KR\sin(\phi_i^F - \psi_0), \\
\dot{\phi}_i^L &= \omega_i^L - \Omega - KR_F\sin(\phi_i^L - \psi_{0F})
\end{aligned} \tag{7.4}
$$

From now on we set $\psi_0 = 0$, without loss of generality, and define $\psi_{0L} - \psi_{0F} \equiv \Delta, \psi_{0F} - \psi_0 \equiv \delta$. In the steady state, a locked leader/follower oscillator satisfies

$$
\begin{aligned}
\omega_i^F - \Omega &= KR\sin\phi_i^F \\
\omega_i^L - \Omega &= KR_F\sin(\phi_i^L - \psi_{0F})
\end{aligned} \tag{7.5}
$$

From the complex self consistency equations of three order parameters Z, Z_F, Z_L, we find 6 equations with 6 unknowns $R, R_F, R_L, \Omega, \Delta, \delta$. Owing to the phase separation between the three order parameters, we need to consider the mixing angles (Fig. 7.1).

$$gR_F = \mathcal{F}(F, R, \Omega)\cos\delta + \mathcal{G}(F, R, \Omega)\sin\delta \tag{7.6}$$

$$(1-g)R_L = \mathcal{F}(L, R_F, \Omega)\cos\Delta + \mathcal{G}(L, R_F, \Omega)\sin\Delta \tag{7.7}$$

$$R = \mathcal{F}(F, R, \Omega) + \mathcal{F}(L, R_F, \Omega)\cos\delta - \mathcal{G}(L, R_F, \Omega)\sin\delta \tag{7.8}$$

$$0 = -\mathcal{F}(F, R, \Omega)\sin\delta + \mathcal{G}(F, R, \Omega)\cos\delta \tag{7.9}$$

$$0 = -\mathcal{F}(L, R_F, \Omega)\sin\Delta + \mathcal{G}(F, R_F, \Omega)\cos\Delta \tag{7.10}$$

$$0 = \mathcal{F}(F, R, \Omega) + \mathcal{F}(L, R_F, \Omega)\sin\delta + \mathcal{G}(L, R_F, \Omega)\cos\delta \tag{7.11}$$

where

$$\mathcal{F}\big(\{\omega_i\}, R, \Omega\big) = \frac{1}{N}\sum_{\omega_i \in locked} \sqrt{1 - \frac{(\omega_i - \Omega)^2}{K^2R^2}}, \tag{7.12}$$

$$\mathcal{G}\big(\{\omega_i\}, R, \Omega\big) = \frac{1}{N}\sum_{\omega_i \in drifting} \left[\frac{\omega_i - \Omega}{KR} - \mathrm{sgn}(\omega_i - \Omega)\sqrt{\frac{(\omega_i - \Omega)^2}{K^2R^2} - 1}\right]. \tag{7.13}$$

Given (R, Ω) we can evaluate the above equations in the following sequence

$$(R, \Omega) \overset{(7.9)}{\longrightarrow} \delta \overset{(7.6)}{\longrightarrow} R_F \overset{(7.8),(7.11)}{\longrightarrow} (R, \Omega) \tag{7.14}$$

$$\overset{(7.10)}{\longrightarrow} \Delta \overset{(7.7)}{\longrightarrow} R_L \tag{7.15}$$

From the first chain of substitutions, we obtain the self consistency condition for (R, Ω).

7.3 Results and discussions

Fig. 7.2 shows typical order parameter trajectories of a synchronized state. Obtained from a numerical simulation at a supercritical value of K. The detailed motion includes highly non-trivial finite size fluctuations near the time averaged value $(\langle R\rangle, \langle\Omega\rangle)$, which becomes steady

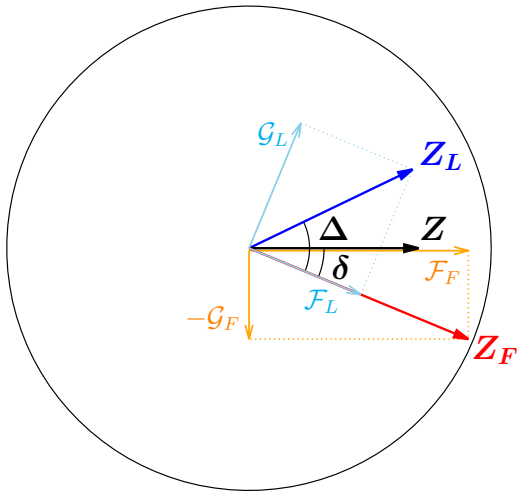

Figure 7.1: Owing to phase seprations of the three order parameters Z, Z_F, Z_L, mixing angles Δ, δ are present in the corresponding self-consistency equations.

after some transient time. The order parameters reach a steady state, $Z(t) \simeq Re^{i\Omega t+\psi_0}$, $Z_L(t) \simeq R_L e^{i\Omega t+\psi_{0L}}$, $Z_F(t) \simeq R_F e^{i\Omega t+\psi_{0F}}$, and $\Omega_L = \Omega_F = \Omega$. It is remarked, however, $V_F < V < V_L$, in contrast. Coherence of the follower group is larger than the leader group $R_L < R_F$, because the followers attract each other while the leaders do not. Moreover, the two groups are not perfectly aligned in-phase, but a nonzero constant phase separation $\psi_L - \psi_F$ is maintained in between. The time averaged coherence R is the order parameter which defines the incoherent to coherent synchronization transition in Fig. 7.3(a). We find that the restricted synchronization model is capable of both continuous and hybrid phase transitions. Hybrid phase transition of the restricted Kuramoto model occurs at a range of restriction parameter $g \in [g_\ell, g_u]$ values at which continuous singularity characterized by the exponent β is found at the top of the order parameter jump [11, 20, 33, 51]. For values of g above and below this range, continuous synchronization transitions occur. We solved the self-consistency equation (7.14) numerically and obtained the curves of Fig. 7.3(b), which look quite similar to the simulation results. However, we remark that the theory also shows some discrepancy to the simulation results. In particular, the self-consistency equations obtains incorrect value of β near unity in the regime $[g_\ell, g_u]$, which has been verified as a hybrid transition regime

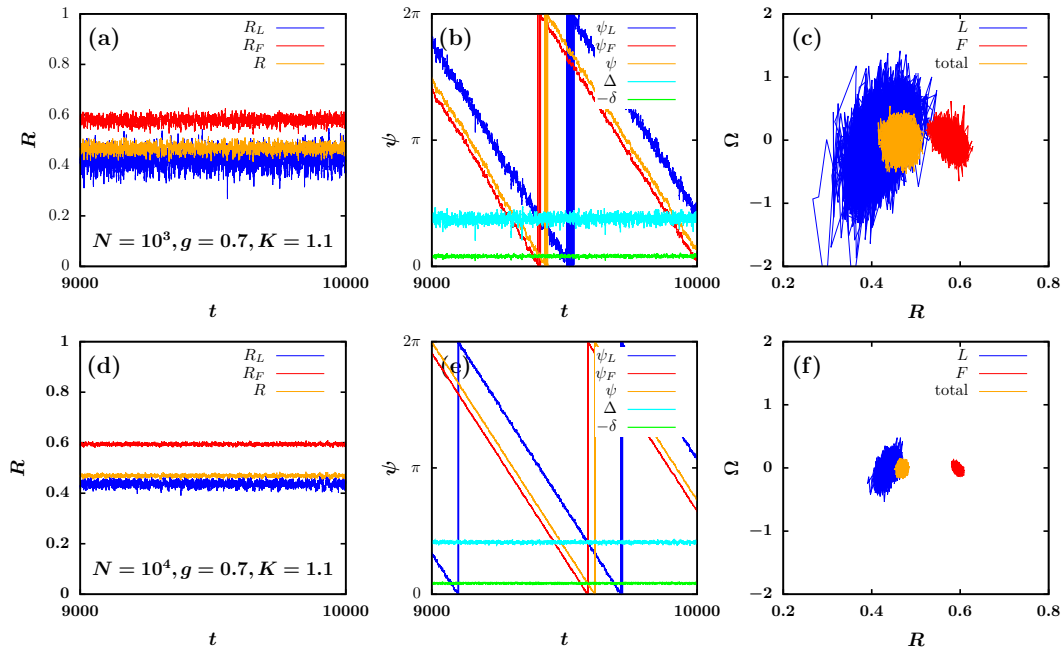

Figure 7.2: Order parameter trajectories $R(t), \psi(t)$, and $\big(R(t), \Omega(t)\big)$ of the restricted Kuramoto model for lorentzian natural frequency distribution $g(\omega) = (\gamma/\pi)/(\gamma^2 + \omega^2)$ obtained by simulations. $g = 0.7, \gamma = 0.5, K = 1.1, N = 10^3, 10^4$. In the thermodynamic limit $N \to \infty$ we expect a steady state characterized by co-rotation $\Omega = \Omega_F = \Omega_L$ and with constant coherence R, R_F, R_L and constant phase separations $\Delta, \psi_F - \psi$.

in the simulations. It is remarked that the self-consistency theory is approximate, because it does not take into account the detailed microscopic dynamic group switchings, which is a critical feature of the restricted synchronization. Dynamic switchings is discussed in detail in the later part of the chapter.

With small number of leaders ($g > g_u \simeq 0.8$), increase of coherence is gradual as in the ordinary Kuramoto model ($g = 1$). Introduction of some leaders (as g is decreased) may bring a leap of coherence. While the follower population shows strong internal cohesion, leaders do not bond to each other, owing to the asymmetric form of interaction in the restricted Kuramoto equation (7.4). Instead each leader may individually bond to a sufficiently large and coherent mass of followers. An increase in total coherence in turn increases attraction in the follower group. Such a mutual cooperation of the two groups can cause a leap of

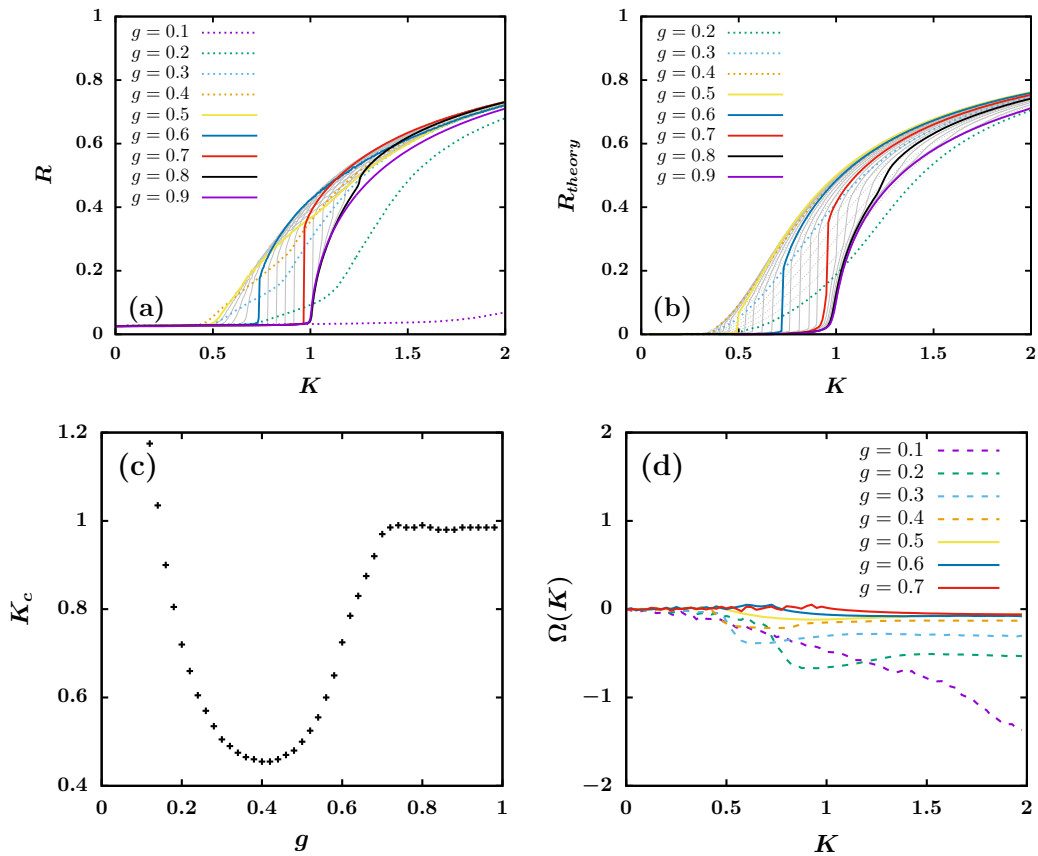

Figure 7.3: (a) Time averaged order parameter curve $R(K)$ and (b) the self-consistency order parameter solution curve $R_{theory}(K)$ of the restricted Kuramoto model for lorentzian natural frequency distribution $g(\omega) = (\gamma/\pi)/(\gamma^2 + \omega^2)$ for $\gamma = 1$ and for various values of $g = 0.1 \sim 0.9$. Hybrid synchronization transition occurs at a range of values of $g \in [g_\ell, g_u] \approx [0.6, 0.7]$. Thinner curves are in spacings of $\Delta g = 0.02$. $N = 10^4$. Simulation measured (c) $K_c(g)$ and (d) the traveling wave order parameter curves $\Omega(K)$ for various values of g. Traveling wave synchronization occurs in the restricted model. $\Omega(K) = 0$ beyond $g > g_u$.

coherence. With increasing numbers of leaders $g \to g_\ell$, the jump size gradually decreases to zero. With presence of too many leaders, leap does not occur. Instead the order parameter curve shows irregular indents. A similar bumpy deviation had occurred in the traveling wave phase of a competing Kuramoto model, which had occurred in between a parameter window $[K_\ell, K_u]$ [20]. Larger values in traveling wave speed had led to larger deviations from static π-state solution curves. Similar behaviors are also observed from in the small g deviations of

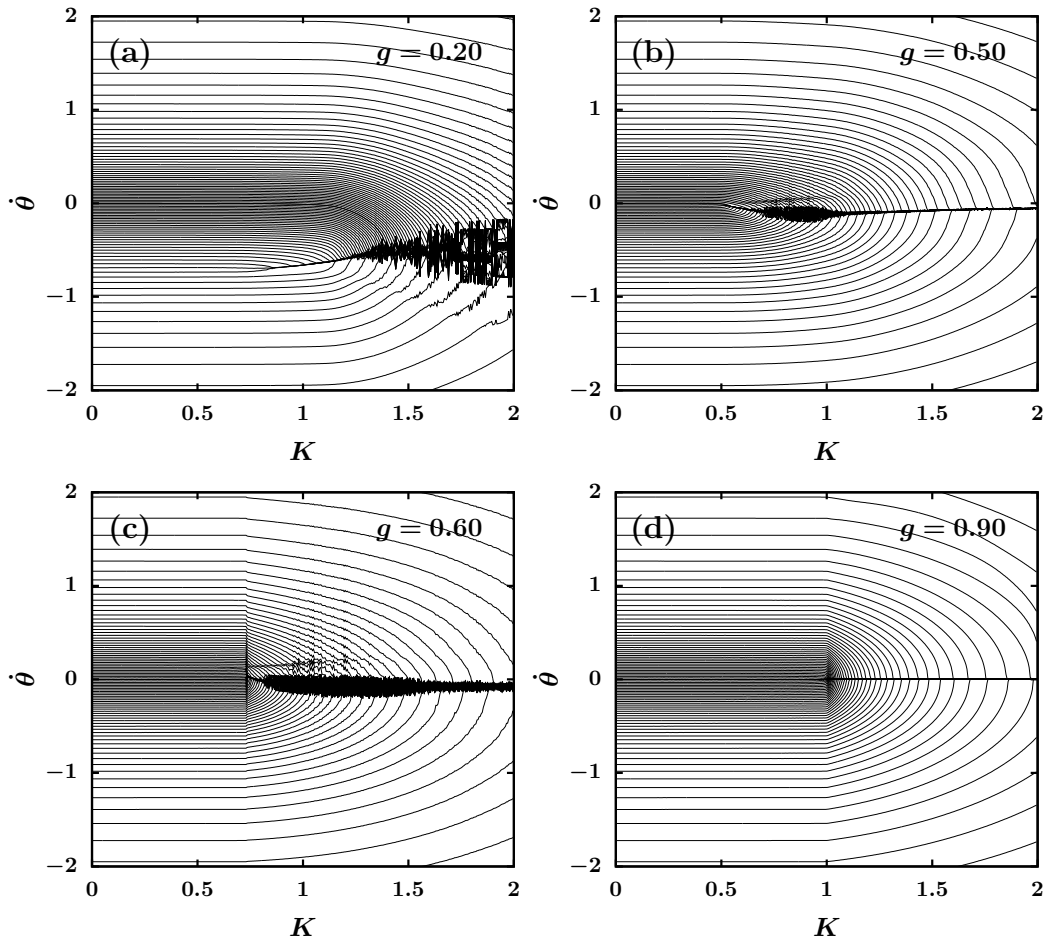

Figure 7.4: Frequency clustering in the restricted Kuramoto model for lorentzian distribution for various values of $g = 0.2, 0.5, 0.6, 0.9$. In (a), (b), and (d) the giant frequency cluster merges oscillators one by one and hence its size is gradually grown from zero beyond the continuous transition point. In (c) hybrid phase transition occurs, which is characterized by a sudden frequency locking of a macroscopic number of clusters. Similar clustering has been noticed in the previous hybrid synchronization transition studies of the ordinary Kuramoto models, where a giant frequency cluster of full system size had emerged at the hybrid transition point [11, 20]. In contrast, the giant cluster of the restricted model continuously grows its size beyond the hybrid transition point.

the restricted model. In Fig. 7.3(d) the traveling wave order parameter curve $\Omega(K)$ proceeds like a breaking ball and hence the coherence order parameter $R(K)$ correspondingly shows nontrivial variations, especially for small values of g. Also, note particularly in Fig. 7.4 that

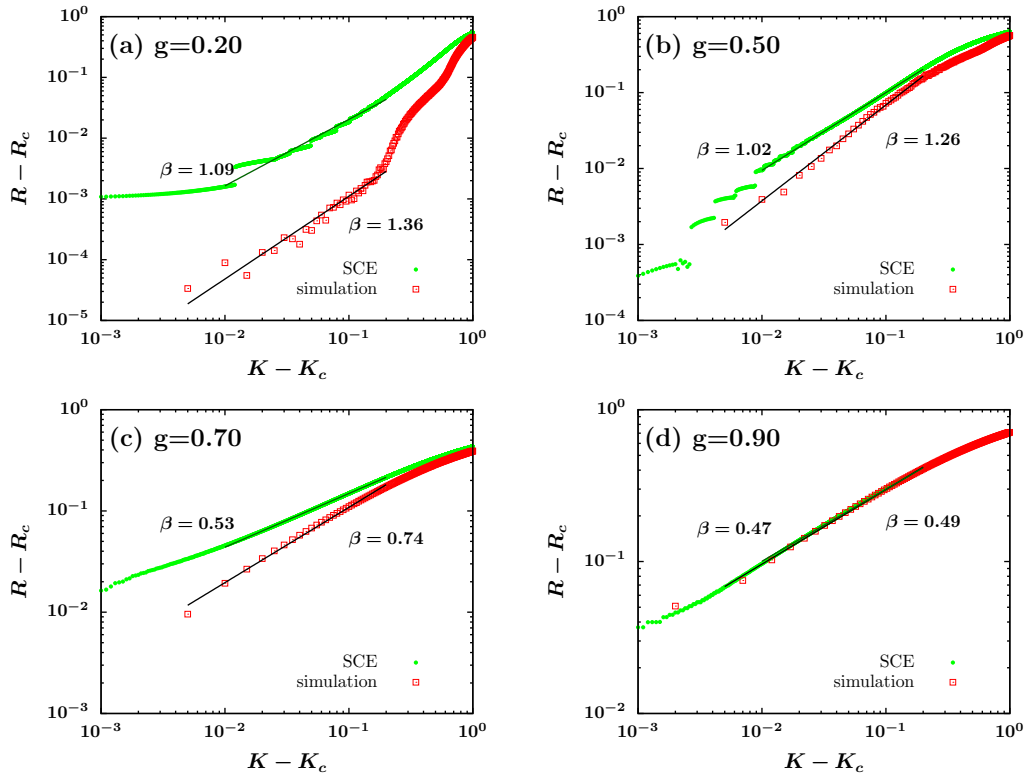

Figure 7.5: (a) Explosive (discontinuous) transition with β near unity is obtained for $g = 0.4, 0.5$. This is in contrast to the usual critical exponent $\beta = 1/2$ for the continuous synchronization transition. (c,d) Continuously varying hybrid critical exponent β is obtained for a range of values of $g \in [g_\ell, g_u] \approx [0.6, 0.7]$. Beyond $g > g_u \approx 0.7$ continuous transition with $\beta = 1/2$ occurs.

the giant cluster frequency Ω immediately after the transition exhibits a larger deviation from zero, as g is decreased further below $g_\ell \approx 0.5$. There the coherent states of the restricted Kuramoto model are traveling waves. Both $g < g_\ell$ and $g > g_u$ are continuous transition regimes. We find that $\beta > 1$ in the former continuous transition while $\beta = 0.5$ in the later continuous transition. Also, $0.5 < \beta < 1$ for hybrid phase transitions in the regime $[g_\ell, g_u]$.

In the ordinary Kuramoto model ($g \to 1$) continuous transition robustly occurs for any unimodal frequency distribution $g(\omega)$ and traveling wave is absent when $g(\omega)$ is symmetric. Self consistency analysis tells that for a $g(\omega)$ symmetric and convex upward $g''(0) < 0$ distribution about the zero mean leads to a supercritical bifurcation of an order parameter curve

with $\beta = 1/2$ [8]. For bimodal, and thus concave upward $g''(0) > 0$ distribution, the transition was discontinuous and much complex bifurcations had occurred [8, 10]. Flat distribution was an exceptional marginal case to exhibit hybrid phase transition [11]. However, the hybrid phase transitions of the previous ordinary and competing Kuramoto models [11–13, 20] require a specific form of frequency distributions or a particular $\lambda = 3$ scale-free network with some frequency-degree correlations [7], in order to organize a maximal competition among the oscillators.

In contrast, the restricted Kuramoto model exhibits discontinuous (or hybrid) transition even for the Lorentzian or gaussian $g(\omega)$. Also, in contrast to the gradual attachments of clusters in Fig. 7.4 (a) and (b), the frequency clustering of a hybrid phase transition (c) is abrupt. A sudden frequency locking had occurred similarly in the hybrid phase transition of the ordinary and competing Kuramoto models [11, 13, 20]. But in the previous models, giant frequency cluster had emerged with the size equal to the system size N. The sudden frequency-clustering in Fig. 7.4(c) involves a finite fraction but not all of the oscillators. Moreover, attachments is continued beyond K_c and hence the giant cluster size also grows gradually after the jump transition. We remark that the increase of phase coherence R should not be confused with the growth of frequency cluster.

Microscopically, each individual oscillator continuously changes its ranking as seen in Fig. 7.6. Fluctuations in the ranking is quite wide for the oscillators of intermediate values of frequency, as in Fig. 7.6 (c,d), although they collectively form a macroscopic frequency cluster in average, as in Fig. 7.6 (a,b). In turn, an intermediate class oscillator rapidly switches its belonging group. On the other hand, a low/high class oscillator rarely switch its role as leader/follower. Fig. 7.7 shows power-law tail in the interevent time distribution of switchings events between the leader group and the follower group. It is remarked, however, presence of this critical phenomenon is not limited to the hybrid transition of the order parameter curve. Power law in the interevent time is orchestrated by the dichotomous dynamics together with the global sorting process, and it seems to happen regardless of the value of coupling strength K.

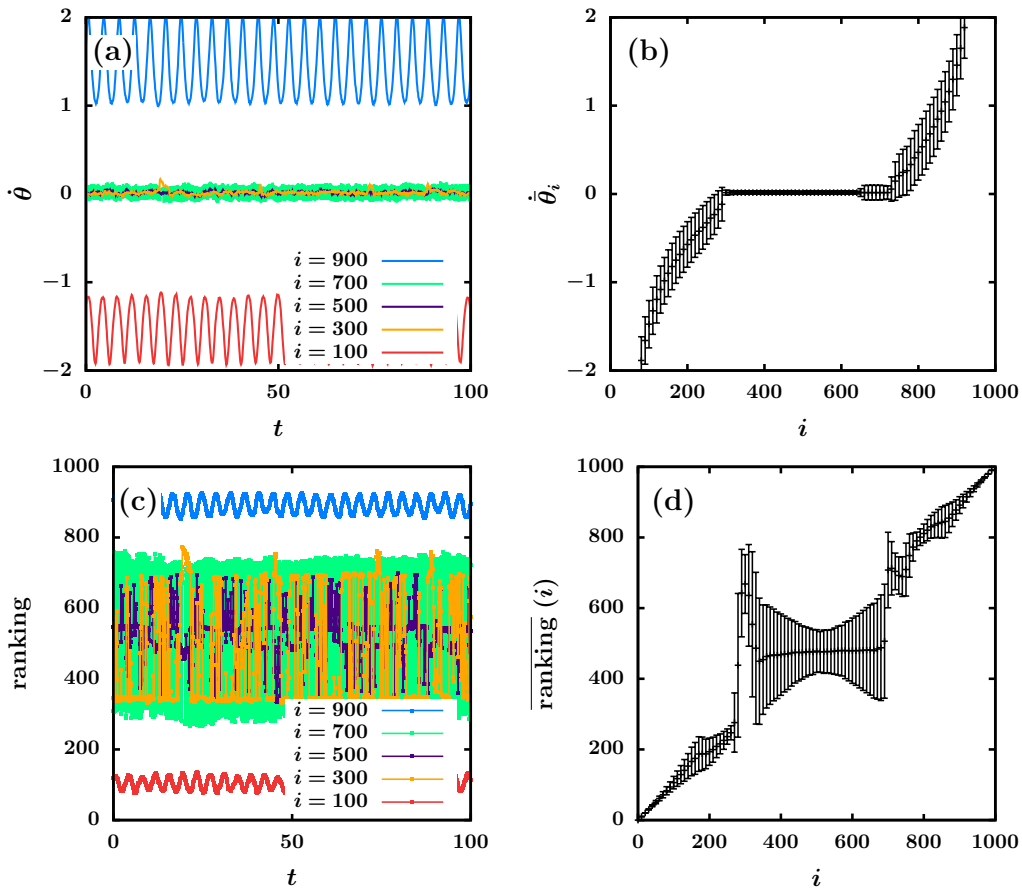

Figure 7.6: Oscillators can change their ranking. Trajectories of (a) angular velocity and (c) ranking, and (b,d) their temporal mean and standard deviations on each oscillator basis. In average, a finite fraction of oscillator population has frequency clustered, and their fluctuations in angular velocities are small. However, those intermediate oscillator class at the same time has quite wide fluctuations in ranking, in contrast to the oscillators at extremes. $N = 10^3$, Lorentzian frequency distribution, $g = 0.7, K = 1$. In (b) and (d) we plotted every 10 oscillators for a better visualization.

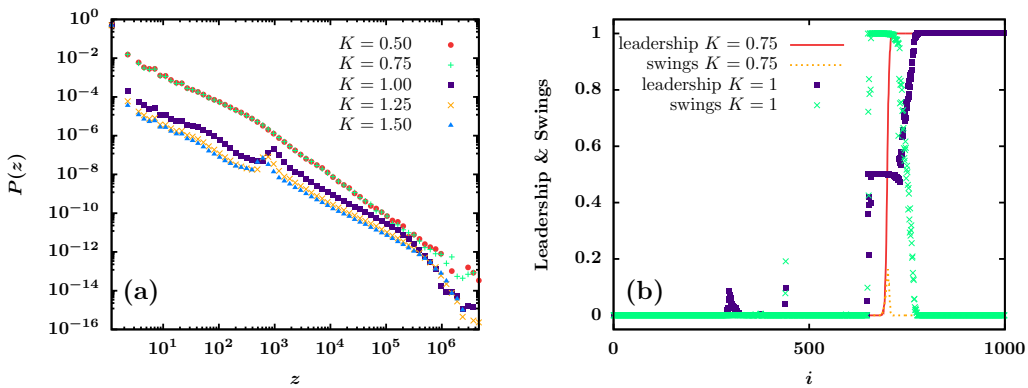

Figure 7.7: (a) The restricted synchronization self-organizes a heavy tail in the interevent time distribution of leader-follower group switchings, regardless of the value of the coupling strength K. In (b), each node's participation rate as a leader and frequency of swings are plotted, for a subcritical coupling $K = 0.75$ and for a supercritical coupling $K = 1$. Notice that there are swinging intermediate class and unwavering populations at sides.

Chapter 8

Conclusion

In conclusion, there are several classes of hybrid phase transitions in complex systems, and their hybrid critical phenomena can be rich. In the cascade class hybrid percolation transition, there is a powder-keg mechanism, a crossover from critical branching to supercritical branching. In the flat-topped class of hybrid synchronization, an absence of synchronization seed leads to an abrupt frequency clustering. Finally, in the restriction class hybrid percolation and hybrid synchronization transitions, there is a dynamic self-organization to criticality through intricate ranking dynamics. In contrast to equilibrium systems, hybrid singular point of the order parameter curve is realized under nonequilibrium drivings. This second-order-like hybrid singular point of nonequilibrium complex systems may associate to diverse critical phenomena, for example, organization of power laws in finite cluster (or avalanche) size distribution and/or interevent time distributions. The dynamic processes at the hybrid phase transition may display rich and intricate phenomena, such as metastable dynamics around saddles, formation of long-range connections, devil's staircase and crackling noise, burst, and wide ranking fluctuations.

Limitations and future directions: The ordinary percolation transition of cluster systems was mappable to a magnetic phase transition. Hence the percolation phase transition and its critical phenomena allows a robust renormalization approach. Concepts of critical exponents and scaling relations were followed. Instead, a hybrid percolation transition displays a wide sample-to-sample fluctuations of giant cluster size at the transition point, which is non-gaussian. There are two diverging scales. One is caused by the fractality displayed by the finite clusters (or avalanches), and the other relates to this non-self-averaging aspect of the

giant cluster size. But the giant itself is compact, i.e. having a fractal dimension equal to the dimensionality of the system, and hence the bulk of which gives no anomaly. Hence a way to coarse-grain the system under the presence of two diverging scales is quite nontrivial, and developing a renormalization theory of the hybrid percolation transition remains challenging.

On the other hand, a static synchronization transition can be viewed as frequency clustering, a cluster growth process. Hybrid synchronization transition is characterized by an abrupt frequency clustering, in the coupling constant domain. Otherwise speaking, a giant synchronized frequency cluster can destruct via cascade of splittings. As a consequence, hybrid synchronization transition is often characterized by an absence of hysteresis, in contrast to the first-order explosive synchronization transition, which in general has hysteresis. However, such a dichotomous view is not always correct. It is remarked that the forward and backward explosive synchronization transitions might be potentially regarded as two independent hybrid transitions, if each of both has a hybrid type singularity. For hybrid synchronization transition, whether there are hybrid critical phenomena directly associated to the hybrid order-parameter-singularity is yet inconclusive, although there are some candidates. Further studies on the critical phenomena of various hybrid synchronization transitions are necessary.

Appendices

Appendix A

Kasteleyn-Fortuin Transformation

The original paper of Fortuin and Kasteleyn is quite complicated. Here, a simplified derivation presented by Edwards and Sokal, and Fortunato is followed [86, 87]. Define joint probability of spin ($\sigma_i = 1, \cdots, q$) and link ($n_{ij} = 0, 1$) configurations as

$$P(\sigma, n) = Z^{-1} \prod_{\langle ij \rangle} \left[(1 - p_{ij}) \delta_{n_{ij},0} + p_{ij} \delta_{\sigma_i,\sigma_j} \delta_{n_{ij},1} \right], \tag{A.1}$$

together with the Fortuin-Kasteleyn-Swendsen-Wang partition function [86]

$$Z = \sum_{\sigma} \sum_{n} \prod_{\langle ij \rangle} \left[(1 - p_{ij}) \delta_{n_{ij},0} + p_{ij} \delta_{\sigma_i,\sigma_j} \delta_{n_{ij},1} \right]. \tag{A.2}$$

The two nearest neighbor sites with same spin alignment is joined with a link by a random probability p. By summing over all link configurations we obtain

$$\begin{aligned}
P(\sigma) &= \sum_{n} P(\sigma, n) && \text{(A.3)} \\
&= Z^{-1} \prod_{\langle ij \rangle} \sum_{n_{ij}=0,1} \left[(1 - p_{ij}) \delta_{n_{ij},0} + p_{ij} \delta_{\sigma_i,\sigma_j} \delta_{n_{ij},1} \right] && \text{(A.4)} \\
&= Z^{-1} \prod_{\langle ij \rangle} \left[(1 - p_{ij}) + p_{ij} \delta_{\sigma_i,\sigma_j} \right] && \text{(A.5)} \\
&= Z^{-1} \prod_{\langle ij \rangle} \exp[-\beta J (1 - \delta_{\sigma_i,\sigma_j})] && \text{(A.6)} \\
&= Z^{-1} e^{-\beta H} && \text{(A.7)}
\end{aligned}$$

where the probability of joining two nearest neighbor sites is p_{ij} is set temperature dependent as $1 - \exp(-\beta J)$ to reduce to the form of Potts Hamiltonian

$$H(\sigma) = -J \sum_{\langle ij \rangle} (\delta_{\sigma_i, \sigma_j} - 1). \tag{A.8}$$

By the normalization condition of $P(\sigma)$ we obtain

$$Z = \sum_{\sigma} e^{-\beta H(\sigma)} \tag{A.9}$$

Instead by summing over all spin configurations we obtain

$$\begin{aligned} P(n) &= \sum_{\sigma} P(\sigma, n) && \text{(A.10)} \\ &= Z^{-1} \sum_{\sigma} \left[\prod_{\langle ij \rangle, n_{ij}=1} p_{ij} \delta_{\sigma_i, \sigma_j} \prod_{\langle ij \rangle, n_{ij}=0} (1 - p_{ij}) \right] && \text{(A.11)} \\ &= Z^{-1} \sum_{\sigma^n} \left[\prod_{\langle ij \rangle, n_{ij}=1} p_{ij} \prod_{\langle ij \rangle, n_{ij}=0} (1 - p_{ij}) \right] && \text{(A.12)} \\ &= Z^{-1} \prod_{\langle ij \rangle, n_{ij}=1} p_{ij} \prod_{\langle ij \rangle, n_{ij}=0} (1 - p_{ij}) q^{c(n)} && \text{(A.13)} \end{aligned}$$

where σ^n denotes a spin configuration which are compatible with the Kastelen-Fortuin clusters. $c(n)$ is the number of clusters and $q^{c(n)}$ is the number of possible colorings [83]. Again, by the normalization condition of $P(n)$ we obtain

$$Z = \sum_{n} \left[\prod_{\langle ij \rangle, n_{ij}=1} p_{ij} \prod_{\langle ij \rangle, n_{ij}=0} (1 - p_{ij}) q^{c(n)} \right]. \tag{A.14}$$

The Potts model and Fortuin-Kasteleyn model are reduced from the Fortuin-Kasteleyn-Swendsen-Wang model, and the three partition functions (A.2), (A.9), (A.14) are equivalent. Note in addition that the $q \to 1$ limit of the Fortuin-Kasteleyn partition function (A.14) corresponds to the graph partition function of the percolation model. Thus percolation model is a $q \to 1$ limit of the q-state Potts model.

Appendix B

Ott–Antonsen and Watanabe-Strogatz reductions

Here, we briefly review the Ott–Antonsen reduction and obtain the reduced system of the Lorentzian case.

The continuum Kuramoto model In the thermodynamic limit $N \to \infty$, a continuum description of the Kuramoto model is possible. The density function

$$\rho(\omega, \theta, t) = \lim_{N\to\infty} \frac{1}{N} \sum_{i=1}^{N} \delta(\omega - \omega_i)\delta\left(\theta - \theta_i(t)\right) \tag{B.1}$$

describes the density of oscillators with natural frequency ω and phase θ at time t. Since the oscillators are conserved, the Kuramoto fluid satisfies the continuity equation

$$\frac{\partial \rho}{\partial t} + \frac{\partial}{\partial \theta}(\rho v) = 0, \tag{B.2}$$

with the velocity field given congruent to the Eq. (4.3) as

$$v(\omega, \theta, t) = \omega + KR\sin(\psi - \theta) = \omega + \frac{K}{2i}\left(Ze^{-i\theta} - Z^* e^{i\theta}\right), \tag{B.3}$$

where the asterisk denotes complex conjugate and the complex order parameter Z of the continuum is given as

$$Z(t) = \iint d\omega d\theta \; \rho(\omega, \theta, t) e^{i\theta}. \tag{B.4}$$

Note since each Kuramoto oscillator has a time-independent natural frequency ω, the flow is in the θ-direction only.

The Ott–Antonsen ansatz The density function can be series expanded in the angular dimension θ as

$$\rho(\omega, \theta, t) = \frac{g(\omega)}{2\pi}\left[1 + \sum_{n=1}^{\infty} \rho_n(\omega, t) e^{in\theta} + c.c.\right], \tag{B.5}$$

where the complex conjugate terms are required to satisfy the reality. The Ott–Antonsen ansatz considers a restricted class of solutions, which relates the complex n-th harmonics to the fundamental harmonic by a geometric series

$$\rho_n(\omega, t) = a^n(\omega, t). \tag{B.6}$$

Plugging in (B.5) to the (B.2) will result a whole tower of equations on harmonics, which is in turn simplified to a single equation by this assumption (B.6). For each frequency mode $a(\omega, t)$,

$$\frac{\partial a}{\partial t} + i\omega a + \frac{K}{2}\left(Za^2 - Z^*\right) = 0, \tag{B.7}$$

where the complex order parameter becomes

$$Z(t) = \int d\omega g(\omega) a^*(\omega, t). \tag{B.8}$$

In particular, for a Lorentzian frequency distribution

$$g(\omega) = \frac{\gamma/\pi}{\gamma^2 + \omega^2}, \tag{B.9}$$

the integral for the complex order parameter (B.7) can be further calculated out as a contour integral in the complex plane, assuming that $a^*(\omega)$ can be analytically continued in the com-

plex ω plane. Remarkably, we find for a Lorentzian distribution that only a single complex mode is relevant to the order parameter.

$$Z(t) = a^*(-i\gamma, t). \tag{B.10}$$

Moreover, the complex order parameter dynamics $Z(t)$ is described by the first-order ordinary differential equation closed in Z

$$\frac{dZ(t)}{dt} = \left(\frac{K}{2} - \gamma\right) Z - \frac{K}{2}|Z|^2 Z. \tag{B.11}$$

For $0 < K < 2\gamma$ we immediately notice that $Z(t) \to 0$. A nontrivial solution emerges for $K \geq 2\gamma$. In the case of Lorentzian natural frequency distribution, dimensional reduction occurs; an infinite number of complex modes reduced to a single complex mode, or two real dimensions. The order parameter dynamics can be tracked exactly.

meaning of the OA anasatz OA ansatz [128] is a restricted class of states with Fourier components following a geometric series. Together with a governing equation it forms an invariant manifold. The transverse attraction of this manifold is proven in Ref. [129], provided that the natural frequency distribution has a finite width. The OA ansatz may be interpreted as follows. In a steady state with $R(t) \simeq Re^{i\Omega t + i\Psi_0}$ where R and Ω being nearly constant, a drifting oscillator $|\omega| > |KR|$ is distributed in the phase circle as

$$\rho_\omega(\theta) \propto \frac{1}{|\dot{\theta}_\omega|} \sim \frac{1}{|\omega - KR\sin\theta|} \sim \frac{1}{1 - a\sin\theta}. \tag{B.12}$$

where $a \equiv |KR/\omega| < 1$. In the next steps we show that the Ott–Antonsen ansatz is naturally obtained from the steady state condition (B.12). The normalized distribution is written (appendix D),

$$\rho_\omega(\theta) = \frac{\sqrt{1-a^2}}{2\pi} \frac{1}{1 - a\sin\theta}. \tag{B.13}$$

Now, the m-th Fourier coefficient is calculated as

$$\rho_{\omega,m} = \int d\theta \rho_\omega(\theta) e^{-im\theta} \tag{B.14}$$

$$= \frac{\sqrt{1-a^2}}{2\pi} \int d\theta \frac{e^{-im\theta}}{1 - a\sin\theta} \tag{B.15}$$

$$= \frac{\sqrt{1-a^2}}{2\pi} \int_{|z|=1} \frac{idz}{z} \frac{z^m}{1 - \frac{a}{2i}(z^{-1} - z)} \tag{B.16}$$

$$= -\frac{\sqrt{1-a^2}}{2\pi i} \frac{2i}{a} \int_{|z|=1} dz \frac{z^m}{z^2 + \frac{2iz}{a} - 1} \tag{B.17}$$

$$= \frac{2i\sqrt{1-a^2}}{a} \frac{z_+^m}{z_+ - z_-} \tag{B.18}$$

$$= \left(\frac{\sqrt{1+a^2} - 1}{a} \right)^m \tag{B.19}$$

$$= \rho_{\omega,1}^m. \tag{B.20}$$

where $z_\pm = -\frac{i}{a} \pm i\sqrt{\frac{1}{a^2} - 1}$, and only $z = z_+$ is enclosed by the contour. The resulting last line is the Ott–Antonsen ansatz (B.6).

Watanabe-Strogatz reduction Another important case is identical oscillators. $\omega_i = \omega$. In this case reduction is possible through the so-called Watanabe-Storgatz transform [126, 127]. The equation of motion of the fully connected identical oscillators is written

$$\frac{d\theta_k}{dt} = \omega(t) + \mathrm{Im}\big[Z(t) e^{-i\theta_k}\big] \tag{B.21}$$

where $\omega(t)$ is an arbitrary function of time and $Z(t)$ is some complex external field, or is given as $(1/N)\sum_{j=1}^N e^{i\theta_j}$ in case of a Kuramoto system. Watanabe and Strogatz showed that this system (B.21) could be reduced from N ordinary differential equations to three ordinary differential equations through a time-dependent transformation

$$\tan\left(\frac{\theta_k(t) - \Phi(t)}{2}\right) = \sqrt{\frac{1+\gamma(t)}{1-\gamma(t)}} \tan\left(\frac{\Psi_k - \Theta(t)}{2}\right) \tag{B.22}$$

which transforms a set of constant angles $\{\Psi_k\}$ to a set of functions $\theta_k(t)$ for $k = 1, \cdots, N$ [126, 127]. By direct substitution, one can check that the resulting $\theta_k(t)$ simultaneously satisfy all N equations of (B.21) as long as the three variables $\phi(t), \gamma(t), \Theta(t)$ satisfy a certain closed set of ordinary differential equations. A modern view to this enigmatic transformation has been provided by [150–152]. Here I follow the approach by Pikovsky [150, 152]. The equation (B.21) is rewritten in terms of phasors as

$$\frac{d}{dt}e^{i\theta_k} = i\omega(t)e^{i\theta_k} + \frac{1}{2}Z(t) - \frac{e^{2i\theta_k}}{2}Z^*(t). \tag{B.23}$$

Now Möbius transform $\{\theta_k\}$ variables into $\{\psi_k\}$ variables.

$$e^{i\theta_k} = \frac{z + e^{i\psi_k}}{1 + z^* e^{i\psi_k}} \tag{B.24}$$

$$e^{i\psi_k} = \frac{-z + e^{i\theta_k}}{1 - z^* e^{i\theta_k}} \tag{B.25}$$

where z is a free complex parameter $|z| \leq 1$. Require the following complex condition to this overly determined system:

$$\frac{1}{N}\sum_k e^{i\psi_k} = 0 \tag{B.26}$$

that is $\langle e^{i\psi_k} \rangle = 0, \langle \dot{\psi}_k e^{i\psi_k} \rangle = 0$ where the angular bracket $\langle \cdot \rangle$ denotes averaging in k. The equation of motion in terms of ψ variables is written as

$$\frac{d}{dt}\left(\frac{z + e^{i\psi_k}}{1 + z^* e^{i\psi_k}}\right) = i\omega(t)\frac{z + e^{i\psi_k}}{1 + z^* e^{i\psi_k}} + \frac{1}{2}Z(t) - \frac{1}{2}Z^*(t)\left(\frac{z + e^{i\psi_k}}{1 + z^* e^{i\psi_k}}\right)^2 \tag{B.27}$$

Hence

$$\begin{aligned}
&(\dot{z} + i\dot{\psi}_k e^{i\psi_k})(1 + z^* e^{i\psi_k}) - (z + e^{i\psi_k})(\dot{z}^* e^{i\psi_k} + iz^*\dot{\psi}_k e^{i\psi_k}) \\
&= i\omega(z + e^{i\psi_k})(1 + z^* e^{i\psi_k}) + \frac{1}{2}Z(1 + z^* e^{i\psi_k})^2 - \frac{1}{2}Z^*(z + e^{i\psi_k})^2
\end{aligned} \tag{B.28}$$

Averaging in k gives

$$\left(\dot{z} - i\omega z - \frac{Z}{2} + \frac{Z^*}{2}z^2\right) - \left(\dot{z}^* + i\omega z^* - \frac{Z^*}{2} + \frac{Z}{2}(z^*)^2\right)\langle e^{2i\psi_k}\rangle = 0 \tag{B.29}$$

where $\langle e^{2i\psi_k}\rangle$ can take an arbitrary value depending on the initial conditions. Hence

$$\dot{z} = i\omega z + \frac{Z}{2} - \frac{Z^*}{2}z^2 \tag{B.30}$$

Substituting it back into the equation before averaging in k gives in the $e^{i\psi_k}$ order, where zeroth order and $e^{2i\psi_k}$ order vanish.

$$\dot{\psi}_k = \omega + \mathrm{Im}[Zz^*] \tag{B.31}$$

Remarkably, the dynamics of ψ_k does not depend on k. In other words, ψ_k variables have no relative motion. This causes a huge amout of reduction.

$$\psi_k(t) = \psi(t) + \psi_k(0) \tag{B.32}$$

$$\frac{d\psi}{dt} = \omega + \mathrm{Im}[Zz^*] \tag{B.33}$$

Thus N equations (B.21) are reduced to just 3 equations (B.30) and (B.33). It should be noted that $z = \rho e^{i\Phi}$ is in general different from the order parameter $Z = \langle e^{i\theta_k}\rangle = Re^{i\Psi}$. The Möbius transform (B.24)

$$e^{i\theta_k - \Phi} = \frac{\rho + e^{i(\psi_k - \Phi)}}{1 + \rho e^{i(\psi_k - \Phi)}} \tag{B.34}$$

yields the well known Watanabe-Strogatz transform. Using the identity $\tan(x/2) = i(1 - e^{ix})/(1 + e^{ix})$,

$$\tan\left(\frac{\theta_k - \Phi}{2}\right) = i\frac{1 - e^{i(\theta_k - \Phi)}}{1 + e^{i(\theta_k - \Phi)}} \tag{B.35}$$

$$= i\frac{(1-\rho)(1 - e^{i(\psi_k - \Phi)})}{(1+\rho)(1 + e^{i(\psi_k - \Phi)})} \tag{B.36}$$

$$= \frac{1-\rho}{1+\rho}\tan\left(\frac{\psi_k - \Phi}{2}\right) \tag{B.37}$$

which is equivalent to the Watanabe-Strogatz transform (B.22) with $\gamma = -2\rho/(1+\rho^2), \Theta = \Phi - \psi, \Psi_k = \psi_k(0)$. Therefore, given an initial condition $\{\theta_k(0)\}$, we can always find the corresponding $\{\psi_k(0)\}$ state and the initial conditions $Z(0)$, and $z(0)$ is determined by the constraint (B.26). By integrating just three equations (B.30) and (B.33), $z(t), \psi(t)$ can be solved, and $\{\psi_k(t)\}, \{\theta_k(t)\}$ are determined. Thus the integration of N dimensional system has been reduced to the integration of the three dimensional system.

Appendix C

Temporal fluctuations of the Kuramoto order parameter

Consider a finite Kuramoto system consists of a large number of oscillators ($N \gg 1$). There exist persistent fluctuations of the complex order parameter $Z(t)$ even in this large but finite N. Symmetric sampling of $\{\omega_i\}$ from a gaussian distribution $g(\omega)$ is assumed. Daido's system size expansion method is as followed. Let [130]

$$w(t) = Z(t) - \hat{Z} \tag{C.1}$$

$$\theta_i(t) = \hat{\psi}_i(t) + \phi_i(t) \tag{C.2}$$

where $\hat{Z}$ and $\hat{\psi}_i(t)$ is the complex order parameter and phase movement, respectively, of a hypothetically infinite Kuramoto system. When N is large, $\hat{Z}$ can be replaced by the time average $\langle Z(t) \rangle$ and $w(t)$ should be small, after some initial transient period has passed. Except at the critical point, correlation length is finite and the central limit theorem may be applied. Up to leading orders of $1/N$ expansions:

$$w = \frac{\tilde{w}}{\sqrt{N}} + O\left(\frac{1}{N}\right) \tag{C.3}$$

$$\theta_i = \psi_i + \frac{\tilde{\phi}_i}{\sqrt{N}} + O\left(\frac{1}{N}\right) \tag{C.4}$$

and $Z(t) = \hat{Z} + w(t) = \hat{Z} + \tilde{w}/\sqrt{N}$. The tilde variables are rescaled in N.

The Kuramoto equation $\dot{\theta}_i = \omega_i + K\,\mathrm{Im}(Z(t)e^{-i\theta_i})$ in the order $O(1/\sqrt{N})$ gives

$$\frac{d\tilde{\phi}_i}{dt} = K\,\mathrm{Im}\left[\left((-i\tilde{\phi}_i)\hat{Z} + \tilde{w}\right)e^{-i\psi_i}\right] \tag{C.5}$$

which has the solution formally written as

$$\tilde{\phi}_i(t) = \int_0^t dt' \exp\left[\int_{t'}^t d\tau K\,\mathrm{Im}\left(-i\hat{Z}e^{-i\psi_i(\tau)}\right)\right] K\,\mathrm{Im}\,\tilde{w}(t')e^{-i\psi_i(t')} \tag{C.6}$$

Hence the order parameter deviation is

$$\begin{aligned}
w(t) &= Z(t) - \hat{Z} && \text{(C.7)}\\
&= \frac{1}{N}\sum_{i=1}^N e^{i\left(\psi_i + \tilde{\phi}_i/\sqrt{N}\right)} - \hat{Z} && \text{(C.8)}\\
&= \left[\frac{1}{N}\sum_{i=1}^N e^{i\psi_i} - \hat{Z}\right] + \frac{i}{N\sqrt{N}}\sum_{i=1}^N e^{i\psi_i}\tilde{\phi}_i + O\left(\frac{1}{N}\right) && \text{(C.9)}\\
&= \left[\frac{1}{N}\sum_{i=1}^N e^{i\psi_i} - \hat{Z}\right] + \frac{iK}{N\sqrt{N}}\sum_{i=1}^N e^{i\psi_i(t)}\\
&\qquad \times \int_0^t dt' \exp\left[\int_{t'}^t d\tau K\,\mathrm{Im}\left(-i\hat{Z}e^{-i\psi_i}\right)\right]\mathrm{Im}\,\tilde{w}e^{-i\psi_i(t')} && \text{(C.10)}\\
&= \left[\frac{1}{N}\sum_{i=1}^N e^{i\psi_i} - \hat{Z}\right]\\
&\quad + \frac{iK}{2N}\sum_{i=1}^N \int_0^t dt' w(t') e^{i(\psi_i(t) - \psi_i(t'))} \exp\left[\int_{t'}^t d\tau K\,\mathrm{Im}\left(-i\hat{Z}e^{-i\psi_i}\right)\right]\\
&\quad - \frac{iK}{2N}\sum_{i=1}^N \int_0^t dt' w^*(t') e^{i(\psi_i(t) + \psi_i(t'))} \exp\left[\int_{t'}^t d\tau K\,\mathrm{Im}\left(-i\hat{Z}e^{-i\psi_i}\right)\right] && \text{(C.11)}\\
&= \left[\frac{1}{N}\sum_{i=1}^N e^{i\psi_i} - \hat{Z}\right] + \frac{K}{2}\int_0^t dt'\left[A_-(t,t')w(t') - A_+(t,t')w^*(t')\right]dt' && \text{(C.12)}
\end{aligned}$$

where it has been let

$$A_{\pm}(t,t') \equiv \lim_{N\to\infty} \frac{1}{N} \sum_{i=1}^{N} \exp\left[i\big(\psi_i(t) \pm \psi_i(t')\big) + K \int_{t'}^{t} d\tau \, \mathrm{Im}\,\big(- \hat{Z} e^{-i\psi_i(\tau)}\big)\right]. \quad \text{(C.13)}$$

In the subcritical disordered phase $\hat{Z} = 0$ and the dominant phase motion is $\psi_i(t) = \theta_i(0) + \Delta_i(t)$ and the kernels $A_{\pm}$ are simplified as

$$A_{-}(t,t') = \lim_{N\to\infty} \frac{1}{N} \sum_{i=1}^{N} e^{i\Delta_i(t-t')} \equiv A(t-t') \quad \text{(C.14)}$$

$$A_{+}(t,t') = \lim_{N\to\infty} \frac{1}{N} \sum_{i=1}^{N} e^{i(\Delta_i(t+t')+2\theta_i(0))} \equiv B(t+t') \quad \text{(C.15)}$$

and

$$w(t) = \frac{1}{N} \sum_{i=1}^{N} e^{i(\Delta_i t + \theta_i(0))} + \frac{K}{2} \int_0^t dt' [A_{-}(t-t')w(t') - B(t+t')w^*(t')] \quad \text{(C.16)}$$

Here, the integrand involving B vanishes in the limit $t \to \infty$ by the Riemann-Lebesgue lemma. Upon Fourier transforms,

$$w(t) = \frac{1}{N} \sum_{i=1}^{N} \frac{e^{i(\theta_i(0)+\Delta_i t)}}{1 - \frac{K}{2}\tilde{A}(\omega_i)} \quad \text{(C.17)}$$

and finally the temporal fluctuations of the order parameter is given by

$$\chi = \lim_{N\to\infty} N\big\langle |w - \langle w\rangle|^2 \big\rangle \quad \text{(C.18)}$$

For a Lorentzian distribution $g(\omega) = (\Gamma/\pi)/(\omega^2+\Gamma^2)$, one finds $\tilde{A}(\omega) = (\Gamma - i\omega)/(\omega^2+\Gamma^2)$ and

$$\chi = \frac{2\Gamma}{2\Gamma - K} \propto (K - K_c)^{-1}. \quad \text{(C.19)}$$

Hence the critical exponent of the temporal fluctuations of the order parameter yields as $\gamma' =$

1 at the subcritical side. Similarly, order parameter fluctuations diverge at the supercritical side, but Daido's calculation had yielded a different exponent $\gamma = 1/4$ [130]. There was a controversy on this exponent value on the supercritical side. Recently, an intensive finite size scaling analysis [131] and an exact Ott-Antonsen calculation obtained $\gamma = 1$ in the supercritical regime [132].

Appendix D

Useful integrals

Gamma function Gamma function is defined as

$$\Gamma(n) = \int_0^\infty dx x^{n-1} e^{-x}. \tag{D.1}$$

Using this integral representation, we can easily evaluate the following integral

$$\int_0^\infty dx x^{n-1} e^{-fx} = \frac{\Gamma(n)}{f^n}, \quad f > 0. \tag{D.2}$$

Feynman's trick Another useful integral representation is

$$f = \int_0^\infty ds e^{-sf}. \tag{D.3}$$

Applying these tricks, we can evaluate for example the normalization constant in (5.1),

$$\begin{aligned}
\int_{-\infty}^\infty \frac{d\omega}{\omega^{2m} + \gamma^{2m}} &= 2\int_0^\infty d\omega \int_0^\infty ds e^{-s(\omega^{2m}+\gamma^{2m})} && \text{(D.4)}\\
&= 2\int_0^\infty ds e^{-s\gamma^{2m}} \int_0^\infty d\omega e^{-s\omega^{2m}} && \text{(D.5)}\\
&= \frac{1}{m}\int_0^\infty ds e^{-s\gamma^{2m}} \int_0^\infty dt\, t^{\frac{1}{2m}-1} e^{-st} && \text{(D.6)}\\
&= \frac{1}{m}\Gamma\Big(\frac{1}{2m}\Big) \int_0^\infty ds\, s^{-1/2m} e^{-s\gamma^{2m}} && \text{(D.7)}\\
&= \frac{\gamma^{2m-1}\Gamma(1-\frac{1}{2m})\Gamma(\frac{1}{2m})}{m} && \text{(D.8)}\\
&= \frac{\gamma^{2m-1}}{m}\frac{\pi}{\sin\frac{\pi}{2m}}. && \text{(D.9)}
\end{aligned}$$

Beta function Integral representation of the beta function is given as

$$\beta(m,n) = \int_0^1 dx x^{m-1}(1-x)^{n-1}. \tag{D.10}$$

A key property of the beta function is its relationship to the gamma function

$$\beta(m,n) = \frac{\Gamma(m)\Gamma(n)}{\Gamma(m+n)}. \tag{D.11}$$

Following asymptotics of the beta function is useful.

$$\beta(m,n) \sim \Gamma(n) m^{-n} \tag{D.12}$$

for fixed n and large m. Now consider the following integral for example.

$$\begin{aligned} I_{2n} &\equiv \int_{-1}^{1} d\theta \, \sin^{2n}\theta \cos\theta, && \text{(D.13)} \\ &= 2\int_0^1 dx \, x^{2n}\sqrt{1-x^2} && \text{(D.14)} \\ &= \int_0^1 dt \, t^{(2n-1)/2}(1-t)^{1/2} && \text{(D.15)} \\ &= \beta\left(\frac{2n+1}{2}, \frac{3}{2}\right). && \text{(D.16)} \end{aligned}$$

for an integer n. The beta function kernel appears naturally in the calculation of the probability distribution of interevent times [51]. For example, for a random uncorrelated sequence of events with occurrence probability p. The probability of waiting time interval z between consecutive events is written as $(1-p)^{z-1}p$, which follows a Poisson distribution. For correlated sequence of events, a power law distribution can occur [51, 108]. For example, for time dependent initiation $p_0(t)$ and selection $p(t)$ probabilities, interevent time distribution accumulated during $[0, t_c]$ is written as [51]

$$P_z = \int_0^{t_c} p_0(t)[1-p(t)]^{z-1}p(t)dt. \tag{D.17}$$

Drifting oscillator's trajectory Use of order parameter decouples the Kuramoto equation to a one-dimensional equation $\dot{\theta} = \omega - KR\sin(\theta - \psi)$. We evaluate the trajectory of a drifting oscillator $|KR/\omega| \equiv |a| < 1$ for stationary (R, ψ),

$$\int \frac{d\theta}{\omega - KR\sin\theta} = \frac{1}{\omega}\int \frac{2dt}{1+t^2}\frac{1}{1-a\frac{2t}{1+t^2}} \tag{D.18}$$

$$= \frac{2}{\omega}\int \frac{dt}{t^2 - 2at + 1} \tag{D.19}$$

$$= \frac{2}{\omega}\int \frac{ds}{s^2 + b^2} \tag{D.20}$$

$$= \frac{2}{\omega}\int \frac{b\sec^2\phi d\phi}{b^2\sec^2\phi} \tag{D.21}$$

$$= \frac{2\phi}{b\omega} + \phi_0 \tag{D.22}$$

$$= \frac{2}{b\omega}\arctan\frac{t+a}{b} + \phi_0 \tag{D.23}$$

$$= \frac{2}{b\omega}\arctan\left(\frac{1}{b}\tan\frac{\theta}{2} + \frac{a}{b}\right) + \phi_0. \tag{D.24}$$

We used the tangent half-angle and trigonometric substitutions $t = \tan(\theta/2) = b\tan\phi$, and let $a \equiv \frac{KR}{\omega}, b \equiv \sqrt{1-a^2}, \psi = 0$. For a time-constant R and ψ the drifting oscillator trajectory is

$$\tan\frac{\theta(t) - \psi}{2} = \sqrt{1 - \frac{K^2R^2}{\omega^2}}\tan\left(\frac{\omega t}{2}\sqrt{1 - \frac{K^2R^2}{\omega^2}} - \phi_0\right) - \frac{KR}{\omega}. \tag{D.25}$$

Period The period of oscillations of a drifting oscillator ($|\omega| > KR$) is followed

$$T = \int_{-\pi}^{\pi}\frac{d\theta}{|\dot{\theta}|} = \int_{-\pi}^{\pi}\frac{d\theta}{|\omega| - KR\sin\theta} = \frac{2\pi}{\sqrt{\omega^2 - K^2R^2}}. \tag{D.26}$$

Drifting oscillator contribution Notice that

$$\int_{-\pi}^{\pi}\frac{\sin\theta}{A - B\sin\theta}d\theta = \frac{2\pi}{B}\left(\frac{A}{\sqrt{A^2 - B^2}} - 1\right), \quad A > |B| > 0, \tag{D.27}$$

is also followed, and by the parities of cosine $(-++-)$ and sine $(--++)$

$$\int_{-\pi}^{\pi} \frac{\cos\theta}{A - B\sin\theta} d\theta = 0, \quad A > |B| > 0. \tag{D.28}$$

Combining the results of the previous two integrals, we find that a drifting oscillator's contribution to the order paramater $\langle e^{i\theta} \rangle$ is purely imaginary

$$\langle e^{i\theta} \rangle = \frac{1}{T} \int_{-\pi}^{\pi} d\theta \frac{e^{i\theta}}{|\dot{\theta}|} = i\left(\frac{\omega}{KR} - \mathrm{sgn}(\omega) \sqrt{\frac{\omega^2}{K^2R^2} - 1} \right). \tag{D.29}$$

Note in the above equation that the drifting oscillator contribution is odd in ω; which will thus cancel pairwisely for symmetric distribution of natural frequencies $g(\omega) = g(-\omega)$. In such case, the imaginary part of the self-consistency equation vanishes.

Self-consistency equation Following indefinite integrals appear frequently in the self consistency equation of the Kuramoto model

$$\int \sqrt{1 - x^2} dx = \frac{1}{2} \left(x\sqrt{1 - x^2} + \arcsin(x) \right) + c \tag{D.30}$$

$$\int \sqrt{x^2 - 1} dx = \frac{1}{2} \left(x\sqrt{x^2 - 1} - \log\left(x + \sqrt{1 - x^2} \right) \right) + c \tag{D.31}$$

where c is the constant of integration.

Appendix E

Numerical Tips

Evaluation of sine The bottleneck in the numerical integration of Kuramoto model is insistent evaluation of sines. For example in a fully connected network of size N, a naive add up of pair interactions will call $O(N^2)$ sine evaluations. Instead, we may benefit from the use of the order parameter. The total number of sine evaluations can be reduced to $O(N)$ per each time step.

$$\dot{\theta}_i = \omega_i + \frac{K}{N}\sum_{j=1}^{N}\sin(\theta_j - \theta_i), \qquad i = 1, \cdots, N \tag{E.1}$$

$$= \omega_i + KR\sin(\psi - \theta_i) \tag{E.2}$$

The procedure is as followed:

$$c_i \leftarrow \cos(\theta_i), \quad s_i \leftarrow \sin(\theta_i) \tag{E.3}$$

$$z_x \leftarrow \frac{1}{N}\sum_i c_i, \quad z_y \leftarrow \frac{1}{N}\sum_i s_i \tag{E.4}$$

$$R\sin(\psi - \theta_i) \leftarrow z_y c_j - z_x s_j. \tag{E.5}$$

where $z_x = R\cos\psi, z_y = R\sin\psi$. For the sake of numerical accuracy and speed, sine addition formula is very useful, rather than invoking further trigonometric function calls such as $\psi = \arctan(z_y/z_x)$ and $\sin(\psi - \theta_i)$.

Modulo operation Modulo operations will cause truncation errors and should be used sparingly. The phase variables need not be kept in range $[0, 2\pi)$ every time step of the numerical integration.

Solving the self consistency equation numerically Self consistency equation of the Kuramoto system is obtained after assuming the steady state of the form $Z(t) \sim Re^{i\Omega t}$ for the complex synchronization order parameter. For a non-traveling solution $\Omega = \langle \omega_i \rangle = 0$, the real self consistency equation of a finite system is written:

$$R = f(R; K, \omega_i) \equiv \frac{1}{N} \sum_{j=1}^{N} \sqrt{1 - \frac{\omega_j^2}{K^2 R^2}} \Theta\big(KR - |\omega_j|\big), \tag{E.6}$$

where the Heaviside $\Theta(x)$ denotes locked oscillators. We may either solve the above equation for R at fixed values of $\{\omega_i\}$ and K, or equivalently solve instead:

$$g(K; R, \omega_i) \equiv R - f(K, R, \omega_i) = 0 \tag{E.7}$$

for K at given set of $\{\omega_i\}$ and a positive $R > 0$. The later method is preferred, because $K(R)$ is usually single-valued while $R(K)$ can become multivalued. Since the problem is one-dimensional root finding, the solution can be roughly seeked by the bisection method and polished using Newton's method if necessary.

For a complex self consistency equation with nontrivial $\Omega \neq \langle \omega_i \rangle = 0$, we need to solve the real and imaginary parts simultaneously and obtain both R and Ω.

$$R = f(R, \Omega; K, \omega_i) \equiv \frac{1}{N} \sum_{j=1}^{N} \sqrt{1 - \frac{(\omega_j - \Omega)^2}{K^2 R^2}} \Theta\big(KR - |\omega_j|\big) \tag{E.8}$$

$$0 = h(R, \Omega; K, \omega_i) \equiv \frac{1}{N} \sum_{j}^{N} \frac{\omega_j - \Omega}{KR} - \frac{1}{N} \sum_{j}^{N} \mathrm{sgn}(\omega_j - \Omega) \sqrt{\frac{(\omega_j - \Omega)^2}{K^2 R^2} - 1} \Theta\big(|\omega_j| - KR\big) \tag{E.9}$$

This two dimensional root finding problem can be attacked by first optimizing $\mathcal{L}(R, \omega) \equiv$

$\big(R - f(R,\Omega)\big)^2 + \big(h(R,\Omega)\big)^2$ to obtain the candidate solutions and then selecting out the solutions. Or, the previous bisection scheme can be applied for K at fixed R, Ω, and $\{\omega_i\}$, utilizing that the domain of (R, Ω) is usually bounded.

Bibliography

[1] P. W. Anderson, "More is different," *Science* **177** 393 (1972).

[2] G. Parisi, "Complex systems: a physicist's viewpoint," *Phys. A* **263**, 557 (1999).

[3] A. B. Harris, "Effect of random defects on the critical behaviour of Ising models," *J. Phys. C* **7**, 1671 (1974).

[4] Y. Imry and S. K. Ma, "Random-field instability of the ordered state of continuous symmetry," *Phys. Rev. Lett.* **35**, 1399 (1975).

[5] D. H. Kim, J. Park and B. Kahng, "Enhanced storage capacity with errors in scale-free Hopfield neural networks: An analytical study," *PloS one* **12** e0184683 (2017).

[6] S. Jang, J. S. Lee, S. Hwang, B. Kahng, "Ashkin-Teller model and diverse opinion phase transitions on multiplex networks," *Phys. Rev. E* **92**, 022110 (2015).

[7] B. C. Coutinho, A. V. Goltsev, S. N. Dorogovtsev and J. F. F. Mendes, "Kuramoto model with frequency-degree correlations on complex networks," *Phys. Rev. E* **87**, 032106 (2013).

[8] Y. Kuramoto, in *International Symposium on Mathematical Problems in Theoretical Physics*, edited by H. Araki, Lecture Notes in Physics, Vol. 30 (Springer, New York, 1975).

[9] A. T. Winfree, *The Geometry of Biological Time* (Springer, Berlin, 1980).

[10] E. A. Martens, E. Barreto, S. H. Strogatz, E. Ott, P. So, T. M. Antonsen, "Exact results for the kuramoto model with a bimodal frequency distribution," *Phys. Rev. E* **79**, 026204 (2009).

[11] Pazó, "Thermodynamic limit of the first-order phase transition in the Kuramoto model," *Phys Rev. E* **72**, 046211 (2005).

[12] L. Basnarkov and V. Urumov, "Phase transitions in the Kuramoto model," *Phys. Rev. E* **76**, 057201 (2007).

[13] J. Park and B. Kahng, "Abnormal hybrid phase transition in the passively competing Kuramoto model," *Physica D* **399**, 186 (2019)

[14] H. Daido, "Population dynamics of randomly interacting self-oscillators. I. tractable models without frustration," *Prog. Theor. Phys.* **77**, 622 (1987).

[15] H. Daido, "Quasientrainment and slow relaxation in a population of oscillators with random and frustrated interactions," *Phys. Rev. Lett.* **68**, 1073 (1992).

[16] B. Ottino-Löffler, S. H. Strogatz, "Volcano transition in a solvable model of frustrated oscillators," *Phys. Rev. Lett.* **120**, 264102 (2018).

[17] C. Börgers, N. Kopell, "Synchronization in networks of excitatory and inhibitory neurons with sparse, random connectivity," *Neural Comput.* **15**, 509 (2003).

[18] D. H. Zanette, "Synchronization and frustration in oscillator networks with attractive and repulsive interactions," *Europhys. Lett.* **72**, 190 (2005).

[19] Hong & Strogatz, "Kuramoto model of coupled oscillators with positive and negative coupling parameters: an example of conformist and contrarian oscillators," *Phys. Rev. Lett.* **106**, 054102 (2011).

[20] J. Park and B. Kahng, "Metastable state en route to traveling-wave synchronization state," *Phys. Rev. E* **97**, 020203(R) (2018).

[21] J. Park and B. Kahng, "Synchronization transitions through metastable state on structured networks," *arXiv:1901.02123* (2019).

[22] S. V. Buldyrev, R. Parshani, G. Paul, H. E. Stanley, S. Havlin, "Catastrophic cascade of failures in interdependent networks," *Nature* **464**, 1025 (2010).

[23] D. J. Thouless, "Long-range order in one-dimensional Ising systems," *Phys. Rev.* **187**, 732 (1969).

[24] A. Bar and D. Mukamel, "Mixed order phase transition in a one-dimensional model," *Phys. Rev. Lett.* **112**, 015701 (2014).

[25] P. M. Chaikin and T. C. Lubensky, *Principles of condensed matter physics* (Cambridge University Press, Cambridge, 2000).

[26] W. L. Bragg and E. J. Williams, "The effect of thermal agitation on atomic arrangement in alloys," *Proc. R. Soc. A* **145**, 699 (1934).

[27] R. Alert, P. Tierno and J. Casademunt, "Mixed order phase transition in a colloidal crystal," *Proc. Natl. Acad. Sci. U.S.A.* **114**, 12906 (2017).

[28] M. Aizenman, J. T. Chayes, L. Chayes and C. M. Newman, *J. Stat. Phys.* **50**, 1 (1988).

[29] F. J. Dyson, "An Ising ferromagnet with discontinuous long-range order," *Commun. Math. Phys.* **21**, 269 (1971).

[30] D. Ruelle, "Statistical mechanics of a one-dimensional lattice gas," *Commun. Math. Phys.* **9**, 267 (1968).

[31] J. Adler, *Physica A* **171**, 453 (1991).

[32] P. M. Kogut and P. L. Leath, *J. Phys. C* **14**, 3187 (1981).

[33] J. Chalupa, P. L. Leath, and G. R. Reich, "Bootstrap percolation on a Bethe lattice," *J. Phys. C* **12**, L31 (1979).

[34] D. Zhou, A. Bashan, R. Cohen, Y. Berezin, N. Shnerb and S. Havlin, "Simultaneous first-and second-order percolation transitions in interdependent networks," *Phys. Rev. E* **90**, 012803 (2014).

[35] G. J. Baxter, S. N. Dorogovtsev, K. E. Lee, J. F. F. Mendes and A. V. Goltsev, "Critical Dynamics of the k-Core Pruning Process,"*Phys. Rev. X* **5**, 031017 (2015).

[36] D. Lee, M. Jo, and B. Kahng, "Critical behavior of k-core percolation: Numerical studies," *Phys. Rev. E* **94**, 062307 (2016).

[37] J. M. Schwarz, A. J. Liu, and L. Q. Chayes, "The onset of jamming as the sudden emergence of an infinite k-core cluster," *Europhys. Lett.* **73**, 560 (2006).

[38] S. N. Dorogovtsev, A. V. Goltsev, and J. F. F. mendes, "k-core organization of complex networks," Phys. Rev. Lett. **96**, 040601 (2006).

[39] G. Parisi and T. Rizzo, "k-core percolation in four dimensions", *Phys. Rev. E* **78**, 022101 (2008).

[40] H. -K. Janssen and O. Stenull, "First-order phase transitions in outbreaks of co-infectious diseases and the extended general epidemic process. *Europhys. Lett.* **113**, 26005 (2016).

[41] W. Choi, D. Lee and B. Kahng, "Mixed-order phase transition in a two-step contagion model with a single infectious seed," *Phys. Rev. E* **95**, 022304 (2017).

[42] W. Choi, D. Lee amd B. Kahng, "Critical behavior of a two-step contagion model with multiple seeds," *Phys. Rev. E* **95**, 062115 (2017).

[43] D. Lee, W. Choi, J. Kértesz and B. Kahng "Universal mechanism for hybrid percolation transitions," *Sci. Rep.* **7**, 5723 (2017).

[44] T. Hasegawa and K. Nemoto "Sudden spreading of infections in an epidemic model with a finite seed fraction," *Eur. Phys. J. B* **91**, 58 (2018).

[45] D. Lee, S. Choi, M. Stippinger, J. Kertész and B. Kahng, "Hybrid phase transition into an absorbing state: Percolation and avalanches," *Phys. Rev. E* **93**, 042109 (2016).

[46] D. Lee, W. Choi, J. Kertész, B. Kahng, "Universal mechanism for hybrid percolation transitions," *Sci. Rep.* **7**, 5723 (2017).

[47] S. W. Son, G. bizhani, C. Christensen, P. Grassberger and M. Paczuski, "Percolation theory on interdependent networks based on epidemic spreading," *Europhys. Lett.* **97**, 16006 (2012).

[48] K. Panagiotou, R. Spöhel, A. Steger, H. Thomas, "Explosive percolation in Erdős-Rényi-like random graph processes," *Electron. Notes Discrete Math.* **38**, 699 (2011).

[49] Y. S. Cho, J. S. Lee, H. J. Herrmann, B. Kahng, "Hybrid percolation transition in cluster merging processes: Continuously varying exponents," *Phys. Rev. Lett.* **116**, 025701 (2016).

[50] K. Choi, D. Lee, Y. S. Cho, J. C. Thiele, H. J. Herrmann and B. Kahng, "Critical phenomena of a hybird phase transition in cluster merging dynamics," *Phys. Rev. E* **96**, 042148 (2017).

[51] J. Park, S. Yi, K. Choi, D. Lee and B. Kahng, "Interevent-time, bursts and hybrid percolation transition," *Chaos* **29**, 091102 (2019).

[52] R. M. D'Souza and J. Nagler, "Anomalous critical and supercritical phenomena in explosive percolation," *Nat. Phys.* **11**, 531 (2015).

[53] S. N. Dorogovtsev, A. V. Goltsev, J. F. F. Mendes, "Criticial phenomena in complex networks," *Rev. Mod. Phys.* **80**, 1275 (2008).

[54] D. Lee, B. Kahng, Y. S. Cho, K. I. Goh and D. S. Lee, "Recent advances of percolation theory in complex networks," *J. Korean Phys. Soc.* **73**, 152 (2018).

[55] L. Basnarkov and V. Urumov, "Kuramoto model with asymmetric distribution of natural frequencies," *Phys. Rev. E* **78**, 011113 (2008).

[56] J. Song, J. Um, J. Park, S. Dorogovtsev, J. F. F. Mendes and B. Kahng, "Effective potential approach for hybrid synchronization transitions," *in preparation*.

[57] Y. Moreno and A. F. Pacheco, "Synchronization of kuramoto oscillators in scale-free networks," *Europhys. Lett.* **68**, 603 (2004).

[58] J. Gómez-Gardeñes, Y. Moreno and A. Arenas, "Paths to synchronization on complex networks," *Phys. Rev. Lett.* **98**, 034101 (2007).

[59] J. Gómez-Gardeñes, S. Gómez, A. Arenas and Y. Moreno, "Explosive synchronization transitions in scale-free networks," *Phys. Rev. Lett.* **106**, 128701 (2011).

[60] P. Ji, T. K. DM. Peron, P. J. Menck, F. A. Rodriguez and J. Kurths, "Cluster explosive synchronization in complex networks," *Phys. Rev. Lett.* **110**, 218701 (2013).

[61] Y. Zou, T. Pereira, M. Small, Z. Liu, J. Kurths, Basin of attraction determines hysteresis in explosive synchronization, *Phys. Rev. Lett.* **112**, 114102 (2014).

[62] X. Zhang, Y. Zou, S. Boccaletti and Z. Liu "Explosive synchronization as a process of explosive percolation in dynamical phase space," *Sci. Rep.* **4**, 5200 (2014).

[63] S. Boccaletti et al., "Explosive transitions in complex networks' structure and dynamics: Percolation and synchronization," *Phys. Rep.* **660**, 1 (2016).

[64] O. Riordan, L. Warnke, "Explosive percolation is continuous," *Science* **333**, 322 (2011) .

[65] J. Park and B. Kahng, "Hybrid synchronization transition in a restricted Kuramoto model," *in preparation*.

[66] S. H. Strogatz, *Sync: The Emerging Science of Spontaneous Order* (Hyperion, New York, 2003).

[67] G. V. Osipov, J. Kurths, C. Zhou, *Synchronization in Oscillatory Networks* (Springer, Berlin, 2007).

[68] S. Boccaletti, *The Synchronized Dynamics of Complex Systems* (Elsevier, Oxford, 2008).

[69] A. Pikovsky, M. Rosenblum, J. Kurths, *Synchronization: A Universal Concept in Nonlinear Sciences* (Cambridge University Press, Cambridge, 2001).

[70] A. Arenas, A. Díaz-Guilera, J. Kurths, Y. Moreno, C. Zhou, "Synchronization in complex networks," *Phys. Rep.* **469**, 93 (2008).

[71] J. A. Acebrón, L. L. Bonilla, C. J. P. Vicente, F. Ritort, R. Spigler, "The kuramoto model: A simple paradigm for synchronization phenomena," *Rev. Mod. Phys.* **77**, 137 (2005).

[72] D. Stauffer, A. Coniglio and M. Adam, "Gelation and critical phenomena," in *Polymer Networks* (Springer, Berlin, Heidelberg, 1982).

[73] Z. Ball, H. M. Phillips, D. L. Callahan and R. Sauerbrey, "Percolative metal-insulator transition in excimer laser irradiated polyimide," *Phys. Rev. Lett.* **73**, 2099 (1994).

[74] J. S. Lee, S. Lee, S. and T. W. Noh, "Resistive switching phenomena: A review of statistical physics approaches," *Appl. Phys. Rev.* **2**, 031303 (2015).

[75] R. Pastor-Satorras and A., Vespignani, "Epidemics and immunization in scale-free networks," in *Handbook of Graphs and Networks: From the Genome to the Internet*, edited by S. Bornholdt and H. G. Schuster, (Wiley-VCH,Berlin, 2003), p. 111.

[76] S. W. Son, H. Jeong and J. D. Noh, "Random field Ising model and community structure in complex networks," *Eur. Phys. J. B* **50**, 431 (2006).

[77] M. Molloy and B. Reed, "A critical point for random graphs with a given degree sequence," *Random Stuct. Algorithms* **6**, 161 (1995).

[78] M. E. J. Newman, S. H. Strogatz and D. J. Watts, "Random graphs with arbitrary degree distributions and their applications," *Phys. Rev. E* **64**, 026118 (2001).

[79] J. Park and M. E. Newman, "Statistical mechanics of networks," *Phys. Rev. E* **70**, 066117 (2004).

[80] P. Erdős and A. Rényi, "On random Graphs. I," *Publ. Math. Debrecen.* **6**, 259 (1959).

[81] P. Erdős and A. Rényi, "On the evolution of random graphs," *Publ. Math. Inst. Hung. Acad. Sci.* **5**, 17 (1960).

[82] K. -I. Goh, B. Kahng and D. Kim, "" *Phys. Rev. Lett.* **87**, 278701 (2001).

[83] C. M. Fortuin and P. W. Kasteleyn, "On the random-cluster model: I. Introduction and relation to other models," *Physica* **57**, 536 (1972).

[84] C. M. Fortuin, "On the random-cluster model II. The percolation model," *Physica* **58**, 393 (1972).

[85] C. M. Fortuin, "On the random-cluster model: III. The simple random-cluster model," *Physica* **59**, 545 (1972).

[86] R. G. Edwards, A. D. Sokal, "Generalization of the Fortuin-Kasteleyn-Swendsen-Wang Representation and Monte Carlo Algorithm," *Phys. Rev. D* **38**, 2009 (1988).

[87] S. Fortunato, "Percolation and deconfinement in SU(2) gauge theory," *arXiv: preprint hep-lat/0012006* (2000).

[88] D. S. Lee, K. -I. Goh, B.Kahng and D. Kim, "Evolution of scale-free random graphs: Potts model formulation," *Nucl. Phys. B* **696**, 351 (2004).

[89] B. Bollobas, *Random Graph* (Cambridge University Press, Cambridge, 2005)

[90] S. N. Dorogovtsev, J. F. F. Mendes and A. N. Samukhin, "Principles of statistical mechanics of uncorrelated random networks," *Nucl. Phys. B* **666**, 396 (2003).

[91] M. E. J. Newman, "Component sizes in networks with arbitrary degree distributions," *Phys. Rev. E* **76**, 045101(R) (2007).

[92] P. L. Krapivsky, S. Redner and E. Ben-Naim, *A Kinetic View of Statistical Physics* (Cambridge University Press, Cambridge, 2010).

[93] D. Achlioptas, R.M. d'Souza, J. Spencer, "Explosive percolation in random networks," *Science* **323**, 1453 (2009).

[94] Y.S. Cho, S. Hwang, H.J. Herrmann, B. Kahng, "Avoiding a spanning cluster in percolation models," *Science* **339**, 1185 (2013).

[95] R.A. da Costa, S.N. Dorogovtsev, A.V. Goltsev, J.F.F. Mendes, "Explosive percolation transition is actually continuous," *Phys. Rev. Lett.* **105**, 255701 (2010).

[96] P. Grassberger, C. Christensen, G. Bizhani, S.-W. Son, M. Paczuski, "Explosive percolation is continuous, but with unusual finite size behavior," *Phys. Rev. Lett.* **106**, 225701 (2011).

[97] da Costa RA, Dorogovtsev SN, Goltsev AV, Mendes JFF "Solution of the explosive percolation quest: Scaling functions and critical exponents," *Phys. Rev. E* **90**, 022145 (2014).

[98] T. Bohman and A. Frieze, "Avoiding a giant component," *Random Struct. Algorithms* **19**, 75 (2001).

[99] E. J. Friedman and A. S. Landsberg, "Construction and Analysis of Random Networks with Explosive Percolation," *Phys. Rev. Lett.* **103**, 255701 (2009).

[100] M. E. Fisher and A. N. Berker "Scaling for first-order phase transitions in thermodynamic and finite systems," *Phys. Rev. B* **26** 2507 (1982).

[101] K. Ziemelis and L. Allen, "Nature insight: Complex systems," *Nature* **410**, 241 (2001).

[102] R. Gallagher and T. Appenzeller, "Complex systems, and following viewpoint articles on complex systems," *Science* **284**, 8 (1999).

[103] D. Sornette and G. Ouillon, "Dragon-kings: mechanisms, statistical methods and empirical evidence," *Eur. Phys. J.: Spec. Top.* **205**, 1 (2012).

[104] P. Bak, K. Christensen, L. Danon, and T. Scanlon, "Unified scaling law for earthquakes," *Phys. Rev. Lett.* **88**, 178501 (2002).

[105] F. Lillo and R. N. Mantegna, "Power-law relaxation in a complex system: Omori law after a financial market crash," *Phys. Rev. E* **68**, 016119 (2003).

[106] B. D. Malamud, G. Morein, and D. L. Turcotte, "Forest fires: an example of self-organized critical behavior," *Science* **281**, 1840–1842 (1998).

[107] D. Lee, J. Y. Kim, J. Lee, and B. Kahng, "Forest fire model as a supercritical dynamic model in financial systems," *Phys. Rev. E* **91**, 022806 (2015).

[108] A. L. Barabasi, "The origin of bursts and heavy tails in human dynamics," *Nature* **435**, 207 (2005).

[109] M. E. Newman, "Power laws, Pareto distributions and Zipf's law," *Contemp. Phys.* **46**, 323 (2005).

[110] D. Sornette, "Predictability of catastrophic events: Material rupture, earthquakes, turbulence, financial crashes, and human birth," *Proc. Natl. Acad. Sci. U. S. A.* **99**, 2522 (2002).

[111] B. A. Carreras, V. E. Lynch, I. Dobson, and D. E. Newman, "Critical points and transitions in an electric power transmission model for cascading failure blackouts," *Chaos* **12**, 985–994 (2002).

[112] R. M. D'souza, "Curtailing cascading failures," *Science* **358**, 860 (2017).

[113] Y. Yang, T. Nishikawa, and A. E. Motter, "Small vulnerable sets determine large network cascades in power grids," *Science* **358**, eaan3184 (2017).

[114] D. L. Gilden, T. Thornton, and M. W. Mallon, "1/f noise in human cognition," *Science* **267**, 1837 (1995).

[115] L. de Arcangelis, C. Perrone-Capano, and H. J. Herrmann, "Self-organized criticality model for brain plasticity," *Phys. Rev. Lett.* **96**, 028107 (2006).

[116] P. Bak, C. Tang, and K. Wiesenfeld, "Self-organized criticality: An explanation of the 1/f noise," *Phys. Rev. Lett.* **59**, 381–384 (1987).

[117] E. Bonabeau, "Sandpile dynamics on random graphs," *J. Phys. Soc. Jpn.* **64**, 327 (1995).

[118] K. I. Goh, D. S. Lee, B. Kahng, and D. Kim, "Sandpile on scale-free networks," *Phys. Rev. Lett.* **91**, 148701 (2003).

[119] Y. Lin, K. Burghardt, M. Rohden, P.-A. Noël, and R. M. D'Souza, "Self-organization of dragon king failures," *Phys. Rev. E* **98**, 022127 (2018).

[120] M. Schröder, S. H. Ebrahimnazhad Rahbari, J. Nagler, "Crackling noise in fractional percolation," *Nat. Commun.* **4**, 2222 (2013).

[121] J. Buck, and E. Buck, "Synchronous fireflies," *Sci. Am.* **234**, 74 (1976).

[122] Z. Néda, E. Ravasz, Y. Brechet, T. Vicsek and A-L. Barabási, "Self-organizing processes: The sound of many hands clapping," *Nature* **403**, 849 (2000).

[123] I. Dobson, "Synchrony and your morning coffee," *Nat. Phys.* **9**, 133 (2013).

[124] P. J. Menck, J. Heitzig, J. Kurths and H. J. Schellnhuber, "How dead ends undermine power grid stability," *Nat. Commun.* **5**, 3969 (2014).

[125] M. G. Rosenblum, A. S. Pikovsky and J. Kurths, "Phase synchronization of chaotic oscillators," *Phys. Rev. Lett.* **76**, 1804 (1996).

[126] S. Watanabe, S. H. Strogatz, "Integrability of a globally coupled oscillator array," *Phys. Rev. Lett.* **70**, 2391 (1993).

[127] S. Watanabe, S. H. Strogatz, "Constants of motion for superconducting josephson arrays," *Physica D* **74**, 197 (1994).

[128] E. Ott and T.M. Antonsen, "Low dimensional behavior of large systems of globally coupled oscillators," *Chaos* **18**, 037113 (2008).

[129] E. Ott and T.M. Antonsen, "Long time evolution of phase oscillator systems," *Chaos* **19**, 023117 (2009).

[130] H. Daido, "Intrinsic fluctuations and a phase transition in a class of large populations of interacting oscillators," *J. Stat. Phys.* **60**, 753 (1990).

[131] H. Hong, H. Chaté, L. H. Tang and H. Park, "Finite-size scaling, dynamic fluctuations, and hyperscaling relation in the Kuramoto model," *Phys. Rev. E* **92**, 022122 (2015).

[132] S. Yoon, M. S. Sindaci, A. V. Goltsev and J. F. F. Mendes, "Critical behavior of the relaxation rate, the susceptibility, and a pair correlation function in the Kuramoto model on scale-free networks," *Phys. Rev. E* **91**, 032814 (2015).

[133] M. A. Buice and C. C. Chow, "Correlations, fluctuations, and stability of a finite-size network of coupled oscillators," *Phys. Rev. E* **76**, 031118 (2007).

[134] S. H. Strogatz and R. E. Mirollo, "Stability of incoherence in a population of coupled oscillators." *J. Stat. Phys.* **63**, 613 (1991).

[135] S. H. Strogatz, R. E. Mirollo and P. C. Matthews, "Coupled nonlinear oscillators below the synchronization threshold: relaxation by generalized Landau damping," *Phys. Rev. Lett.* **68**, 2730 (1992).

[136] S. H. Strogatz, "From kuramoto to crawford: exploring the onset of synchronization in populations of coupled oscillators," *Physica D* **143**, 1 (2000).

[137] Y. Maistrenko, B. Penkovksy, M. Rosenblum, "Solitary state at the edge of synchrony in ensembles with attractive and repulsive interactions," *Phys. Rev. E* **89**, 060901(R) (2014).

[138] H. Hong, S. H. Strogatz, "Mean-field behavior in coupled oscillators with attractive and repulsive interactions," *Phys. Rev. E* **85**, 056210 (2012).

[139] D. Iatsenko, S. Petkoski, P. V. E. McClintock, A. Stefanovska, "Stationary and travelling wave states of the kuramoto model with an arbitrary distribution of frequencies and coupling strengths," *Phys. Rev. Lett.* **110**, 064101 (2013).

[140] M. T. Alkire, A. G. Hudetz and G. Tononi, "Consciousness and anesthesia," *Science* **322**, 876 (2008).

[141] A. E. Hudson, D. P. Calderon, D. W. Pfaff and A. Proekt, "Recovery of consciousness is mediated by a network of discrete metastable activity states," *Proc. Natl. Acad. Sci. U.S.A.* **111**, 9283 (2014).

[142] J. -Y. Moon et al., "Structure shapes dynamics and directionality in diverse brain networks: mathematical principles and empirical confirmation in three species," *Sci. Rep.* **7**, 46606 (2017).

[143] U. Lee et al., " Functional brain network mechanism of hypersensitivity in chronic pain," *Sci. Rep.* **8**, 243 (2018)

[144] H. Hong, S. H. Strogatz, "Conformists and contrarians in a kuramoto model with identical natural frequencies," *Phys. Rev. E* **84**, 046202 (2011).

[145] O. Burylko, Y. Kazanovich, R. Borisyuk, "Bifurcation study of phase oscillator systems with attractive and repulsive interaction," *Phys. Rev. E* **90**, 022911 (2014).

[146] T. Qiu, S. Boccaletti, I. Bonamassa, Y. Zou, J. Zhou, Z. Liu and S. Guan, "Synchronization and Bellerophon states in conformist and contrarian oscillators," *Sci. Rep.* **6**, 36713 (2016).

[147] M. Nagy, Z. Akos, D. Biro and T. Vicsek "Hierarchical group dynamics in pigeon flocks," *Nature* **464**, 890 (2010).

[148] H. Su and S. Wang, "Flocking of multi-agents with a virtual leader," *IEEE Trans. Automat. Control* **54**, 293 (2009).

[149] T. Vicsek, A. Czirók, E. Ben-Jacob, I. Cohen and O. Shochet, "Novel type of phase transition in a system of self-driven particles," *Phys. Rev. Lett.* **75**, 1226 (1995).

[150] A. Pikovsky and M. Rosenblum, "Partially integrable dynamics of hierarchical populations of coupled oscillators," *Phys. Rev. Lett.* **101**, 264103 (2008).

[151] S. A. Marvel, R. E. Mirollo, S. H. Strogatz, "Identical phase oscillators with global sinusoidal coupling evolve by möbius group action", *Chaos* **19**, 043104 (2009).

[152] A. Pikovsky and M. Rosenblum, "Dynamics of heterogeneous oscillator ensembles in terms of collective variables," *Physica D* **240**, 872 (2011).

[153] J. Park, S. Yi and B. Kahng, "Hysteresis and criticality in the restricted Erdős–Rényi model," *in preparation*.

초 록

복잡계(complex system)는 복잡하고 어렵다는 의미보다는 복합적이라는 의미에서 바라보아야 한다. 계를 구성하는 요소가 여러 종류이거나 복합적인 상호작용이 있는 경우 단일 종 사이의 단순한 상호작용에서는 볼 수 없는 복합적인 효과가 나타날 수 있다. 복잡계 네트워크는 계를 구성하는 요소(노드)들과 복합적 상호작용의 연결 관계(링크)에 대한 수학적인 표현 방법이다. 어떤 복잡계가 특정한 기능을 하는지 여부는 전체적인 연결망의 상태와 더불어 내부 상호작용의 방식과도 관련될 수 있다. 상전이는 계의 기능 여부와 같은 어떤 질적인 변화를 기술한다. 여과 상전이(percolation phase transition)와 동기화 상전이(synchronization phase transition)는 복잡계에서 연구되는 대표적인 상전이이다. 여과 상전이는 전체적인 연결이 없는 상태에서 전체적인 연결이 있는 상태로의 네트워크의 구조적 변화다. 한편 동기화 상전이는 시스템의 운동에서 나타나는, 결맞음성이 없는 무질서한 상태로부터 동기화된 상태로의 동역학적 변화다. 상전이는 연속 상전이와 불연속 상전이로 구분되는데, 두 개의 상이 공존할 수 있는 불연속 상전이와 달리 연속 상전이에서는 임계점에서 두 개의 상이 하나로 합치된다. 이에 연속상전이의 임계점에서는 계 전체가 강한 상관관계에 있기 때문에 부분의 변화가 전체의 변화로 이어질 수 있고 임계현상이 나타난다. 불연속 상전이에서는 임계 현상이 있을 수도 있고 없을 수도 있다. 하이브리드 상전이(hybrid phase transition)란 연속상전이의 특징인 임계현상을 동반하는 불연속 상전이를 의미한다. 따라서 어떻게 불연속 상전이가 임계현상을 가질 수 있는가 하는 의문점이 생긴다. 본 학위 논문에서는 복잡계에서 나타나는 하이브리드 상전이와 그 메커니즘을 알아본다. 특히 하이브리드 여과 상전이(percolation hybrid transition)와 하이브리드 동기화 상전이(synchronization hybrid transition)를 중점적으로 살펴본다. 여과 상전이의 경우 연쇄 파급 과정(cascade process)과 클러스터 성장 과정(merging process)에서 각기 다른 종류의 하이브리드 상전이가 일어난다. 구라모토 진동자들의 동기화 상전이에서는 고유진동수의

분포에 따라 연속, 불연속, 하이브리드 상전이가 가능한데, 하이브리드 상전이는 분포가 납작해지는 경우에 발생한다. 또한 어떤 순위(ranking)에 따라 두 개의 그룹으로 나뉘어 제한된 상호작용을 하는 경우에도 하이브리드 동기화 상전이가 가능하다. 특히 이러한 메커니즘은 여러 모형에서 보편적(universal)으로 나타나기도 하는데, 이를 바탕으로 비평형 복잡계에서의 하이브리드 상전이를 분류해 볼 수 있다.

주요어 : 하이브리드 상전이, 복잡계, 여과 상전이, 동기화 상전이, 구라모토 모형, 제한된 여과 모형, 제한된 동기화 모형

학번 : 2014-21361